Comparison of Control Techniques for Robust Performance on Uncertain Structural Systems

by

Simon C. O. Grocott

B.A.Sc. University of Toronto (1991)

SUBMITTED TO THE DEPARTMENT OF
AERONAUTICS AND ASTRONAUTICS
IN PARTIAL FULFILLMENT OF THE REQUIREMENTS
FOR THE DEGREE OF

S.M.

at the

Massachusetts Institute of Technology

February, 1994

Signature of Author _____

Department of Aeronautics and Astronautics
January 12, 1994

Certified by _____

David W. Miller
Thesis Advisor, Principal Research Scientist, Department of Aeronautics and Astronautics

Accepted by _____

Professor Harold Y. Wachman
Chairman, Department Graduate Committee

Comparison of Control Techniques for Robust Performance on Uncertain Structural Systems

by

Simon C. O. Grocott

SUBMITTED TO THE DEPARTMENT OF AERONAUTICS AND ASTRONAUTICS
ON JANUARY 12, 1994, IN PARTIAL FULFILLMENT OF THE
REQUIREMENTS FOR THE DEGREE OF
S.M.

The objective of this thesis is to compare several control techniqueswhich provide robustness to parametric uncertainty in structural systems. The techniques are compared analytically, through the design of compensators for a low order sample problem, and experimentally on the Middeck Active Control Experiment (MACE) test article. From the sample problem, the techniques are compared on the basis of computation required, the performance sacrifice for the level of robustness achieved, and, for techniques that provide guarantees of robustness, the conservativeness of the guarantees. On the MACE test article, the techniques are compared on the basis of the maximum performance that could be achieved in both single-input, single-output (SISO) and multiple-input, multiple-output (MIMO) configurations.

Through the comparison, it was found that $\mathcal{H}_\infty$ synthesis for parameter uncertainty was not suitable for control designs on structural systems. The robustness guarantees provided by $\mathcal{H}_\infty$ were extremely conservative, and the performance sacrificed to achieve robustness was much larger than for any of the other techniques. Though significant performance was not sacrificed, μ-synthesis was found to be unsuitable, due to the rapid increase in system order that results from incorporating the D-scale dynamics for large order systems with multiple uncertainties. The Multiple Model, Maximum Entropy, and SWLQG techniques were all found to be suitable for control of MACE. Results consisently showed that Multiple Model controllers achieve better performance than ME and SWLQG controllers. Furthermore, a design process was developed in which preliminary SWLQG or ME compensators are used as initial guesses for Multiple Model, thus reducing the computational burden of designing Multiple Model controllers.

Thesis Supervisor: Dr. David W. Miller
Principal Research Scientist, Aeronautics and Astronautics

Acknowledgments

This research is supported by the NASA In-Step and CSI Offices, with Mr. Gregory Stover and Dr. Jerry Newsom as contract monitors, under contract NAS1-18690, and by NASA Headquarters Grant NAGW-1335 to the MIT Space Engineering Research Center, with Dr. Robert Hayduk as technical monitor.

I would like to thank Doug MacMartin for his help in steering me at the start of my research, and helping me to determine the best sample problem for this work.

I would like to thank Roger Glaese for developing the finite element models that were used to design controllers.

I would like to thank Jon How for his guidance in the preparation of this thesis.

I would like to thank Dave Miller, my advisor, for his guidance and support throughout this endeavour.

Most importantly, I would like to thank my wife, Ariana, for her love and support without which I could not have persevered.

Contents

List of Figures

List of Tables

Chapter 1

Introduction

The use of feedback control to enhance the behavior of mechanical systems is quite common. For spacecraft, such mechanical systems include astrophysical and earth-observing instruments. These instruments are subject to increasingly stringent performance and weight requirements which can cause the control bandwidth of these control systems to overlap with the flexible dynamics of the spacecraft. Thus control of structural systems has emerged in recent years to address this issue.

The use of modern control techniques to develop feedback compensators requires a detailed model of the dynamics of the structural system. However, models developed using the finite element method and other modelling techniques often contain significant errors. The emerging field of robust control is well suited to deal with errors in these models.

Modelling errors are often divided into two categories; unmodelled dynamics and parametric uncertainty. Unmodelled dynamics frequently arise in structural control applications due to the infinite order nature of structural dynamics. Dynamics well above the bandwidth of interest in a system are typically truncated, and therefore are unmodelled. In addition, sensor and actuator dynamics and time delays are often ignored leading to additional unmodelled dynamics.

Within the bandwidth of interest, modelling errors often arise due to modelling assumptions and the approximate nature of the modelling techniques. Therefore, model parameters, such as modal frequencies and mode shapes, contain errors. These

errors then make the modal parameters of the actual system uncertain. Compensators designed using optimal control techniques often encounter performance degradation and instability due to the uncertainty in these parameters. Therefore, it is necessary to consider robust control techniques for the design of compensators for these systems.

An example of a flexible structural system requiring the use of robust control to meet performance objectives is the Middeck Active Control Experiment (MACE) test article. This test article was designed to simulate a satellite with multiple independently pointing instruments. The performance objective is to minimize the degradation in pointing precision of one payload while the other payload is in operation, so that both can meet requirements and be operated simultaneously Motivated by the need to maintain good pointing performance, in the presence of parametric uncertainty, the objective of this thesis is to compare existing robust control techniques to determine which are most useful in the design of robust compensators for structural systems such as the MACE test article.

While the literature on robust control techniques is quite extensive, very little comparison of robust techniques has been made. Comparisons that have been made tend to be very limited in scope. Tahk and Speyer [1], for example, compare two asymptotic Linear Quadratic Gaussian (LQG) techniques: LQG/Loop Transfer Recovery [2] (LQG/LTR) and Parameter Robust LQG [3] (PRLQG). However, their comparison deals only with whether or not robustness is achieved using these techniques. The broader issues of the cost associated with achieving robustness, in terms of performance and computational effort, are ignored.

Cheung and Yurkovich [4] build on the comparison by Tahk and Speyer by including an additional robust control technique, Maximum Entropy [5]. Their work includes a rudimentary discussion of the computation required for each technique, and a comparison of the performance of controllers designed using the three techniques. However, the compensators that were compared did not have equivalent robustness properties, so it was difficult to draw any conclusions regarding how robustness and performance are traded off in

This thesis will present a much more thorough and comprehensive comparison

of the existing robust control techniques. It is comprehensive because a total of nine robust control techniques are considered. These techniques are divided into two categories on the basis of whether or not robustness is guaranteed. The desensitizing techniques, which do not provide guarantees, include: Trajectory Sensitivity Optimization (TSO) [6], Sensitivity Weighted LQG (SWLQG) [7], PRLQG[3, 1], and Maximum Entropy [5]. The techniques presented which provide some guarantees consist of Multiple Model[8, 9], the Bourret Approximation method[10], $\mathcal{H}_\infty$-synthesis[11], μ-synthesis [12], and Popov controller synthesis [13]. These techniques span the spectrum of existing robust control techniques.

The comparison is thorough because it considers a wide range of properties associated with robust control. These include the computation required and effectiveness of each technique, as well as the effects of adding robustness on closed loop properties such as performance and bandwidth. Compensators will be designed for two systems. The first is a low order sample problem which is representative of structural control applications. The second is the MACE test article. The use of two systems permits two different and complementary approaches to the comparison.

The first approach, used on the sample problem, will be similar to the approach used in Ref. [4]. Several controllers, designed with different amounts of uncertainty, will be designed at the same level of control authority for each of the robust control techniques. The effectiveness of each technique can be evaluated by comparing the stability robustness that is achieved. For compensators with equivalent robustness properties, the performance degradation and bandwidth increase that occur as a result of increasing robustness will be compared. In addition, the computation required for each technique will be determined. Finally, the amount of conservatism in the robust techniques that provide guarantees will be examined. For this purpose, the conservatism of a technique is defined as the difference between the robustness achieved by a compensator and the robustness guaranteed. For example, if a compensator is stable for 15% perturbations in a parameter, but is guaranteed to be stable for only 5% perturbations, the difference is a measure of conservatism.

The second approach, used for the MACE test article, is to compare the best pos-

sible performance improvement that can be achieved using each technique. Experimentally, compensators designed from optimal control techniques often destabilize the system because they lack sufficient robustness. Therefore on experimental systems, it is more meaningful to talk about performance improvement that can be gained by designing more robust compensators. Thus a comparison of the maximum performance that can be gained using each control technique complements the comparison of properties based on the sample problem.

1.1 Outline

In the following chapter, the MACE test article is introduced in greater detail. The Finite Element Method (FEM) based control design model developed by Glaese [14] is also presented. A comparison between the control design model and measured transfer functions gives an indication of some of the modelling errors that are present, and motivates the use of an uncertainty set that consists of some of the modal frequencies in the model.

In Chapter 3, background information is presented which is necessary for an understanding of the various robust control techniques. The chapter begins by fixing a standard notation. This is followed by a summary of the derivation of LQG, and each of the robust control techniques. Following the presentation of the control techniques, a qualitative and quantitative comparison of the computational requirements of each method is made. Finally, some of the techniques are eliminated from the comparison on the basis of similarity with other techniques, excessive computational burden, or maturity of computer algorithms. Five of the control design techniques are carried over to the sample problem for comparison.

In Chapter 4, analysis tools are presented. The analysis techniques consist of two sets. The first set is primarily comparative in nature, and the tools in this set are used in the sample problem to help interpret the results and make comparisons between compensators and control techniques. The second set is predictive in nature. This set is used in experimental control design. The second set of tools provide predictions

of stability and performance which aid the control designer in selecting parameters for compensator design.

The bulk of the comparative work is presented in Chapters 5 and 6. Chapter 5 focuses on comparing the robust control techniques using the low order sample problem. Control designs for two different input-output configurations are presented to add breadth to the comparison. For each configuration, several compensators are designed using each robust control technique. For each technique, compensators with varying robustness properties are studied to identify the means by which robustness is added. Then, compensators from each technique with equal robustness properties are compared to determine the performance degradation and bandwidth increase that result from added robustness.

Chapter 6 presents the results of experimentals conducted on the MACE test article. For breadth, two input-output configurations are again used. The first is a single input, single output (SISO) configuration. The means by which robustness is added to the SISO compensators is studied, and differences between compensators designed from each technique are illustrated. Closed loop performance is then compared for compensators from each technique. The second configuration is multiple-input, multiple-output (MIMO). Direct comparsion of compensators is limited for the MIMO case. However, closed loop performance is compared for compensators designed using the different robust control techniques.

Chapter 7 takes the observations from the sample problem and experiments, and formulates some observations which are more generalizable to other applications. In addition, a robust control synthesis approach is presented which exploits the strengths of several of the design techniques in the design of high authority robust controllers.

Finally, in Chapter 8 the conclusions based on computation and the analytical and experimental comparisons are summarized. Future directions for this research are also suggested.

Chapter 2

Middeck Active Control Experiment (MACE)

The Middeck Active Control Experiment (MACE) test article is an example of a flexible structural system requiring high authority control. Due to limitations in the Finite Element Method (FEM) based control design model, this structure exhibits significant parametric uncertainty. Therefore, it is useful as a testbed on which to compare robust control techniques. This chapter begins with a description of the MACE program, a NASA In-Step sponsored program scheduled for launch in December 1994. This is followed by a description of the MACE test article hardware. Finally, a discussion of the FEM model of the test article rounds out the chapter.

Many future spacecraft will require active structural control to meet stringent performance specifications. However, prior to launch, the controllers for these vehicles can only be analyzed and tested on the ground. Unfortunately, these ground tests are affected by gravity and the suspension system which couple with the structural dynamics. Thus, it is very difficult to use ground tests to validate the controller that is selected for on-orbit operations. Therefore, techniques are required that will provide a program manager with confidence that the spacecraft will operate as required once on-orbit.The objective of MACE is to develop a well verified set of Controlled Structures Technology (CST) techniques that gives designers of future spacecraft, which cannot be adequately tested on the ground in a sufficiently realistic zero-gravity simulation,

confidence in the eventual on-orbit performance.

The configuration of the MACE test article was chosen to be representative of flexible spacecraft, such as Earth observing platforms, with multiple, independently pointing or scanning payloads. For this type of spacecraft, the motion of one payload can substantially affect the pointing accuracy of another[15]. Furthermore, the interaction between the payloads includes substantial structural flexibility effects. Ground testing for this mission class is highly susceptible to gravity and suspension effects, such as structural sag, pendulum, and compound pendulum modes. Therefore, the test article has been designed to couple these effects with the flexible behavior[16].

2.1 MACE Hardware

The experiments described in this section were carried out on the hardware shown in Figure 2.1. The test article consists of a flexible bus, to which two payloads, a reaction wheel assembly for attitude control, and a variety of other sensors and actuators are mounted. Each payload is mounted to the structure using a two-axis gimbal that provides pointing capability. The hardware is suspended using three pneumatic/electric low frequency suspension devices [17]. For reference, the X-axis is aligned with the bus. In the nominal configuration (shown in Figure 2.1), the gimbals point in the $-Y$ direction, and the Z-axis points out of the figure.

The sensors used in these experiments include two rate gyros in the primary payload, and three rate gyros suspended beneath the reaction wheels. The actuators include two motors in each gimbal and three reaction wheels. The angular rates of the two gimbals relative to the bus are measured using optical encoders.

The control is implemented using a real-time computer operating at a 500 Hz sampling rate. Anti-aliasing Bessel filters are included on all analog sensor channels. These can be modelled as an effective time delay up to frequencies higher than the control bandwidth. The combination of the computational delay, the zero-order hold, and the anti-aliasing filters introduces a substantial net time delay into all control transfer functions.

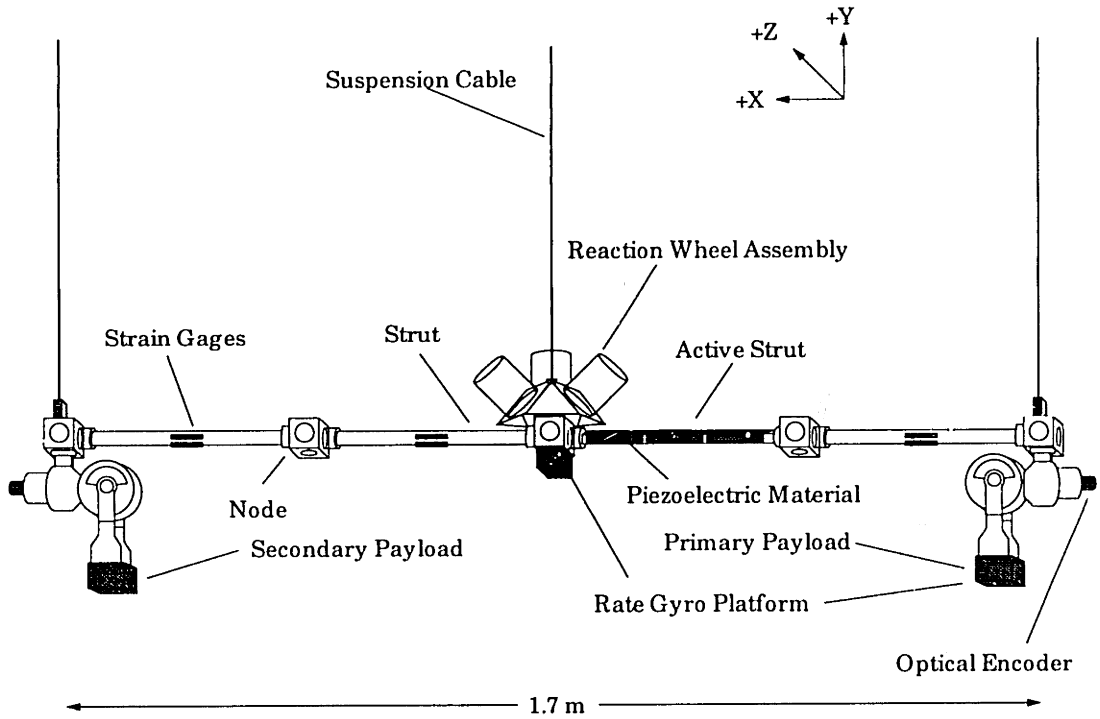

Figure 2.1: Middeck Active Control Experiment (MACE) test article suspended in 1-g.

Since many spacecraft use low frequency servo control systems to point attached payloads, such a servo control is also used on the MACE hardware. All four gimbal motors have proportional-integral (PI) servo loops closed around them, using the encoder rate and integrated rate signals for feedback. The result is that below a frequency of 3 Hz, the input signal to each gimbal commands the relative angular position of the payload with respect to the bus. The structural control is designed for implementation on this servo controlled system. The performance improvement that can be attributed to CST is the improvement over the performance of the system with this servo control operating.

2.2 Control Design Model

The model used for control design in this thesis is derived from a finite element model (FEM) of the MACE test article developed by Glaese[14]. Experimentally determined

modal damping ratios are combined with the analytic predictions of the modal frequencies and mode shapes from the FEM to form the state space representation of the test article.

The baseline model of the MACE test article includes servo loops around the four gimbal axes and a speed control servo around the reaction wheels. These servos are included in the model. In addition, the phase delay associated with the sensor dynamics, anti-aliasing filters, computational delay and zero order hold are included using Padé approximations on the appropriate input-output channels.

The finite element model used to generate this control design model was generated through a model updating procedure [14]. The model that has been used in this thesis has had the stiffness parameters updated once. The update occurred on a previous configuration of the hardware, in which one of the gimbals was of an earlier design and the active strut was not present. The stiffnesses of the various components were updated by matching modal frequencies with a measurement model. The measurement model used in the update was a Z-axis model, *i.e.* all motion involoved rotationas about the Z-axis that included the Z-axis primary and secondary gimbals and Z-axis reaction wheels as inputs with Z-axis payload and bus rate gyros as outputs. Since the suspension cables, the structural bus, and the gravity vector all lie in the same plane, the dynamics of the structure decouple into vertical, or Z-axis, and horizontal, or XY-axis, dynamics. The actuators and sensors on the structure are grouped into Z and XY-axis as well. Although the update was performed using only the Z-axis dynamics, the parameters used in the update also affect the XY-axis dynamics, and improvements were seen in the XY-axis transfer functions. This indicates that the new estimates better reflect the true values of the physical parameters. Using the updated stiffness parameters, and models of the new gimbal and active strut, a new FEM was created for the current configuration. The damping used in this model was taken from measured values from the previous configuration.

The MACE model consists of 127 states with 7 inputs (4 gimbals and 3 reaction wheels) and 5 rate gyro outputs. The model includes 50 structural modes from the finite element model (100 states) and 27 states corresponding to the time delays. In

Table 2.1: List of important structural modal frequencies in the finite element model (FEM), with errors when compared to measured data, and their mode number in the reduced order models for the SISO and MIMO topologies. Mode numbers are not consecutive due to non-structural modes in the design model.

Description	Finite Element Model Frequency (Hz)	Errors in Model (%)	Mode Number in Reduced Models	
			SISO	MIMO
Y twist	0.23	-4.7	NP	1
Z tilt	0.45	2.3	NP	NP
X rotation	1.39	0.0	1	2
1st Z bending	1.99	1.2	NP	NP
1st Y bending	3.35	-0.9	2	3
1st Violin	6.81	0.7	NP	NP
1st Violin	6.82	-4.6	4	5
1st Violin	6.82	-5.2	5	6
1st Violin	6.84	-5.1	6	7
2nd Y bending	9.42	1.3	7	8
2nd Z bending	11.30	-0.3	NP	NP
3rd Z bending	12.58	3.9	NP	NP
2nd Violin	13.18	3.7	NP	NP
2nd Violin	13.72	-4.0	NP	NP
2nd Violin	13.72	-18.6	NP	NP
2nd Violin	13.74	-5.2	8	9
3rd Y bending	18.73	9.8	9	10
3rd Violin	20.67	-4.0	NP	NP
3rd Violin	20.68	-4.1	10	11
4th Y bending	22.77	5.8	11	12
5th Y bending	50.42	3.8	13	16
6th Y bending	54.16	0.3	14	17
NP-not present in reduced model				

Chapter 6 robust control techniques will be compared experimentally based on control designs for two sensor and actuator groupings. For both, the problem is reduced so that only the XY-axis dynamics are considered. The servoed X-axis Secondary Gimbal motor is used as a disturbance source. The X-axis angular displacement of the Primary Gimbal is considered the performance metric. However, different actuators and sensors are used in the control loops for the two sets of experiments. The first uses as single-input single-output (SISO) control loop with the servoed X-axis Primary Gimbal motor as the actuator, and the X-axis Primary Gimbal rate gyro as the sensor. The second topology is multiple-input multiple-output (MIMO). In addition to the servoed X-axis Primary Gimbal motor, the X-axis and Y-axis reaction wheels are used as actuators. For sensors, the X-axis and Y-axis bus rate gyros and the X-axis Primary Gimbal rate gyro are used. Using these actuators and sensors, the control design model was reduced to a more manageable size by eliminating the states which have low Hankel Singular Values. For the SISO designs of Section 6.1 the model was reduced to 37 states. For the MIMO designs of Section 6.2 the model was reduced to 42 states. The frequencies of 22 of the most prominent modes in the full order model are shown in Table 2.1. The table indicates which modes are present in the reduced models, and lists the mode number for later reference.

The table also includes the error between the frequencies in the FEM and those measured experimentally. The effects of this modelling error can be seen in Figure 2.2, which shows a typical transfer function for this system. The transfer function for this input-output pair clearly shows modelling error in one of the suspension cable first violin modes at 6.8 Hz, one of the second violin modes at 13.7 Hz, and the fourth Y-axis bending mode at 22.8 Hz. When the control design model has eerors of this magnitude, attempts to achieve large performance improvements without considering these errors will often drive the system unstable. Through the use of robust control techniques which take into consideration errors in the model of the system, it is possible to achieve high performance.

Motivated by the need to use robust control for the design of compensators when errors of this magnitude are present, this thesis seeks to compare different robust

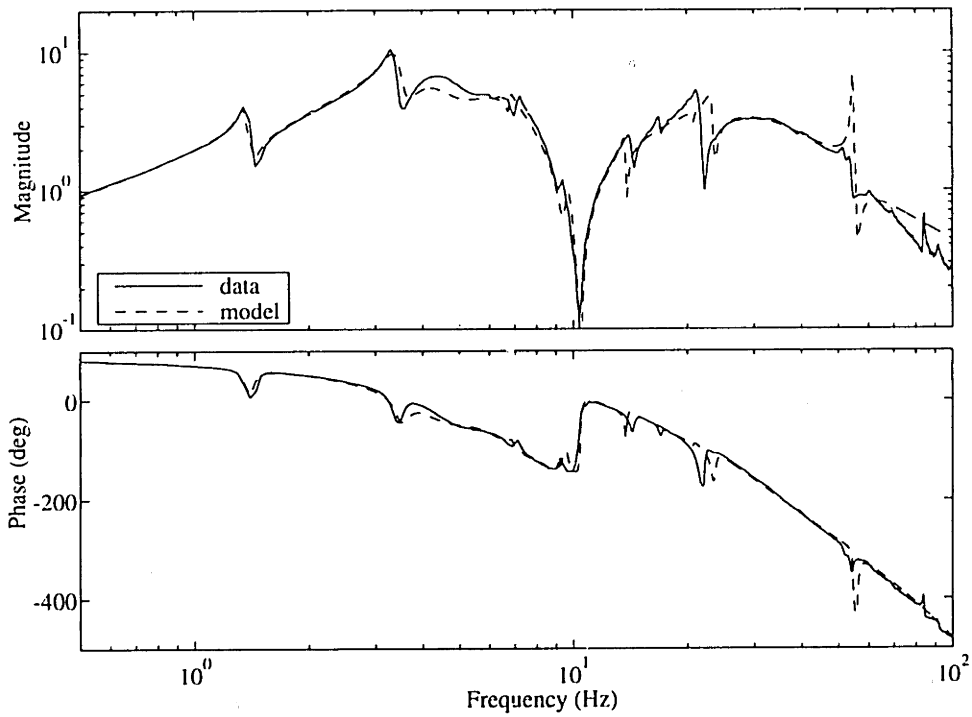

Figure 2.2: Transfer function from servoed X-axis Primary Gimbal motor to X-axis Primary Gimbal rate gyro.

control techniques to determine the usefulness and effectiveness of each. In the following chapter, the robust control techniques that will be considered in this thesis are reviewed.

Chapter 3

Robust Control Formulation

In this chapter, Linear Quadratic Gaussian (LQG) and a number of robust control methodologies are presented. This provides a review of the theoretical basis for each technique, along with a discussion of the solution procedure. The robust techniques are divided into two broad groupings: desensitizing techniques and techniques which provide robustness guarantees.

3.1 Background

This section presents background information which is useful for the robust control techniques presented later in this chapter.

3.1.1 Standard Control Problem

In modern control theory, the standard control problem is to minimize some property (*e.g.* $\mathcal{H}_2$ norm or $\mathcal{H}_\infty$ norm) of a dynamic system through the use of feedback. The standard system is represented in state space as:

$$\begin{aligned} \dot{x} &= Ax + B_w w + B_u u \\ z &= C_z x + D_{zw} w + D_{zu} u \\ y &= C_y x + D_{yw} w + D_{yu} u\,, \end{aligned} \tag{3.1}$$

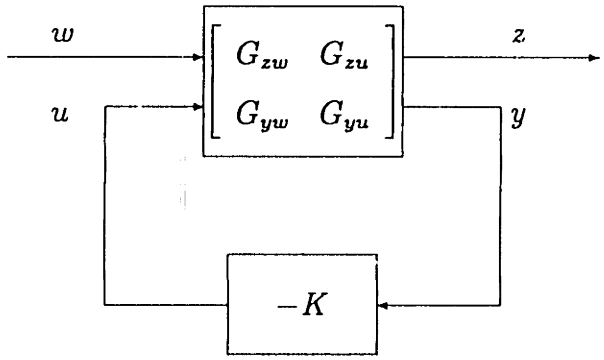

Figure 3.1: Standard Control Problem.

where x represents the states of the system, w is a set of disturbances, u are control inputs, z are performance variables, and y are measurements used for feedback. The transfer function of the open loop system is represented by the matrix

$$G(s) = \begin{bmatrix} G_{zw}(s) & G_{zu(s)} \\ G_{yw}(s) & G_{yu}(s) \end{bmatrix}, \tag{3.2}$$

where $G_{ij}(s) = C_i(sI - A)^{-1}B_j + D_{ij}$.

The standard control problem is shown schematically in Figure 3.1 where $K(s)$ is the transfer function of the feedback compensator. The transfer function for the closed loop system is

$$G_{cl}(s) = G_{zw}(s) - G_{zu}(s)K(s)(I + G_{yu}(s)K(s))^{-1}G_{yw}(s). \tag{3.3}$$

The objective of the standard control problem is to minimize some properties of the closed loop system G_{cl}.

3.1.2 Linear Quadratic Gaussian (LQG)

In comparing robust control techniques, it will be useful to compare controllers designed by these techniques to compensators derived from a technique which does not explicitly address robustness. The Linear Quadratic Gaussian (LQG) technique [18] provides such a comparison, and is presented here as background.

For the system in Equation 3.1, the general stochastic time invariant LQG problem

is to find the compensator which minimizes the quadratic cost

$$J = \lim_{T\to\infty} \frac{1}{T} \mathsf{E}\left\{ \int_0^T [x^T R_{xx} x + 2x^T R_{xu} u + u^T R_{uu}] u \, \mathrm{dt} \right\} , \tag{3.4}$$

subject to the constraints that

$$D_{zw} = 0 , \tag{3.5}$$

$$V = \begin{bmatrix} B_w \\ D_{yw} \end{bmatrix} \begin{bmatrix} B_w^T & D_{yw}^T \end{bmatrix} = \begin{bmatrix} V_{xx} & V_{xy} \\ V_{xy}^T & V_{yy} \end{bmatrix} \geq 0 \ , \ V_{yy} > 0 , \tag{3.6}$$

$$R = \begin{bmatrix} C_z^T \\ D_{zu}^T \end{bmatrix} \begin{bmatrix} C_z & D_{zu} \end{bmatrix} = \begin{bmatrix} R_{xx} & R_{xu} \\ R_{xu}^T & R_{uu} \end{bmatrix} \geq 0 \ , \ R_{uu} > 0 , \tag{3.7}$$

where E is the expectation operator.

Note that the quadratic minimization in Equation 3.4 can also be written as

$$J = \lim_{T\to\infty} \frac{1}{T} \mathsf{E}\left\{ \int_0^T z^T z \, \mathrm{dt} \right\} = \|G_{zw}\|_2^2 . \tag{3.8}$$

The LQG compensator thus minimizes the $\mathcal{H}_2$ norm from the disturbance to performance variables.

The solution is the compensator (K) with state space representation

$$\begin{aligned} \dot{x_c} &= A_c x_c + B_c y \\ -u &= C_c x_c \ , \end{aligned} \tag{3.9}$$

with

$$\begin{aligned} A_c &= A - B_u F - H C_y + B_u D_{yu} C_y \\ B_c &= H \\ C_c &= F , \end{aligned} \tag{3.10}$$

where

$$F = R_{uu}^{-1} \left[R_{xu}^T + B_u^T P \right] \tag{3.11}$$

$$H = \left[Q C_y^T + V_{xy} \right] V_{yy}^{-1} , \tag{3.12}$$

and P and Q solve the following Riccati equations

$$0 = PA + A^T P + R_{xx} - \left[PB_u + R_{xu}\right] R_{uu}^{-1} \left[R_{xu}^T + B_u^T P\right] \tag{3.13}$$

$$0 = AQ + QA^T + V_{xx} - \left[QC_y^T + V_{xy}\right] V_{yy}^{-1} \left[V_{xy}^T + C_y Q\right] . \tag{3.14}$$

Equations 3.13 and 3.14 can be identified as the Linear Quadratic Regulator (LQR) and Kalman Filter (KF) Riccati equations, respectively. The LQR problem seeks the optimal full state feedback gains to minimize Equation 3.4. The KF problem seeks the linear least squares estimate of the states of the system based on noisy measurements from the sensors when the system is driven by a white noise process. The LQG controller is formed by combining these two problems, so that the optimal full state feedback gains are applied to the state estimates which result from the Kalman Filter. The fact that the LQG solution is the combination of these two problems is known as the *separation principle*[18]. Note that while both LQR and KF exhibit built-in robustness properties [19] of $\pm 60°$ phase margin in each control channel, independently and simultaneously, and gain margin of $[1/2, \infty]$, LQG provides no robustness guarantees [20].

Thus two approaches can be used to design LQG controllers. Each of the elements of V and R can be regarded as free parameters which can be altered individually so long as the constraints in Equations 3.6 and 3.7 are satisfied. Given a set of parameters, there is some fictitious set of disturbances and performance variables for which the $\mathcal{H}_2$ norm in Equation 3.8 is minimized. Note that $V_{yy} > 0$ implies that noise is present in all sensor measurements, and $R_{uu} > 0$ implies that all of the control signals are present in the performance variables.

Alternatively, disturbances and performance variables can be set *a priori*. This significantly reduces the number of free parameters. The remaining free parameters are the relative weightings of the various disturbances and performance variables. The relative weightings can be applied by incorporating additional scaling matrices so that

$$V = \begin{bmatrix} B_w \\ D_{yw} \end{bmatrix} V_{ww} \begin{bmatrix} B_w^T & D_{yw}^T \end{bmatrix}, \text{ and } R = \begin{bmatrix} C_z^T \\ D_{zu}^T \end{bmatrix} R_{zz} \begin{bmatrix} C_z & D_{zu} \end{bmatrix} . \tag{3.15}$$

For systems with a single-input, single output (SISO) control loop and one performance variable (apart from the control signal) and one disturbance (apart from sensor noise), there are only two free parameters which will be denoted ρ (control weighting) and θ (sensor noise). In this case $R_{uu} = \rho$ and $V_{yy} = \theta$. This is equivalent to setting the first element of R_{zz} to unity and the last element to ρ, and similarly the first element of V_{ww} to unity and the last element to θ. By reducing the control weighting, the bandwidth of the regulator loop is increased. By reducing the sensor noise, the bandwidth of the estimator loop is increased. Both of these parameters influence the bandwidth of the compensator in the same way. Therefore, higher bandwidth control is obtained by reducing the control weighting and/or the sensor noise. It has been suggested that the bandwidth of the regulator and estimator should not differ greatly[18]. By setting the ratio of ρ and θ to a constant, the number of free parameters may be reduced to one.

For multiple-input, multiple-output (MIMO) problems, more free parameters in V_{ww} and R_{zz} are present. However, the performance variables can be partitioned to control outputs and measurement outputs, and the disturbances can be partitioned to sensor noises and process disturbances. Relative weightings can be specified within each of the partitioned groups. Then the bandwidth can be controlled by adjusting ρ, a relative weighting between control outputs and other outputs, and θ, a relative weighting between sensor noises and other disturbances.

3.1.3 Closed Loop LQG Cost

It is useful to look at the LQG cost in terms of the closed loop system dynamics as well as the open loop dynamics (Equation 3.4). The closed loop expression is used to illustrate the derivation of the many of the robust techniques later in this chapter.

Consider the system in Equation 3.1 cascaded with the compensator in Equation 3.9. With a non-zero D_{zw} term, there is no finite $\mathcal{H}_2$ cost. So with $D_{zw} = 0$, the

closed loop dynamics are as follows:

$$\begin{bmatrix} \dot{x} \\ \dot{x_c} \end{bmatrix} = \begin{bmatrix} A & B_u C_c \\ -B_c C_y & A_c - B_c D_{yu} C_c \end{bmatrix} \begin{bmatrix} x \\ x_c \end{bmatrix} + \begin{bmatrix} B_w \\ -B_c D_{yw} \end{bmatrix} w$$

$$z = \begin{bmatrix} C_z & D_{zu} C_c \end{bmatrix} \begin{bmatrix} x \\ x_c \end{bmatrix}, \tag{3.16}$$

or

$$\begin{aligned} \dot{\tilde{x}} &= \tilde{A}\tilde{x} + \tilde{B}w \\ z &= \tilde{C}\tilde{x}, \end{aligned} \tag{3.17}$$

where $\tilde{(\cdot)}$ is used to distinguish closed loop matrices from open loop matrices.

The cost functional in Equation 3.8 is equivalent to

$$J = \mathrm{tr}\left\{\tilde{Q}\tilde{C}^T\tilde{C}\right\} \tag{3.18}$$

where $\tilde{Q}$ is the solution of the Lyapunov equation

$$0 = \tilde{A}\tilde{Q} + \tilde{Q}\tilde{A}^T + \tilde{B}\tilde{B}^T. \tag{3.19}$$

The two Riccati equation solution for LQG can be derived by appending the Lyapunov equation, Equation 3.19, to the cost functional, Equation 3.18, with a matrix Lagrange multiplier. Taking the gradient with respect to the free parameters (the elements of the compensator matrices) results in Equations 3.13 and 3.14 [21].

3.1.4 Loop Transfer Recovery (LQG/LTR)

A special case of the LQG method, called LQG/LTR, was developed by Doyle and Stein [2]. This method is based on frequency domain loop shaping ideas. If a plant, with frequency response $G(s)$ is minimum phase, *i.e.* has no zeros in the right half plane, then as control weighting approaches zero, the frequency domain properties of the Kalman Filter loop are recovered asymptotically [2]. The loop transfer function of the system, $G_{yu}(s)K(s)$ will asymptotically approach the frequency response of the Kalman Filter loop. Similarly the sensitivity transfer function, $(I + G_{yu}(s)K(s))^{-1}$,

and the complementary sensitivity transfer function, $(I + G_{yu}(s)K(s))^{-1}G(s)K(s)$, will approach those of the Kalman Filter loop. In addition, LQG/LTR recovers the built-in robustness properties of the Kalman Filter. The dual result also applies. These robustness properties are more useful in dealing with unmodelled dynamics rather than parametric uncertainty. LQG/LTR generally leads to poorer parameter robustness because the compensator inverts the stable dynamics of the plant (cancels poles with zeros and zeros with poles) and replaces it with the desired loop shaped dynamics. However LQG/LTR is presented as an introduction since one of the robust techniques extends the results to parametric uncertainty.

3.2 Desensitizing Methods

In this thesis, robust control techniques are divided into two groups; techniques that provide some guarantees of robust stability and techniques that merely desensitize the compensator to parameter uncertainty, but without providing guarantees. The desensitizing methods will be presented in this section.

It is impossible to present every robust control algorithm ever conceived. But it is possible to present a general outline of a few of the more common and interesting techniques to demonstrate desensitizing methods. The techniques that will be presented are Trajectory Sensitivity Optimization (TSO) [6], Sensitivity Weighted LQG (SWLQG) [7], Parameter Robust LQG PRLQG [3, 1], and Maximum Entropy [5].

3.2.1 Trajectory Sensitivity Optimization

The basic principle of the Trajectory Sensitivity Optimization (TSO) presented by Okada and Skelton [6] is that uncertainty is modelled by the "trajectory sensitivity", otherwise known as the state differential sensitivity[22] or simply state sensitivity. This algorithm is the culmination of work by Yedevalli and Skelton[23] and Wagie and Skelton[24] using the concept of sensitivity states which has been around for more than two decades[22].

To introduce the concept of trajectory sensitivity, consider the following simple

system in which the dynamics depend on a parameter α:

$$\begin{aligned} \dot{x} &= Ax + Bu \\ y &= Cx\,. \end{aligned} \tag{3.20}$$

Differentiating Equation 3.20 with respect to α yields the following differential sensitivity equation:

$$\begin{aligned} \frac{\partial \dot{x}}{\partial \alpha} &= A\frac{\partial x}{\partial \alpha} + \frac{\partial A}{\partial \alpha}x + B\frac{\partial u}{\partial \alpha} + \frac{\partial B}{\partial \alpha}u \\ \frac{\partial y}{\partial \alpha} &= C\frac{\partial x}{\partial \alpha} + \frac{\partial C}{\partial \alpha}x\,. \end{aligned} \tag{3.21}$$

Combining Equations 3.20 and 3.21 yields the following system:

$$\begin{aligned} \begin{bmatrix} \dot{x} \\ \frac{\partial \dot{x}}{\partial \alpha} \end{bmatrix} &= \begin{bmatrix} A & 0 \\ \frac{\partial A}{\partial \alpha} & A \end{bmatrix} \begin{bmatrix} x \\ \frac{\partial x}{\partial \alpha} \end{bmatrix} + \begin{bmatrix} B \\ \frac{\partial B}{\partial \alpha} \end{bmatrix} u + \begin{bmatrix} 0 \\ B \end{bmatrix} \frac{\partial u}{\partial \alpha} \\ \begin{bmatrix} y \\ \frac{\partial y}{\partial \alpha} \end{bmatrix} &= \begin{bmatrix} C & 0 \\ \frac{\partial C}{\partial \alpha} & C \end{bmatrix} \begin{bmatrix} x \\ \frac{\partial x}{\partial \alpha} \end{bmatrix}, \end{aligned} \tag{3.22}$$

where $\frac{\partial x}{\partial \alpha}$ is known as the sensitivity states of the system. This shows the structure of the sensitivity system. A summary of the derivation for TSO follows.

Beginning with the standard system, Equation 3.1, with n_α uncertain parameters, the following assumptions are made in Ref. [6]:

$$D_{zw} = 0\,,\ D_{yu} = 0\,, \tag{3.23}$$

$$C_z D_{zu}^T = 0\,,\ B_w D_{yw}^T = 0\,, \tag{3.24}$$

$$\frac{\partial D_{zu}}{\partial \alpha} = 0\,,\ \text{and}\ \frac{\partial D_{yw}}{\partial \alpha} = 0\,. \tag{3.25}$$

Equation 3.23 implies that there is no feedthrough between the performance and disturbance or input and output of the system. Equation 3.24 implies that there is no cross weighting between performance outputs and controls in the cost functional and that the sensor and process noises are uncorrelated. Also implied by Equations 3.24 and 3.25 is that the sensor noise and control weighting are known and determined by the designer and thus do not vary with the uncertain parameter.

Next, write the dynamics of the n^{th} order compensator in the form

$$\begin{aligned} \dot{x_c} &= (\underline{A} - \underline{B_u}F - H\underline{C_y})x_c + Hy \\ u &= Fx_c\,, \end{aligned} \tag{3.26}$$

where $\underline{(\cdot)}$ indicates that the compensator is determined from the nominal values for the uncertain matrices. With the assumption that at the optimum, $\frac{\partial F}{\partial \alpha} = 0$ and $\frac{\partial H}{\partial \alpha} = 0$, the gradient of the compensator matrices is zero. Therefore, to first order, the compensator is not a function of the uncertain parameters.

Next the closed loop system is formed as in Equation 3.17, and the sensitivity states of the closed loop system are augmented to form

$$\begin{aligned} \begin{bmatrix} \dot{\tilde{x}} \\ \frac{\partial \dot{\tilde{x}}}{\partial \alpha} \end{bmatrix} &= \begin{bmatrix} \tilde{A} & 0 \\ \frac{\partial \tilde{A}}{\partial \alpha} & \tilde{A} \end{bmatrix} \begin{bmatrix} \tilde{x} \\ \frac{\partial \tilde{x}}{\partial \alpha} \end{bmatrix} + \begin{bmatrix} \tilde{B} \\ \frac{\partial \tilde{B}}{\partial \alpha} \end{bmatrix} w \\ \begin{bmatrix} \tilde{z} \\ \frac{\partial \tilde{z}}{\partial \alpha} \end{bmatrix} &= \begin{bmatrix} \tilde{C} & 0 \\ \frac{\partial \tilde{C}}{\partial \alpha} & \tilde{C} \end{bmatrix} \begin{bmatrix} \tilde{x} \\ \frac{\partial \tilde{x}}{\partial \alpha} \end{bmatrix}, \end{aligned} \tag{3.27}$$

or

$$\begin{aligned} \dot{\bar{x}} &= \bar{A}\bar{x} + \bar{B}w \\ \bar{z} &= \bar{C}\bar{x}\,, \end{aligned} \tag{3.28}$$

where

$$\begin{aligned} \frac{\partial \tilde{A}}{\partial \alpha} &= \begin{bmatrix} \frac{\partial A}{\partial \alpha} & \frac{\partial B_u}{\partial \alpha}F \\ H\frac{\partial C_y}{\partial \alpha} & 0 \end{bmatrix} \\ \frac{\partial \tilde{B}}{\partial \alpha} &= \begin{bmatrix} \frac{\partial B_w}{\partial \alpha} \\ 0 \end{bmatrix} \\ \frac{\partial \tilde{C}}{\partial \alpha} &= \begin{bmatrix} \frac{\partial C_z}{\partial \alpha} & 0 \end{bmatrix}. \end{aligned} \tag{3.29}$$

Note that as with LQG it is assumed that the disturbance inputs are Gaussian white noise processes. It is also assumed that these disturbances processes are independent of the parameter uncertainty so that $\frac{\partial w}{\partial \alpha} = 0$.

A new cost functional is then introduced. The cost functional in Equation 3.8 is modified so that

$$J = \lim_{T\to\infty} \frac{1}{T} \mathsf{E}\left\{ \int_0^T z^T R_{zz} z + \sum_{i=1}^{n_\alpha} \beta_i \frac{\partial z}{\partial \alpha_i}^T R_{zz} \frac{\partial z}{\partial \alpha_i} \, \mathrm{dt} \right\}, \tag{3.30}$$

with $\beta_i \geq 0$ and R_{zz} as in Equation 3.15. The TSO cost functional thus includes a penalty on the performance (output and control) and the performance sensitivities. This cost functional can be rewritten as

$$J = \mathrm{tr}\left\{ \bar{Q} \bar{C}^T \bar{C} \right\} \tag{3.31}$$

where R_{zz} and β_i have been incorporated by scaling the rows of the $\bar{C}$ matrix. The matrix $\bar{Q}$ is the solution of the following Lyapunov equation:

$$0 = \bar{A}\bar{Q} + \bar{Q}\bar{A}^T + \bar{B}\bar{B}^T . \tag{3.32}$$

Appending this Lyapunov equation to the cost functional using a matrix Lagrange multiplier and differentiating with respect to the free parameters yields a second Lyapunov equation in the Lagrange multiplier and an expression for the compensator gains F and H in terms of the two Lyapunov solutions. However, the solutions of the Lyapunov equations depend upon F and H. Therefore the solution is iterative.

At each iterative step two $2n(n_\alpha + 1)\times 2n(n_\alpha + 1)^{th}$ order Lyapunov equations must be solved, where n is the number of states in the nominal plant. Because of the lower triangular structure of $\bar{A}$, this can be reduced to $2n_\alpha^2 + 5n_\alpha + 3$ $n\times n$ Lyapunov equations. For five uncertainties, this would require 78 $n\times n$ Lyapunov equations at each iteration.

3.2.2 Sensitivity Weighted LQG (SWLQG)

Sensitivity Weighted LQG (SWLQG) is very similar to TSO. It aims to increase the robustness to parametric variation of a controller by minimizing a cost which is sensitive to the parametric variation. Some simplifying assumptions are made which eliminate the need for iteration, resulting in a two Riccati equation solution similar to LQG.

SWLQG uses a cost functional similar to that used in TSO (Equation 3.30). The LQG cost function (Equation 3.4) is augmented with a quadratic term involving the sensitivity states. In this way the cost is sensitized to variations in the parameters represented by these states. Note that cross weighting terms may also be included, but have been left out for simplicity. The new cost is :

$$J = \lim_{T\to\infty} \frac{1}{T} \mathbb{E} \left\{ \int_0^T x^T R_{xx} x + \frac{\partial x}{\partial \alpha}^T R_{\alpha\alpha} \frac{\partial x}{\partial \alpha} + 2x^T R_{xu} u + u^T R_{uu} u \; \mathrm{d}t \right\} . \tag{3.33}$$

where in addition to the previous constraints, $R_{\alpha\alpha} \geq 0$.

The presence of the $\frac{\partial u}{\partial \alpha}$ term in Equation 3.22 implies that the control signals are a function of the uncertain parameter. In TSO, $u = Fx_c$. Therefore with the assumption that $\frac{\partial F}{\partial \alpha} = 0$, $\frac{\partial u}{\partial \alpha} = F\frac{\partial x_c}{\partial \alpha}$. This expression results in the coupling of the Lyapunov equations in TSO which forces an iterative solution. To prevent the coupling, so that iteration is not necessary, it is assumed that this term is small, and it is dropped.

The presence of sensitivity states in TSO results in a system n_α times larger than the original system. This state inflation significantly increases the computational burden as will be shown in Section 3.4. In an effort to keep the number of states of the system equal to the number of states in the original plant, a second approximation is made. It is assumed that

$$\frac{\partial \dot{x}}{\partial \alpha} \approx 0 . \tag{3.34}$$

This is the same assumption that is made when eliminating high frequency dynamics, or dynamics with low observability or controllability from the system.

Using these two assumptions, it is possible to write the sensitivity states as a linear combination of the original states of the system and the control. From Equations 3.21 and 3.34,

$$0 = A\frac{\partial x}{\partial \alpha} + \frac{\partial A}{\partial \alpha} x + \frac{\partial B}{\partial \alpha} u \tag{3.35}$$

or

$$\frac{\partial x}{\partial \alpha} = -A^{-1} \left(\frac{\partial A}{\partial \alpha} x + \frac{\partial B}{\partial \alpha} u \right) . \tag{3.36}$$

Substituting Equation 3.36 into Equation 3.33 yields the following new cost functional which depends only upon the control and the original states of the system,

$$J = \lim_{T\to\infty} \frac{1}{T} \mathbb{E} \left\{ \int_0^T x^T (R_{xx} + \frac{\partial A^T}{\partial \alpha} A^{-T} R_{\alpha\alpha} A^{-1} \frac{\partial A}{\partial \alpha}) x \right.$$
$$+ 2x^T (R_{xu} + \frac{\partial A^T}{\partial \alpha} A^{-T} R_{\alpha\alpha} A^{-1} \frac{\partial B}{\partial \alpha}) u \qquad (3.37)$$
$$\left. + u^T (R_{uu} + \frac{\partial B^T}{\partial \alpha} A^{-T} R_{\alpha\alpha} A^{-1} \frac{\partial B}{\partial \alpha}) u \ \mathrm{d}t \right\} .$$

This can be rewritten as

$$J = \lim_{T\to\infty} \frac{1}{T} \mathbb{E} \left\{ \int_0^T x^T R'_{xx} x + 2x^T R'_{xu} u + u^T R'_{uu} u \ \mathrm{d}t \right\} , \qquad (3.38)$$

where

$$R'_{xx} = R_{xx} + \frac{\partial A^T}{\partial \alpha} A^{-T} R_{\alpha\alpha} A^{-1} \frac{\partial A}{\partial \alpha} \qquad (3.39)$$

$$R'_{xu} = R_{xu} + \frac{\partial A^T}{\partial \alpha} A^{-T} R_{\alpha\alpha} A^{-1} \frac{\partial B}{\partial \alpha} \qquad (3.40)$$

$$R'_{uu} = R_{uu} + \frac{\partial B^T}{\partial \alpha} A^{-T} R_{\alpha\alpha} A^{-1} \frac{\partial B}{\partial \alpha} , \qquad (3.41)$$

which is of the same form as Equation 3.4.

To this point in the derivation, sensitivity weighting has only affected the regulator portion of the problem. This derivation is due to Sesak [7] with the objective of increasing parameter robustness in the LQR problem. Two possibilities exist for completing the problem with dynamic compensation. The first is simply to estimate the states using a Kalman Filter; solving Equations 3.12 and 3.14 as is done in the LQG problem. The second method is to apply the dual of the above sensitivity weighting to the Kalman Filter. In this case, the noise intensity matrices from Equations 3.6 and 3.14 will be the dual of weighting matrices in Equations 3.39, 3.40, and 3.41:

$$V'_{xx} = V_{xx} + \frac{\partial A}{\partial \alpha} A^{-1} V_{\alpha\alpha} A^{-T} \frac{\partial A^T}{\partial \alpha} \qquad (3.42)$$

$$V'_{xy} = V_{xy} + \frac{\partial A}{\partial \alpha} A^{-1} V_{\alpha\alpha} A^{-T} \frac{\partial C^T}{\partial \alpha} \qquad (3.43)$$

$$V'_{yy} = V_{yy} + \frac{\partial C}{\partial \alpha} A^{-1} V_{\alpha\alpha} A^{-T} \frac{\partial C^T}{\partial \alpha} , \qquad (3.44)$$

with $V_{\alpha\alpha} \geq 0$. The additional noise can be interpreted as a white noise disturbance entering through the uncertainty.

Combining this Kalman Filter with augmented noise and the sensitivity weighting on the cost produces Sensitivity Weighted LQG (SWLQG). Equations 3.39–3.44 show that SWLQG is simply LQG with a method by selecting the weighting matrices for increased robustness. It can be used as an $\mathcal{H}_2$ suboptimal control algorithm by selecting R_{xx}, R_{xu} and R_{uu} as in Equation 3.7 and then applying Equations 3.39–3.44.

Input and Output Matrix uncertainty in SISO and MIMO systems

Note that for SISO problems, R'_{uu} and R_{uu} in Equation 3.41 are scalar variables. Therefore the effect of an uncertainty in the B (input) matrix of the system simply results in a larger control weight, R_{uu}. Similarly, a C (output) matrix uncertainty results in large sensor noise intensity, V_{yy}.

For MIMO problems, this is not necessarily the case. Since R_{uu} and V_{yy} are matrices, B or C matrix uncertainty does not result in an overall increase in control cost or sensor noise intensity. Rather, a B matrix uncertainty results in a increased control weight in a certain direction, *i.e.* particular combination of input channels. Similarly, C matrix uncertainty will lead to a preferential direction for estimation.

Multiple Uncertainties

This derivation can be modified for systems with multiple uncertainties. For each uncertainty, an n-state model requires n sensitivity states. Each set of sensitivity states is coupled only to the original states of the system. For multiple uncertainties, with the assumption that $\frac{\partial u}{\partial \alpha} \approx 0$, Equation 3.22 becomes

$$
\begin{bmatrix} \dot{x} \\ \frac{\partial \dot{x}}{\partial \alpha_1} \\ \vdots \\ \frac{\partial \dot{x}}{\partial \alpha_i} \\ \vdots \\ \frac{\partial \dot{x}}{\partial \alpha_n} \end{bmatrix} = \begin{bmatrix} A & 0 & \cdots & 0 \\ \frac{\partial A}{\partial \alpha_1} & A & & \\ \vdots & & \ddots & 0 \\ \frac{\partial A}{\partial \alpha_i} & & A & \\ \vdots & 0 & & \ddots \\ \frac{\partial A}{\partial \alpha_n} & & & A \end{bmatrix} \begin{bmatrix} x \\ \frac{\partial x}{\partial \alpha_1} \\ \vdots \\ \frac{\partial x}{\partial \alpha_i} \\ \vdots \\ \frac{\partial x}{\partial \alpha_n} \end{bmatrix} + \begin{bmatrix} B \\ \frac{\partial B}{\partial \alpha_1} \\ \vdots \\ \frac{\partial B}{\partial \alpha_i} \\ \vdots \\ \frac{\partial B}{\partial \alpha_n} \end{bmatrix} u
$$

$$
\begin{bmatrix} y \\ \frac{\partial y}{\partial \alpha_1} \\ \vdots \\ \frac{\partial y}{\partial \alpha_i} \\ \vdots \\ \frac{\partial y}{\partial \alpha_n} \end{bmatrix} = \begin{bmatrix} C & 0 & \cdots & 0 \\ \frac{\partial C}{\partial \alpha_1} & C & & \\ \vdots & & \ddots & 0 \\ \frac{\partial C}{\partial \alpha_i} & & C & \\ \vdots & 0 & & \ddots \\ \frac{\partial C}{\partial \alpha_n} & & & C \end{bmatrix} \begin{bmatrix} x \\ \frac{\partial x}{\partial \alpha_1} \\ \vdots \\ \frac{\partial x}{\partial \alpha_i} \\ \vdots \\ \frac{\partial x}{\partial \alpha_n} \end{bmatrix}. \tag{3.45}
$$

This equation shows that each set of sensitivity states can be reduced from the system independently of the others. Therefore, Equation 3.36 applies to each set. Again the cost functional can be altered to include a penalty on each uncertainty, in which case the cost is now expressed as

$$
J = \lim_{T \to \infty} \frac{1}{T} \mathbb{E} \left\{ \int_0^T x^T R_{xx} x + \sum_{i=1}^{n_\alpha} \frac{\partial x}{\partial \alpha_i}^T R_{\alpha\alpha_i} \frac{\partial x}{\partial \alpha_i} + 2x^T R_{xu} u + u^T R_{uu} u \, \mathrm{d}t \right\}. \tag{3.46}
$$

This in turn permits Equations 3.39–3.44, to be restated as

$$
\begin{aligned}
R'_{xx} &= R_{xx} + \sum_{i=1}^{n_\alpha} \frac{\partial A}{\partial \alpha_i}^T A^{-T} R_{\alpha\alpha_i} A^{-1} \frac{\partial A}{\partial \alpha_i} \\
R'_{xu} &= R_{xu} + \sum_{i=1}^{n_\alpha} \frac{\partial A}{\partial \alpha_i}^T A^{-T} R_{\alpha\alpha_i} A^{-1} \frac{\partial B}{\partial \alpha_i} \\
R'_{uu} &= R_{uu} + \sum_{i=1}^{n_\alpha} \frac{\partial B}{\partial \alpha_i}^T A^{-T} R_{\alpha\alpha_i} A^{-1} \frac{\partial B}{\partial \alpha_i} \\
V'_{xx} &= V_{xx} + \sum_{i=1}^{n_\alpha} \frac{\partial A}{\partial \alpha_i} A^{-1} V_{\alpha\alpha_i} A^{-T} \frac{\partial A}{\partial \alpha_i}^T \\
V'_{xy} &= V_{xy} + \sum_{i=1}^{n_\alpha} \frac{\partial A}{\partial \alpha_i} A^{-1} V_{\alpha\alpha_i} A^{-T} \frac{\partial C}{\partial \alpha_i}^T \\
V'_{yy} &= V_{yy} + \sum_{i=1}^{n_\alpha} \frac{\partial C}{\partial \alpha_i} A^{-1} V_{\alpha\alpha_i} A^{-T} \frac{\partial C}{\partial \alpha_i}^T .
\end{aligned} \tag{3.47}
$$

This shows that the net effect of multiple uncertainties is simply the sum of the individual effects. Thus, multiple uncertainties do not require any special treatment, and single uncertainties can be used for notational simplicity.

SWLQG with Frequency Uncertainty

Some simplification occurs if the uncertainty set is restricted to include only modal frequencies. In complex diagonal form, the system equation for a single degree of freedom oscillator with one input and one output is the following:

$$\begin{aligned} \dot{x}_{cd} &= \begin{bmatrix} -\zeta\omega + j\omega\sqrt{1-\zeta^2} & 0 \\ 0 & -\zeta\omega - j\omega\sqrt{1-\zeta^2} \end{bmatrix} x_{cd} + \begin{bmatrix} 1 \\ 1 \end{bmatrix} u \\ y &= \begin{bmatrix} c & \bar{c} \end{bmatrix} x_{cd}\,, \end{aligned} \tag{3.48}$$

where $\overline{(\cdot)}$ denotes complex conjugate, $(\cdot)_{cd}$ denotes the complex diagonal form, and c is the complex residue. The residues are determined from the mode shapes, therefore in the complex diagonal form, the B and C matrices are independent of the modal frequency.

The complex diagonal form may be transformed to the real modal form, denoted $(\cdot)_{rm}$, through the following transformation

$$x_{cd} = \begin{bmatrix} 1 & -j \\ 1 & j \end{bmatrix} x_{rm} = T x_{rm}\,. \tag{3.49}$$

Applying the similarity transformation, the system dynamics can be expressed in real modal form as

$$\begin{aligned} \dot{x}_{rm} &= T^{-1} A_{cd} T x_{rm} + T^{-1} B_{cd} \\ y &= C_{cd} T x_{rm}\,. \end{aligned} \tag{3.50}$$

Since neither B_{cd}, C_{cd}, nor T is a function of ω, only A_{rm} is a function of frequency:

$$A_{rm} = T^{-1} A_{cd} T = \begin{bmatrix} -\zeta\omega & \omega\sqrt{1-\zeta^2} \\ -\omega\sqrt{1-\zeta^2} & -\zeta\omega \end{bmatrix}. \tag{3.51}$$

After dropping the $(\cdot)_{rm}$ subscript, the frequency sensitivities of the real modal form are

$$\frac{\partial B}{\partial \omega} = 0\,,\ \frac{\partial C}{\partial \omega} = 0 \text{ and } \frac{\partial A}{\partial \omega} = \begin{bmatrix} -\zeta & \sqrt{1-\zeta^2} \\ -\sqrt{1-\zeta^2} & -\zeta \end{bmatrix}. \tag{3.52}$$

Therefore, only the R'_{xx} and V'_{xx} terms in Equations 3.39-3.44 are affected by the frequency uncertainty. Note that

$$A^{-1} = \frac{1}{\omega}\begin{bmatrix} -\zeta & -\sqrt{1-\zeta^2} \\ \sqrt{1-\zeta^2} & -\zeta \end{bmatrix}. \tag{3.53}$$

Therefore,

$$A^{-1}\frac{\partial A}{\partial \omega} = \begin{bmatrix} \frac{1}{\omega} & 0 \\ 0 & \frac{1}{\omega} \end{bmatrix} = \frac{1}{\omega} I_2\,, \tag{3.54}$$

where I_n denotes the $n \times n$ identity matrix.

For multimode systems, a frequency uncertainty in the i^{th} mode of the system yields,

$$\frac{\partial A}{\partial \omega_i} = \begin{bmatrix} 0 & \cdots & & & 0 \\ & \ddots & & & \\ & & -\zeta_i & \sqrt{1-\zeta_i^2} & \\ & & -\sqrt{1-\zeta_i^2} & -\zeta_i & \\ & & & & \ddots \\ 0 & & \cdots & & 0 \end{bmatrix}, \tag{3.55}$$

so that

$$A^{-1}\frac{\partial A}{\partial \omega_i} = \frac{1}{\omega_i}\begin{bmatrix} 0 & \cdots & 0 \\ & \ddots & \\ & I_2 & \\ & & \ddots \\ 0 & \cdots & 0 \end{bmatrix}. \tag{3.56}$$

Substituting into Equations 3.39 and 3.42 yields,

$$R'_{xx} = R_{xx} + \frac{1}{\omega_i^2} \begin{bmatrix} 0 & \cdots & 0 \\ & \ddots & \\ & R^i_{\alpha\alpha} & \\ & & \ddots \\ 0 & \cdots & 0 \end{bmatrix} \tag{3.57}$$

$$V'_{xx} = V_{xx} + \frac{1}{\omega_i^2} \begin{bmatrix} 0 & \cdots & 0 \\ & \ddots & \\ & V^i_{\alpha\alpha} & \\ & & \ddots \\ 0 & \cdots & 0 \end{bmatrix}, \tag{3.58}$$

where $(\cdot)^i$ denotes the i^{th} 2x2 subblock of the matrix.

To complete the derivation, one final assumption is made. In order to penalize the uncertainty as it affects the performance variables, the uncertainty weighting matrices are selected as $R_{\alpha\alpha} = \beta R_{xx}$ and $V_{\alpha\alpha} = \beta V_{xx}$, where β is now a single parameter which acts to increase the penalty on uncertainty and, hence, the robustness of the compensator.

3.2.3 Parameter Robust LQG

Parameter Robust LQG (PRLQG) [3, 1] is an extension of the LQG/LTR method for parameter robustness. Recall that with the LQG/LTR technique, the frequency domain properties of either the Kalman Filter or the Linear Quadratic Regulator are recovered asymptotically for minimum phase systems. However, the gain and phase margin guarantees associated with LQR and KF are usually insufficient to achieve robustness to parameter uncertainty.

The derivation of PRLQG begins with the introduction of an *internal feedback loop* (IFL) representation of the uncertainty. Consider the special case of A matrix uncertainty (It is shown in Ref.[3] that B and C matrix uncertainty can be brought

into the A matrix and treated in this fashion as well.),

$$A = A_0 + \triangle A \qquad\qquad \triangle A = B_0 \delta C_0 \,. \tag{3.59}$$

This is termed IFL because it is equivalent to a system with dynamics represented by A_0, B_0, and C_0 with a static output feedback gain of δ.

If in Equation 3.13, $R_{xu} = 0$, $R_{xx} = L^T L$ and $C_0 = XL$, where X is any correctly dimensioned matrix, and the system is minimum phase, then as the control cost (R_{uu}) approaches zero, the Kalman Filter asymptotically achieves robustness to any parameter represented by Equation 3.59. Similarly if in Equation 3.14, $V_{xy} = 0$, $V_{xx} = LL^T$ and $B_0 = LX$, and the system is minimum phase, then as the sensor noise,V_{yy} approaches zero, the LQR asymptotically achieves robustness to any parameter represented by Equation 3.59. However, if $\text{rank}\{B_0\} > \text{rank}\{C\} = \text{rank}\{L\}$, then a suitable X cannot be found. This implies that if more uncertainties than sensors exist, the asymptotic properties cannot be achieved. The dual also holds for the regulator.

It should be noted, however, that there are no guarantees of parameter robustness with LQR or the Kalman Filter. While both LQR and KF individually tend to be more robust than LQG, no guarantees of stability are provided. Also, asymptotic robustness is achieved at the expense of $\mathcal{H}_2$ performance, since $R_{xx} \neq C_z^T C_z$ and $V_{xx} \neq B_w B_w^T$.

However, in practice, this technique can be used by setting $R_{xx} = C_z^T C_z + \alpha C_0^T C_0$, where α is a weighting on the uncertainty. Again the dual applies to the Kalman Filter by setting $V_{xx} = B_w B_w^T + \alpha B_0 B_0^T$. In this case, the rank condition on B_0 and C_0 is no longer relevant since the Internal Feedback Loop is simply used as a weighting for LQR and the Kalman Filter. In this form, PRLQG is the same as the robust LQG presented by Blelloch and Mingori[25].

Frequency Uncertainty

It can be shown that PRLQG is closely related to SWLQG. Both accomplish robustness by adding to the state weighting and process noise matrices of LQG. For frequency uncertainty, consider the following single degree of freedom system in sec-

ond order canonical form.

$$\dot{x} = \begin{bmatrix} 0 & 1 \\ -\omega^2 & -2\zeta\omega \end{bmatrix} x \,. \tag{3.60}$$

For frequency uncertainty in a lightly damped system, consider only the ω^2 term uncertain. Then using the internal feedback loop representation for the uncertainty, $B_0 = [0\ 1]^T$ and $C_0 = [1\ 0]$. For comparison with SWLQG, convert these to the real modal form using the transformation

$$T = \begin{bmatrix} 1 & 0 \\ -\zeta\omega & \omega\sqrt{1-\zeta^2} \end{bmatrix} . \tag{3.61}$$

then

$$C_{0_{\rm rm}}^T C_{0_{\rm rm}} = \begin{bmatrix} 1 & -\zeta\omega \\ -\zeta\omega & \zeta^2\omega^2 \end{bmatrix} \tag{3.62}$$

$$B_{0_{\rm rm}} B_{0_{\rm rm}}^T = \begin{bmatrix} 0 & 0 \\ 0 & \frac{1}{\omega^2} \end{bmatrix} . \tag{3.63}$$

In the framework of SWLQG, the expressions in Equations 3.62 and 3.63 may be viewed as alternative $R_{\alpha\alpha}$ and $V_{\alpha\alpha}$ matrices.

3.2.4 Maximum Entropy

The Maximum Entropy design technique was developed by Hyland [5, 26] based on a multiplicative white noise model of parametric uncertainty. Solution of the resulting stochastic differential equation in the sense of Stratonovich leads to a modified Lyapunov equation which provides the covariance of the system averaged over the uncertainty. The solution to the modified Lyapunov equation is used in a new cost functional from which the necessary conditions are derived.

As originally conceived, Maximum Entropy included uncertainty in the A, B and C matrices of the system. Recently, however, a more limited set of uncertainty has been permitted based on covariance averaging results[27]. In the new framework, uncertainty is considered only in the damped natural frequency of the modes of a

system, *i.e.*,

$$A = A_0 + \alpha_i A_i \qquad\qquad A_i = \begin{bmatrix} 0 & 1 \\ -1 & 0 \end{bmatrix} \tag{3.64}$$

where A_0, is in the real modal form shown in Equation 3.51.

Consider the following simplified system with multiplicative noise

$$\dot{x} = (A_0 + \sum_{i=1}^{n_\alpha} \alpha_i \sigma_i A_i)x + Bw\,, \tag{3.65}$$

where each σ_i and w is an uncorrelated unit intensity white noise process. Then the steady state covariance, Q, interpreted in the sense of Stratonovich stochastic calculus, is given by the solution of the following modified Lyapunov equation [26],

$$\begin{aligned} 0 &= (A_0 + \frac{1}{2}\sum_{i=1}^{n_\alpha} \alpha_i^2 A_i^2)Q + Q(A_0 + \frac{1}{2}\sum_{i=1}^{n_\alpha} \alpha_i^2 A_i^2)^T + \sum_{i=1}^{n_\alpha} \alpha_i^2 A_i Q A_i^T + BB^T \\ &= A_s Q + Q A_s^T + \sum_{i=1}^{n_\alpha} \alpha_i^2 A_i Q A_i^T + BB^T\,. \end{aligned} \tag{3.66}$$

A new cost functional is then derived based on this modified Lyapunov equation,

$$J = \mathrm{tr}\left\{\tilde{Q}\tilde{C}^T\tilde{C}\right\} \tag{3.67}$$

where $\tilde{(\cdot)}$ denotes the closed loop system defined in Section 3.1.3. Here, $\tilde{Q}$ satisfies Equation 3.66 which can be rewritten as

$$0 = \tilde{A}_s\tilde{Q} + \tilde{Q}\tilde{A}_s^{\ T} + \sum_{i=1}^{n_\alpha} \alpha_i^2 \tilde{A}_i \tilde{Q} \tilde{A}_i^{\ T} + \tilde{B}\tilde{B}^T\,, \tag{3.68}$$

where $\tilde{A}_i = \mathrm{diag}\{A_i, 0\}$.

The modified Lyapunov equation is appended to the cost with a matrix Lagrange multiplier and the gradients with respect to the free parameters are calculated in order to determine the first order necessary conditions. After extensive manipulation[21], these can be stated as a coupled set of the following two Riccati equations and two Lyapunov equations[28]:

$$0 = PA + A^T P + R_{xx} - P_a^T R_{uu}^{-1} P_a + \sum_{i=1}^{n_\alpha} \alpha_i^2 A_i^T (P + \hat{P}) A_i \tag{3.69}$$

$$0 = AQ + QA^T + V_{xx} - Q_a V_{yy}^{-1} Q_a^T + \sum_{i=1}^{n_\alpha} \alpha_i^2 A_i^T (Q + \hat{Q}) A_i \tag{3.70}$$

$$0 = (A_s - Q_a V_{yy}^{-1} C_y)^T \hat{P} + \hat{P}(A_s - Q_a V_{yy}^{-1} C_y) + P_a^T R_{uu}^{-1} P_a \tag{3.71}$$

$$0 = (A_s - B_u R_{uu}^{-1} P_a)\hat{Q} + \hat{Q}(A_s - B_u R_{uu}^{-1} P_a) + Q_a V_{yy}^{-1} Q_a^T \tag{3.72}$$

where

$$P_a = R_{xu}^T + B_u^T P, \qquad Q_a = QC_y^T + V_{xy}\,. \tag{3.73}$$

The solution is then expressed as the compensator with the usual parameters A_c, B_c and C_c given by

$$\begin{aligned} A_c &= A_s - B_u R_{uu}^{-1} P_a - Q_a V_{yy}^{-1} C_y + Q_a V_{yy}^{-1} D_{yu} R_{uu}^{-1} P_a \\ B_c &= Q_a V_{yy}^{-1} \\ C_c &= R_{uu}^{-1} P_a\,. \end{aligned} \tag{3.74}$$

It can easily be seen that when all $\alpha_i = 0$, Equations 3.69 and 3.70 are identical to Equations 3.13 and 3.14, and Equations 3.74 and 3.10 are the same. Thus, as expected, the Maximum Entropy controller with zero uncertainty is identical to the LQG controller.

When first derived, these equations were solved iteratively due to their coupled nature. Recently a new homotopy algorithm has been designed which has significantly improved convergence [28]. Note also that a similar set of equations exists for solving the problem of reduced order design[29]. The Maximum Entropy/Optimal Projection (MEOP) problem will not be considered since compensator order is not an issue in this thesis.

3.3 Methods That Provide Guarantees

In this section, robust control techniques that provide guarantees of stability and/or performance over a set of uncertain plants are presented. These algorithms are typically more complex than desensitizing algorithms and hence, are more computationally intensive. The techniques that will be presented in this section are a multiple model technique, the Bourret approximation to the exact average cost, $\mathcal{H}_\infty$-synthesis, μ-synthesis and Popov control synthesis.

3.3.1 Multiple Model

The multiple model technique is very simple in its conception, but requires a great deal of computational power. The principle is to minimize a weighted average of the $\mathcal{H}_2$ norms of a discrete set of plants[8, 9]. If a solution is found, it is guaranteed to stabilize each of the plants in the set. However, there are no guarantees that the resulting compensator will stabilize the system for plants outside of the set. If, for example, an uncertainty set contains two models in which a single parameter takes on a maximum and minimum value, the system is guaranteed to be stable only for these two values of the parameter. However, if the parameter variation is small, it is likely that the system will be stable for intermediate values of the parameter.

The cost functional for the multiple model technique is a weighted sum of the LQG costs (Equation 3.18) of each individual model

$$J = \sum_{i=1}^{n_{models}} \beta_i \, \mathrm{tr} \left\{ \tilde{Q}_i \tilde{C}_i^T \tilde{C}_i \right\} \tag{3.75}$$

where β_i is a weighting factor, and each Q_i satisfies a Lyapunov equation

$$0 = \tilde{A}_i \tilde{Q}_i + \tilde{Q}_i \tilde{A}_i^T + \tilde{B}_i \tilde{B}_i^T \, . \tag{3.76}$$

There is no known closed form solution [9], therefore numerical optimization must be used. Appending Equation 3.76 to the cost (Equation 3.75) using a set of matrix Lagrange multipliers ($\tilde{P}_i$), the augmented cost functional becomes

$$J_a = \sum_{i=1}^{n_{models}} \beta_i \, \mathrm{tr} \left\{ \tilde{Q}_i \tilde{C}_i^T \tilde{C}_i + \tilde{P}_i (\tilde{A}_i \tilde{Q}_i + \tilde{Q}_i \tilde{A}_i^T + \tilde{B}_i \tilde{B}_i^T) \right\} \, . \tag{3.77}$$

A necessary condition for optimality is that each $\tilde{P}_i$ satisfies an adjoint Lyapunov equation

$$\frac{\partial J_a}{\partial \tilde{Q}_i} = \tilde{P}_i \tilde{A}_i + \tilde{A}_i^T \tilde{P}_i + \tilde{C}_i^T \tilde{C}_i = 0 \, . \tag{3.78}$$

Differentiating the augmented cost with respect to the free parameters (A_c, B_c, C_c) yields the following gradients, which are then used in a quasi-Newton optimization [30]:

$$\frac{\partial J_a}{\partial A_c} = \sum_{i=1}^{n_{models}} \beta_i \, (\tilde{P}_i \tilde{Q}_i)_{22} \tag{3.79}$$

$$\frac{\partial J_a}{\partial B_c} = \sum_{i=1}^{n_{models}} \beta_i (\tilde{P}_{i21} B_{i_w} D_{i_{yw}}^T - \tilde{P}_{i22} B_c D_{i_{yw}} D_{i_{yw}}^T + (\tilde{P}_i \tilde{Q}_i)_{21} C_{i_y}^T + (\tilde{P}_i \tilde{Q}_i)_{22} C_c^T D_{i_{yu}}^T) \quad (3.80)$$

$$\frac{\partial J_a}{\partial C_c} = \sum_{i=1}^{n_{models}} \beta_i (D_{i_{zu}}^T C_{i_z} \tilde{Q}_{i21} + D_{i_{zu}} D_{i_{zu}}^T C_c \tilde{Q}_{i22} + B_{i_u}^T (\tilde{P}_i \tilde{Q}_i)_{21} - D_{i_{yu}}^T B_c^T (\tilde{P}_i \tilde{Q}_i)_{22}) . \quad (3.81)$$

where $(\cdot)_{11}$, $(\cdot)_{12}$, $(\cdot)_{21}$ and $(\cdot)_{22}$ denote the $n_i \times n_i$, $n_i \times n_c$, $n_c \times n_i$ and $n_c \times n_c$ partitions of the respective matrix.

One of the main drawbacks of the multiple model technique is the combinatorial nature of dealing with multiple uncertainties. Since both the convergence time and the iteration time of the algorithm depend upon the number of models used, it is beneficial to restrict the number of models. Using fewer models can cuse uncertainty correlation which to a further approximation of the effects of uncertainty.

3.3.2 Bourret Approximation to the Average Cost

Hagood [10] has suggested using cost averaging techniques for robust control. The cost averaging technique is a formula for robust stability, but not performance, because it considers the average cost over a continuous set of plants in which parameters vary. This technique does not provide a finite upper bound for the worst case cost over the set. The use of cost averaging was motivated by the possibility that bounding the worst case cost over the uncertainty set may result in a higher cost over the remainder of the set than would result from using an average cost. An average cost requires a finite cost over the entire set, which implies stability, but does not place as much emphasis on the worst case model.

In Ref. [10], Hagood compares the exact average with two approximations to the average and two guaranteed cost techniques which overbound the cost over the entire set. The author concluded that the exact average is impossible to calculate for all but the simplest plants thus requiring the use of approximations to the average. The author also concluded that the Bourret approximation to the exact average cost yields the best results, therefore only this method is presented here.

This method is based on an expansion of the averaging operator. For control design purposes the Bourret approximation leads to the following cost functional

$$J = \mathrm{tr}\left\{\tilde{Q_B}\tilde{C}^T\tilde{C}\right\} \tag{3.82}$$

where $\tilde{Q_B}$ is the solution to the following set of coupled Lyapunov equations:

$$0 = \tilde{A}_0\tilde{Q_B} + \tilde{Q_B}\tilde{A}_0{}^T + \tilde{B}\tilde{B}^T + \sum_{i=1}^{n_\alpha}\sigma_i(\tilde{A}_i\tilde{Q}_i + \tilde{Q}_i\tilde{A}_i{}^T) \tag{3.83}$$

$$0 = \tilde{A}_0\tilde{Q}_i + \tilde{Q}_i\tilde{A}_0{}^T + \sigma_i(\tilde{A}_i\tilde{Q_B} + \tilde{Q_B}\tilde{A}_i{}^T), \tag{3.84}$$

with the uncertainty represented by $\tilde{A}(\alpha) = \tilde{A}_0 + \sum_{i=1}^{n_\alpha}\alpha_i\tilde{A}_i$, and σ_i^2 equal to the average of α_i^2.

To solve these equations, a similar approach to the multiple model technique is used. Equations 3.83 and 3.84 are appended to the cost. The augmented cost is then differentiated with respect to the free parameters in the compensator. The resulting gradients are used in a quasi-Newton numerical optimization to yield the desired compensator.

There are two drawbacks to this method. The first is computational intensity. Equations 3.83 and 3.84 must be solved at each step in the gradient search to calculate the optimal Bourret compensator. Since these Lyapunov equations are coupled, they can either be solved iteratively or simultaneously as a single $(n_\alpha + 1)(n + n_c)\times(n_\alpha + 1)(n + n_c)^{\text{th}}$ order Lyapunov equation. Similarly, the dual to these equations must be solved. In Ref.[10] it is suggested that the iterative approach is less computationally intensive.

The second drawback is the fact that the Bourret approximation is only an approximation to the average. Therefore, there is no guarantee of stability. Hagood suggests a test for stability[10], but this can only be applied *a posteriori*. In fact, it can easily be shown that for a single uncertairty the Bourret approximation is identical to the multiple model approach, which implies the same guarantees.

Consider two models to represent a system with uncertainty, each with equal weighting in the cost, $A = A_0 + \alpha A_1$ and $A = A_0 - \alpha A_1$. The multiple model

Lyapunov equations for this system are

$$0 = (A_0 + \alpha A_1)Q_1 + Q_1(A_0 + \alpha A_1)^T + BB^T \tag{3.85}$$

$$0 = (A_0 - \alpha A_1)Q_2 + Q_2(A_0 - \alpha A_1)^T + BB^T . \tag{3.86}$$

Adding and subtracting Equations 3.85 and 3.86, then dividing by two yields

$$0 = A_0(\frac{Q_1 + Q_2}{2}) + (\frac{Q_1 + Q_2}{2})A_0^T + BB^T + \alpha A_1(\frac{Q_1 - Q_2}{2}) + \alpha(\frac{Q_1 - Q_2}{2})A_1^T \tag{3.87}$$

$$0 = A_0(\frac{Q_1 - Q_2}{2}) + (\frac{Q_1 - Q_2}{2})A_0^T + \alpha A_1(\frac{Q_1 + Q_2}{2}) + \alpha(\frac{Q_1 + Q_2}{2})A_1^T . \tag{3.88}$$

These are identical to Equations 3.83 and 3.84 with $Q_B = \frac{Q_1+Q_2}{2}$ and $Q_i = \frac{Q_1-Q_2}{2}$. This result is also shown in Ref. [27] using a derivation on the basis of covariance averaging.

3.3.3 $\mathcal{H}_\infty$ Synthesis

The principle behind $\mathcal{H}_\infty$ control is the small gain theorem. Consider the system G in feedback with an uncertain system Δ depicted in Figure 3.2. The small gain theorem [31] states that if

$$\overline{\sigma}(\Delta(j\omega))\overline{\sigma}(G(j\omega)) < 1 \qquad \forall\omega \tag{3.89}$$

then the interconnection of G and Δ is stable. Therefore, $\|G\|_\infty < \gamma$ and $\|\Delta\|_\infty \leq \frac{1}{\gamma}$ is a sufficient condition for stability of the closed-loop system. It also implies that the system G is stable for all perturbations within $\{\Delta : \|\Delta\|_\infty \leq \frac{1}{\gamma}\}$. To use $\mathcal{H}_\infty$ control for systems with parametric uncertainty, a delta block representation for all the uncertainty in the system must be created. Then, the objective is to design an $\mathcal{H}_\infty$ controller which guarantees that the $\mathcal{H}_\infty$ norm of the closed loop system is less than the inverse of the norm of the delta block. The delta block representation can be attained using the internal feedback loop representation of the uncertainty shown in Section 3.2.3. To simplify things, all the uncertainties can be scaled so that each has a delta block with a maximum singular value of unity. Then if a compensator can

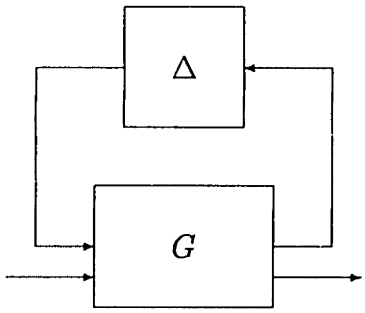

Figure 3.2: Feedback interconnection of system G and uncertain system Δ.

be found which yields a closed loop $\mathcal{H}_\infty$ norm less than unity, stability is guaranteed. Note that performance can also be represented in the delta block, and that an $\mathcal{H}_\infty$ norm less than unity will guarantee robust performance as well when this is the case [12].

Using the standard system, Equation 3.1, depicted in Figure 3.1, the $\mathcal{H}_\infty$ control problem is to minimize $\gamma = \|G_{zw}\|_\infty$. The solution procedure is as follows. Consider the case in which $D_{zw} = 0$, $D_{yu} = 0$, $C_z^T D_{zu} = 0$, $D_{zu}^T D_{zu} = I$, $B_w D_{yw}^T = 0$ and $D_{yw}^T D_{yw} = I$. Under these conditions the compensator $K(A_c, B_c, C_c)$ stabilizes G and guarantees $\|G_{zw}\|_\infty < \gamma$ [11], where

$$A_c = A - (B_u B_u^T - \frac{1}{\gamma^2} B_w B_w^T)X + (I - \frac{1}{\gamma^2} YX)^{-1} Y C_y^T C_y \tag{3.90}$$

$$B_c = -(I - \frac{1}{\gamma^2} YX)^{-1} Y C_y^T \tag{3.91}$$

$$C_c = -B_u^T X \tag{3.92}$$

and

$$0 = XA + A^T X + C_z^T C_z - X(B_u B_u^T - \frac{1}{\gamma^2} B_w B_w^T)X \tag{3.93}$$

$$0 = YA^T + AY + B_w B_w^T - Y(C_y^T C_y - \frac{1}{\gamma^2} C_z^T C_z)Y \tag{3.94}$$

under the conditions that

$$i) \quad X \geq 0 \tag{3.95}$$

$$ii) \quad Y \geq 0 \tag{3.96}$$

$$iii) \quad A - (B_u B_u^T - \frac{1}{\gamma^2} B_w B_w^T) X \text{ is stable} \tag{3.97}$$

$$iv) \quad A - Y(C_y^T C_y - \frac{1}{\gamma^2} C_z^T C_z) \text{ is stable} \tag{3.98}$$

$$v) \quad \rho(YX) < \gamma^2 \tag{3.99}$$

where $\rho(\cdot)$ denotes the spectral radius. If any of these conditions is not satisfied then there is no stabilizing compensator which can guarantee $\|G_{zw}\|_\infty < \gamma$. To find the minimum γ, a simple bisection method is used to solve for the minimum within some tolerance. The general solution in which none of the simplifying assumptions is made can be found in Ref. [32]. It follows a similar pattern, but is much more complex.

The major drawback of $\mathcal{H}_\infty$ control for parameter robustness is in the nature of the small gain theorem. In order to guarantee stability it is necessary to have $\|G_{zw}\|_\infty < 1/\|\Delta\|_\infty$. However, this permits a Δ which is arbitrarily full and complex. When multiple real parameter uncertainties are considered, this is extremely conservative. As a result, it is often not possible to obtain an $\mathcal{H}_\infty$ compensator for which γ is less than unity.

3.3.4 μ-Synthesis

The structured singular value, μ [33], is an extension of the small gain theorem in which information about the structure of the delta block *is* used. The structured singular value was proposed as a measure of stability for uncertainty in which the Δ block is not arbitrarily full. It is defined as follows

$$\mu(G) \triangleq \begin{cases} 0 & \text{if } \det(I - G\Delta) \neq 0 \ \forall \Delta \in \Delta_a \\ \left[\min_{\Delta \in \Delta_a} \{\bar{\sigma}(\Delta) | \det(I - G\Delta) = 0\}\right]^{-1}, \end{cases} \tag{3.100}$$

where Δ_a denotes the set of possible perturbations to the system. The structured singular value, therefore, is the inverse of the smallest perturbation from the set of admissible perturbations, Δ_a, which destabilizes the system.

Unfortunately this is very difficult, if not impossible, to compute for the general case. An upper bound for μ which is a fairly tight upper bound for the case of complex

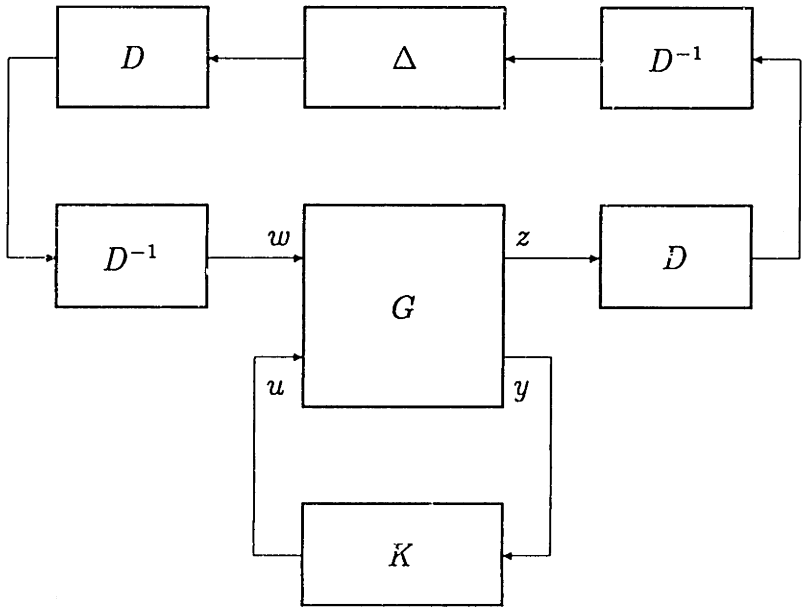

Figure 3.3: System Interconnection with D Scales

uncertainty is

$$\mu(G) \leq \inf_{D} \overline{\sigma}(DGD^{-1}), \tag{3.101}$$

where D is a block-diagonal positive-definite Hermitian matrix which commutes with $\Delta \in \Delta_a$. For the case of independent complex uncertainties, Δ can be represented as $\Delta = \text{diag}\{\Delta_1, \Delta_2, \ldots\}$, where each Δ_i can be scaled such that $\|\Delta_i\|_\infty \leq 1$. $\mu(G)$ is a function of frequency, and therefore the infimum must be obtained at every frequency, which results in a frequency dependent function $D(j\omega)$ called the D-scales. If $\mu(G)$ is less than unity at all frequencies, the system is robustly stable to all uncertainties $\Delta \in \Delta_a$.

The synthesis problem is to design a compensator for which $\mu(G_{cl})$ is less than unity at all frequencies. The most common procedure is the $D - K$ iteration [12]. This is an iterative procedure with two steps at each iteration. The first is an analysis step (D) in which Equation 3.101 is solved. This yields both a value for μ and the D-scales which minimize the right hand side of Equation 3.101. The magnitude of the D-scales is then fit with a set of stable minimum-phase dynamics. The second step is an $\mathcal{H}_\infty$ compensator (K) design for the plant DGD^{-1} shown in Figure 3.3.

Note that since Δ and D commute, $D\Delta D^{-1} = \Delta$. Therefore, the uncertainty is not altered by the scaling. In general, however, G does not commute with D, so it is altered by the addition of the D-scales. Designing an $\mathcal{H}_\infty$compensator for the new system minimizes $\|DGD^{-1}\|_\infty = \bar{\sigma}(DGD^{-1})$, which is the upper bound for μ. The D and K steps are repeated until μ converges or $\mu < 1$ is achieved. Unfortunately, while both the $\mathcal{H}_\infty$ and μ-analysis problems are convex, the D-K iteration is not convex and, therefore, convergence is not guaranteed.

Another drawback of this technique is the need to fit the D-scales at each iteration. Because the D-scales are appended to the system G for $\mathcal{H}_\infty$design, the order of the system can increase dramatically. This increases both the necessary computation and the order of the resulting compensator. The compensator can usually be reduced *a posteriori*, with a re-analysis of μ, but this is not necessarily the case.

Finally, this method is still conservative when dealing with real parametric uncertainty because the Δ block, while no longer arbitrarily full, is still complex. Research into mixed-μ which extends the μ framework to deal with either complex or real uncertainties is on-going. Very recently, Young [34] has devised an upper bound to μ for the case of real or complex uncertainty which requires the addition of a second scaling function (N-scales) for each real uncertainty. The synthesis problem is difficult and results in a vastly increased compensator order.

3.3.5 Popov Control Synthesis

Popov Control Synthesis (PCS) is a technique very recently developed by How [13]. It has been developed from recent research on the Popov stability criterion from *absolute stability theory*. The absolute stability criteria provide sufficient conditions for the stability of a system in feedback with a particular class of sector-bounded, static nonlinear functions. Popov's contribution was to include a stability multiplier, $W(s) = 1 + \gamma s$, in the stability test. The multiplier is selected for a particular class of nonlinear functions, and thus includes phase information in the stability condition. The nonlinear functions considered in absolute stability theory can be associated with the set of parametric uncertainties considered in robust control. How and Hall [35]

have demonstrated that the multiplier is closely related to the N-scales in research on mixed-μ.

Using the concepts of supply rates and storage functions [36] to form parameter dependent Lyapunov functions, a state space version of the Popov stability criterion was developed. Using the internal feedback loop representation for uncertainty shown in Section 3.2.3, parameter uncertainty can be represented in the form $A = A_0 + B_0\delta C_0$. Then for the Popov multiplier $W(s) = H_0 + N_0 s$ with $M_1 \leq \delta \leq M_2$, $H_0 > 0$, $N_0 \geq 0$, $M_2 - M_1 > 0$, and H_0, N_0, M_1, M_2, and δ all diagonal, if there exists a symmetric positive definite P which is the solution of the following Riccati equation

$$0 = \hat{A}^T P + P\hat{A} + C^T C + [H_0 C_0 + N_0 C_0 \hat{A} - B_0^T P]^T R_0^{-1} [H_0 C_0 + N_0 C_0 \hat{A} - B_0^T P] \quad (3.102)$$

where

$$\hat{A} = A_0 - B_0 M_1 C_0 \quad (3.103)$$

$$R_0 = H_0(M_2 - M_1)^{-1} + N_0 C_0 B_0 + [H_0(M_2 - M_1)^{-1} + N_0 C_0 B_0]^T > 0 \,, \quad (3.104)$$

then the system is guaranteed stable for all perturbations δ in the class of nonlinear functions. This class includes linear functions which equate the uncertainty to a range of values between M_1 and M_2.

For control synthesis, it is noted that the cost

$$J = \mathrm{tr}\left\{[\tilde{P} + \tilde{C_0}^T (M_2 - M_1) N_0 \tilde{C_0}] \tilde{B}\tilde{B}^T\right\} \geq \sup_{\Delta\tilde{A}} \mathrm{tr}\left\{\tilde{P}_{\Delta\tilde{A}} \tilde{B}\tilde{B}^T\right\} \quad (3.105)$$

where $\tilde{P}$ solves Equation 3.102 for the closed loop system, and $\tilde{P}_{\Delta\tilde{A}}$ is the solution to

$$0 = (\tilde{A}_0 + \Delta\tilde{A})^T \tilde{P}_{\Delta\tilde{A}} + \tilde{P}_{\Delta\tilde{A}} (\tilde{A}_0 + \Delta\tilde{A}) + \tilde{C}^T \tilde{C} \,. \quad (3.106)$$

Because the cost in Equation 3.105 overbounds the cost, $\mathrm{tr}\left\{\tilde{P}_{\Delta\tilde{A}} \tilde{B}\tilde{B}^T\right\}$, for every $\Delta\tilde{A}$, robust performance is guaranteed.

The compensator is derived by appending the closed loop version of the Riccati equation (Equation 3.102) to the cost J with a matrix Lagrange multiplier and differentiating with respect to the free parameters. Again, a quasi-Newton approach

is used to solve for the minimum cost based on the gradient information which this provides. Note that the multiplier terms, H_0 and N_0, can also be treated as free parameters. In this case, the analysis and synthesis are performed simultaneously. This avoids the problems inherent in the $D - K$ iteration in the μ-synthesis technique.

3.4 Computational Considerations

In order to compare the computational differences in the methods, it is useful to summarize the order and type of equations which must be solved for each technique. The dependence of the computation on the order of the plant and the number of uncertainties will be compared. In addition, note that methods that do not provide guarantees require some iteration in order to choose the appropriate weighting factors on uncertainties, therefore an additional computational burden is imposed by the number of iterations. This information is summarized in Table 3.1. Included in the table is the number of MFLOPS required to solve for a compensator for an 8^{th} order plant. These values were calculated for the system in Chapter 5, and therefore, contain only a reduced set of the control techniques.

For the purpos of this thesis, the computation order dependence will be normalized so that the solution of an n^{th} order Lyapunov equation requires n^3 operations. Note that in this case the solution of an n^{th} order Riccati equation requires $2 \cdot (2n)^3$ or $16n^3$ operations.

The LQG compensator is derived from the solution of two n^{th} order Riccati equations. In Sensitivity Weighted LQG (SWLQG), the state weighting matrices from LQG are augmented with terms that depend on the sensitivity weights, but the computational burden is the same. Finding an acceptable set of weights is usually iterative, however. While the number of uncertainties does not affect the order of the Riccati equations, it may have an affect on the number of iterations which must be performed in order to achieve an acceptable design. The same is true for Parameter Robust LQG (PRLQG). The computation for each iteration is identical to LQG.

The process is iterative, and the number of uncertainties may affect the number of iterations which must be performed in order to achieve an acceptable design.

The Trajectory Sensitivity Optimization (TSO) has a much higher computational burden. The solution process is iterative on two accounts. First, it is a desensitizing method, so that it shares with SWLQG and PRLQG the iterative process of assigning weights to different uncertainties. But at each of these iterations, the solution for the compensator is itself iterative. Using the iteration scheme proposed [6], at each iteration the solution of $(2n_\alpha^2 + 5n_\alpha + 3)$ n^{th} order Lyapunov equations is required. The number of steps in this iteration is not clear and convergence is not guaranteed. A further iteration on weights in the cost functional makes this a very cumbersome and computationally burdensome process.

The Maximum Entropy (ME) approach uses a homotopy method [28] to solve for the optimal robust compensator. For a given set of uncertainty weights and from an LQG initial guess, 30 iterations are typically required to converge to a solution. Each iteration requires the solution of a coupled set of two n^{th} order Lyapunov and two n^{th} order Riccati equations. An efficient method to solve these coupled equations is shown in Appendix F of Ref. [28], but the state dependence is difficult to quantify. It is however at least $O(n^3)$. In this method the number of uncertainties has a very small effect on the computational burden, however, as with SWLQG, no robustness guarantees are available, and an iteration is required to determine the uncertainty weights.

The Multiple Model (MM) technique involves finding the compensator which minimizes a weighted average of the $\mathcal{H}_2$ cost of a set of models. The system is guaranteed to be stable for each model. A Quasi-Newton approach is used to minimize the average cost. At each iteration, two $(2n)^{th}$ order Lyapunov equations must be solved for each model. Typically, 100 iterations yields a good compensator. The choice of models determines the robustness characteristics of the compensator. For a single uncertainty, three models can be used. One is the nominal, the other two have the uncertain parameter evaluated at its largest and smallest possible values. Using this scheme for multiple uncertainties, the number of models increases combinatorially.

Since the uncertainty input for this approach is representative of the actual error models, iteration is generally not required.

The Bourret Approximation technique is considerably more computationally intensive. Based on the same Quasi-Newton approach as the MM technique, the computation suffers from the fact that at each Quasi-Newton step, an iterative solution of $2 \cdot (1 + n_\alpha)$ $(2n)^{th}$ order Lyapunov equations is required. In Ref. [10] it is stated that five iterations was used successfully. It was shown in Section 3.3.2 that for a single uncertainty, the method is equivalent to MM. Thus it is clear that some guarantees accompany this technique. This generally eliminates the need for iteration on the uncertainties. However, the number of uncertainties enter the problem linearly by adding two additional $(2n)^{th}$ order Lyapunov equations assuming that convergence properties do not change.

The (sub)optimal $\mathcal{H}_\infty$ compensator is solved using a bisection method. At each iteration, two n^{th} order Riccati equations are solved to obtain a compensator that guarantees the closed loop $\mathcal{H}_\infty$ norm, γ. In practice, the bisection method stops when the minimum is reached within some tolerance, so the compensator is suboptimal. The number of iterations required to find the (sub)optimal compensator depends upon the termination tolerance. A tolerance of 1% was used throughout this thesis, and the average number of iterations was 15. If the uncertainty is scaled so that it is unit norm, then the system is guaranteed to be stable for perturbations of magnitude $1/\gamma$. However a great deal of iteration on weighting functions is often required in order to achieve an $\mathcal{H}_\infty$ norm of unity which then guarantees stability for the full magnitude of the uncertainty. In fact, it is often not possible to achieve an $\mathcal{H}_\infty$ norm which guarantees to the desired bounds.

Compensators are derived in μ-synthesis using the $D - K$ iteration. In this procedure, an initial compensator, K, is designed using the $\mathcal{H}_\infty$ technique. The structured singular value, μ, is calculated at each frequency point, resulting in a set of D-scales for each uncertainty block. The D-scales are fit with a state space system and appended to the original dynamics. A new K is then obtained by solving for the $\mathcal{H}_\infty$ compensator of the augmented system. At each iteration, the computation is depen-

dent upon the frequency spacing used in the calculation of the structured singular value, and the dimension of the D-scales. Considering only the burden of the K step, at each iteration, two $(n + 2n_D)^{th}$ order Riccati equations must be solved, where n_D is the order of the D-scale fit. For the compensators discussed in this paper, 5–7 $D - K$ iterations were required. If the uncertainty is scaled so that it is unit norm, the system is guaranteed to be stable for perturbations of magnitude $1/\mu$. As with the $\mathcal{H}_\infty$ design process, some iteration of frequency weights is often required. Also, it is often not possible to achieve a value of μ less than unity which would guarantee stability for the desired bounds on uncertainty.

Finally, Popov Controller Synthesis uses a Quasi-Newton approach similar to MM. At each iteration it requires the solution of a $(2n)^{th}$ order Lyapunov equation and a $(2n)^{th}$ order Riccati equation. Guarantees of robustness are provided using this method so that iteration on the uncertainties is not required. The number of uncertainties considered increases the number of free parameters in the Quasi-Newton algorithm, but does not increase the order of the equations to be solved at each iteration. An increase in free parameters may require a greater number of iterations.

Table 3.1 summarizes the dependence of the computational effort required per iteration on the system order and number of uncertainties. In addition, it provides the number of MFLOPS required to solve for a compensator using LQG, SWLQG, ME, MM, $\mathcal{H}_\infty$ and μ-synthesis. Note that the LQG and SWLQG techniques require the least effort. The compensator derived using μ-synthesis required roughly 7000 times the number of FLOPS. This was due to the fact that the D-scales increased the order of the system to 78 from 8. Clearly this state inflation is a serious drawback for systems with multiple uncertainties.

3.5 Selection of Control Techniques for Application

In the Chapter 5, a low order example representative of structural control applications will be studied. Not all of the control design techniques which have been presented will

Table 3.1: Computational dependence of robust control techniques.

Control Technique	state dependence	uncertainty dependence	MFLOPS 8^{th} order
LQG	$4 \cdot (2n)^3$	—	0.933
SWLQG	$4 \cdot (2n)^3$	iterative	0.933
PRLQG	$4 \cdot (2n)^3$	iterative	N/A
TSO	$(2n_\alpha^2 + 5n_\alpha + 3) \cdot n^3$	$O(n_\alpha^2)$ + iterative	N/A
Maximum Entropy	$O((2n)^3)$	iterative	6.380
Multiple Model	$2 \cdot (2n)^3$	$O(2^{n_\alpha})$	98.165
Bourret Approximation	$10 \cdot (1 + n_\alpha) \cdot (2n)^3$	$O(n_\alpha)$	N/A
$\mathcal{H}_\infty$	$4 \cdot (2n)^3$	iteration	23.262
μ-synthesis	$4 \cdot [2(n + 2n_D)]^3$	$O(n_D^3)$	6970.821
PCS	$17 \cdot (2n)^3$	very small	N/A
N/A - Not Available			

be investigated further. LQG designs will be made to compare the results obtained by robust controllers to those obtained when robustness issues are not considered. Of the desensitizing techniques, SWLQG and Maximum Entropy will be addressed. The Multiple Model, $\mathcal{H}_\infty$ and μ-synthesis techniques will be investigated from the techniques which provide guarantees.

Trajectory Sensitivity Optimization will not be addressed. From the derivation in Section 3.2.1, it can be seen that TSO is similar to the SWLQG technique. Fewer approximations in the derivation make it a more rigorous technique, but theoretical rigor is gained at the expense of a feasible method of olution. Because of the computational burden associated with the large number of Lyapunov equations that must be solved at each step in the iterative process, combined with the lack of convergence guarantees, thir technique will not be addressed further.

The PRLQG technique is also similar to SWLQG. It requires the solution of only

two Riccati equations and operates by making additions to the state weighting and process noise matrices from LQG. As seen in Section 3.2.3, it is very closely related to SWLQG for frequency uncertainty, which will be considered throughout this work. For this reason, PRLQG will not be considered further.

The Bourret approximation technique will not be investigated. As shown in Section 3.3.2 the Bourret approximation is closely related to the multiple model technique. In fact, for a system with a single uncertainty, the Bourret approximation is exactly the same as the multiple model technique with equal weighting on two models equally spaced from the nominal. Also, the computational burden of this technique is very large since at each step in the solution process, coupled Lyapunov equations must be solved. For these reasons, the Bourret approximation technique will not be investigated further.

The Popov Control Synthesis technique shows a great deal of promise. However, the solution process is still in its infancy. Because computer algorithms are still in development at this time, it will not be investigated further.

Chapter 4

Analysis Techniques used in Comparison

Having introduced the control synthesis techniques in the preceding chapter, this chapter focuses on analysis techniques that are used in this thesis to aid in the design and comparison of compensators. The first section discusses the basis by which comparison of the control techniques will be made. This is followed by a discussion of the analysis techniques that are used in the comparison of control techniques for the sample problem in Chapter 5. In the last section, the analysis techniques that are used in the design of compensators in the experiments of Chapter 6 are discussed.

4.1 Basis of Comparison

To provide a comparison of robust control techniques, compensators are designed using the control techniques of Chapter 3 for two different systems. The use of different systems allows the comparison to be made using two complementary approaches.

In the first approach, several compensators are designed using each technique at the same level of control authority but with differing amounts of robustness. As the robustness is increased, the closed loop performance tends to decrease and the system bandwith increase. This behavior is noted for all of the robust control techniques. It is then possible to compare the performance decrease and bandwidth increase

for compensators with equivalent robustness properties that were designed using the different techniques. In order to determine the robustness bounds exactly, so that a fair comparison is made, this approach uses the low order sample problem. The parameters in the sample problem are determined ahead of time, and parameter uncertainty can be introduced by varying known parameters. This permits exact calculation of the uncertainty bounds.

In the second approach, compensators are designed at different levels of control authority, using each of the control techniques, to determine the maximum performance that can be achieved by each of the techniques. This complements the study of performance degradation on the above system by showing the consequences of robustness on the best performance than can be achieved. It is difficult to study maximum achievable performance on a sample problem since physical limitations often do not arise. Therefore, control designs on the MACE test article are used for this comparison. However, for an experimental system, the parameter uncertainty is truly uncertain. Therefore, it is not possible to determine robustness bounds exactly. Equivalent robustness characteristics are imposed by the need to stabilize the system in the presence of the modelling errors that were noted in Chapter 2.

A further comparison is made for the control techniques which provide guarantees of robustness. Because robustness is achieved with a degradation in performance and increase in bandwidth, it is desirable to minimize these effects. Therefore the conservatism of a technique which provides guarantees is an important quantity. Conservatism is a measure of how much achieved robustness bounds exceed the guaranteed bounds. This is important because if the achieved robustness level grossly exceeds the guaranteed level, then it is likely that a larger than necessary bandwidth increase and performance degradation has been sustained. Conservatism of this sort would result in reducing the maximum performance that could be achieved using such a technique.

Finally, to gain an understanding of how and why performance degrades and bandwidth increases when robust control techniques are used, the differences between compensators designed for various levels of robustness will be studied. The

differences have been classified into two categories. The *primary* effects of increasing robustness are those changes in the compensator which directly affect its robustness. The effects are most often localized to the frequency region over which the uncertainty has a strong effect (the uncertain region). *Secondary* effects are the changes in the compensator that occur outside of the uncertain region which do not seem to directly affect the robustness. It seems logical that a well designed robust compensator should closely approximate the LQG compensator outside of the uncertain region. This corresponds to a compensator with small secondary effects because outside of the uncertain region, performance is the only design objective. LQG provides the solution to this problem. Thus comparing the primary and secondary effects can provide very useful information regarding the performance sacrifice and bandwidth increases that occur.

In order to measure these effects, the use of certain analysis tools is required. The following section details the analysis techniques that will be used to help illustrate the primary and secondary effects of robustification, as well as, provide performance and bandwidth values so that the techniques may be compared fairly.

4.2 Analysis Techniques for the Sample Problem

It is difficult to compare robust controllers developed using different techniques. A complete investigation must compare the physical attributes of these compensators and how they interact with the uncertain system. This requires the use of a number of analysis techniques which investigate different aspects of the compensator and the closed loop system.

The following is a list of the seven analysis methods used with a description of the information that each provides.

(i) Plotting the frequency response of the compensators.

Comparing the transfer functions of a series of compensators derived using the same technique, but with different amounts of uncertainty, shows the changes that occur in the compensator as robustness is increased. The changes in the

compensator help to illustrate the method by which a robust control technique provides robustness. Also, a comparison of the frequency response of compensators derived using different robust control techniques, but that provide comparable robustness levels, can be used to illustrate some of the key differences between the control formulations.

(ii) Plotting the poles and zeros of the compensators.

Comparing the poles and zeros of different compensators in the complex plane gives a more quantitative measure of some of the differences between compensators than simply comparing the frequency responses. For example, for compensators with near pole-zero cancellations, it is often difficult to determine the damping ratio of the poles and zeros from the frequency response alone. However, the damping ratio and the separation between the poles and zeros is immediately obvious when shown in the complex plane.

(iii) Plotting the loop transfer function.

For the sample problems, all control loops are SISO so that the loop transfer function, $G_{yu}K$, can be studied. This transfer function can be used to determine stability margins for nominal and off-nominal systems. It can also be useful in determining if a compensator is gain stabilizing or phase stabilizing to a particular uncertainty.

(iv) Plotting the complementary sensitivity transfer function.

The complementary sensitivity transfer function, $(I + G_{yu}K)^{-1}G_{yu}K$, provides a measure of the frequency range over which a system tracks input signals. The bandwidth of a compensator is defined [37] as the frequency at which input tracking is reduced by 3 dB from unity. For lightly damped systems this may happen more than once. Therefore, the bandwidth is taken as the highest frequency at which this occurs. Plotting the complementary sensitivity shows the effects of the robust control techniques on the bandwidth of the system.

(v) Plotting state cost as a function of the uncertain parameter.

The $\mathcal{H}_2$ state cost of the closed loop system, or the variance of the performance output caused by a unit intensity disturbance input, is taken as the metric by which the performance of all compensators will be compared. Plotting this metric for the system with different controllers, as a function of the uncertain parameter, gives an indication of performance robustness. That is, it indicates by how much performance degrades for off-nominal values of the uncertain parameter.

(vi) Plotting the performance transfer function.

The performance differences incurred through the use of different levels of uncertainty and different robust control techniques can also readily be seen by observing the closed loop performance transfer function. Rather than giving a single number for performance, this transfer function shows the frequency dependence of the performance which can help to explain performance degradation.

(vii) Plotting nominal state cost as a function of uncertainty bounds.

The uncertainty bounds for a compensator are the largest positive and negative values of the uncertainty for which the system remains stable. Note that all control techniques will be analyzed using a rank two uncertainty form. The bounds are computed using a bisection method to calculate the largest (both positive and negative) gain for which the multivariable Nyquist criterion (refer to Section 4.3) is satisfied for a system with inputs B_0 and outputs C_0. In other words, it is a measure of the largest real perturbation in the delta block for which the system remains stable. Note also that the worst case bound, the smaller in magnitude of the positive and negative bounds, will sometimes be used.

The $\mathcal{H}_2$ state cost calculated on the nominal plant, shown as a function of the uncertainty bounds of a compensator, indicates the degree to which performance is sacrificed to achieve robustness.

Methods (i) and (ii) are used together to give a full quantitative and qualitative indication of the effects on the compensator of increasing robustness. Along with method (iii) these illustrate the method by which each robust technique increases robustness. Methods (iv)–(vii) are used to determine the effects that the changes in the compensator have on the closed loop properties, bandwidth and performance, of the system. Together, these methods are used to determine the key differences between compensators derived using the different control methodologies and the effects that the differences have on the system as a whole. This will allow conclusions to be drawn regarding the effectiveness of each robust control technique.

4.3 Analysis Techniques for the Experiments

For the MACE Experiments in Chapter 6, a different set of analysis techniques is used to aid in the design of compensators. Because modelling errors are present in the nominal experimental system (and not the sample problem) it is important that every compensator be analyzed prior to implementation to check for stability and performance of the closed loop system. The analysis methods in this thesis make use of both the design model and open loop data in order to make predictions of the closed loop behavior. The use of the open loop data has been found to be a reliable method of prediction which increases the rate at which design iterations can take place since it foregoes the experimental testing of intermediate compensator designs.

The analysis techniques can be split into two categories; those which relate to the closed loop stability of the system and those which relate to the closed loop performance. Stability prediction techniques will be discussed first.

Testing the stability of the closed loop system using the design model is very simple. Assuming that state space methods have been used to derive the compensator, then a state space closed loop system can be produced by generating the feedback interconnection of the state space models of the plant and compensator. Then the eigenvalues of the combined system can be calculated to determine stability. Unless a

mistake has been made, the closed loop system is stable since most control techniques guarantee that the nominal closed loop system will be stable.

Since modelling error is always present, it is useful to have tests that can predict the stability on the actual system, not just the model of the system. One such test is the Nyquist Criterion. The Nyquist Criterion is a frequency domain test in which the frequency response of the loop transfer function, $G_{yu}(j\omega)K(j\omega)$, is plotted in the complex plane over the frequency range $-\infty < \omega < \infty$. Note that because the locus of $G_{yu}(-j\omega)K(-j\omega)$ is a reflection about the real axis of $G_{yu}(j\omega)K(j\omega)$ it is sufficient to plot the function over the frequency range $0 < \omega < \infty$. However, care must be taken if the open loop system has poles on the $j\omega$ axis. In such a test, the measured open loop frequency response data can be used in addition to the frequency response of the model [37]. Thus the test can be performed to check for stability of the system based on both the measured open loop data and the model. Then, the test is a good prediction of stability for the actual system and not simply for the model. The net number of clockwise encirclements of the critical point $(-1 + j0)$ is equal to the number of closed loop unstable poles minus the number of open loop unstable poles. Therefore for closed loop stability, the net number of *counter*clockwise encirclements of the critical point must equal the number of unstable poles in the open loop system $G_{yu}(j\omega)K(j\omega)$.

As stated above, this Nyquist Criterion applies only to SISO systems. However, it has been generalized to the multivariable case [38, 39]. The Multivariable Nyquist Criterion for stability states that the net number of *counter*clockwise encirclements of the critical point of the Nyquist function,

$$H_n(j\omega) = -1 + \det(I + G_{yu}(j\omega)K(j\omega)), \tag{4.1}$$

must equal the number of unstable poles in the open loop system $G_{yu}(j\omega)K(j\omega)$. For a SISO system,

$$\det(I + G_{yu}(j\omega)K(j\omega)) = 1 + G_{yu}(j\omega)K(j\omega), \tag{4.2}$$

therefore,

$$H_n(j\omega) = G_{yu}(j\omega)K(j\omega), \tag{4.3}$$

Thus the criteria are equivalent in the SISO case.

Since the locus of the frequency response of a lightly damped mode is a circle in the Nyquist plane, the Nyquist plot tends to have many overlapping circles. It is difficult to distinguish the circles when the full frequency range is plotted on a single graph. In particular, when many overlapping circles are present, the Nyquist plot can be difficult to interpret. A second problem with the Nyquist plot is the range of values for the Nyquist function when high authority control is used. It can be very difficult to distinguish the critical point (which has a magnitude of unity) when the Nyquist function has a magnitude greater than ten.

If instead of being plotted in the complex plane, the Multivariable Nyquist function is plotted log(magnitude) versus phase, then it becomes much easier to distinguish the locus of the function. Phase accumulation tends to reduce the overlap of circles on the plot, and a very large range of magnitudes can be seen without losing track of the critical point. In fact, there is now a multiplicity of critical points located at a magnitude of 1 with phase of $-180 \pm n360$ degrees, $n = 0, 1, \ldots, \infty$. For a SISO system, the Nyquist function plotted in this manner is called a Nichols plot[37]. Therefore for the MIMO system, this plot will be referred to as the Multivariable Nichols plot, or simply the Nichols plot. The Nyquist Criterion for stability must be modified for the Nichols plot because an encirclement of the critical point in the Nyquist plane is not necessarily an encirclement of a critical point in the magnitude-phase plane. In fact, the net number of counterclockwise encirclements of the critical point in the Nyquist plane is equal to the net number of left to right passes over a critical point in the magnitude-phase plane. Therefore, for a stable plant and compensator, if the closed loop system is stable, the locus of the Multivariable Nyquist function must have no net passes over the critical points.

Figure 4.1 [40] shows an example of the Multivariable Nichols plot for a stable MIMO system. Note that both the frequency response of the model and the measured frequency response were used to calculate the Multivariable Nyquist function. It is often useful to compare these two loci for an indication of where errors in the model cause potential stability problems. Notice that the locus of the Nyquist function

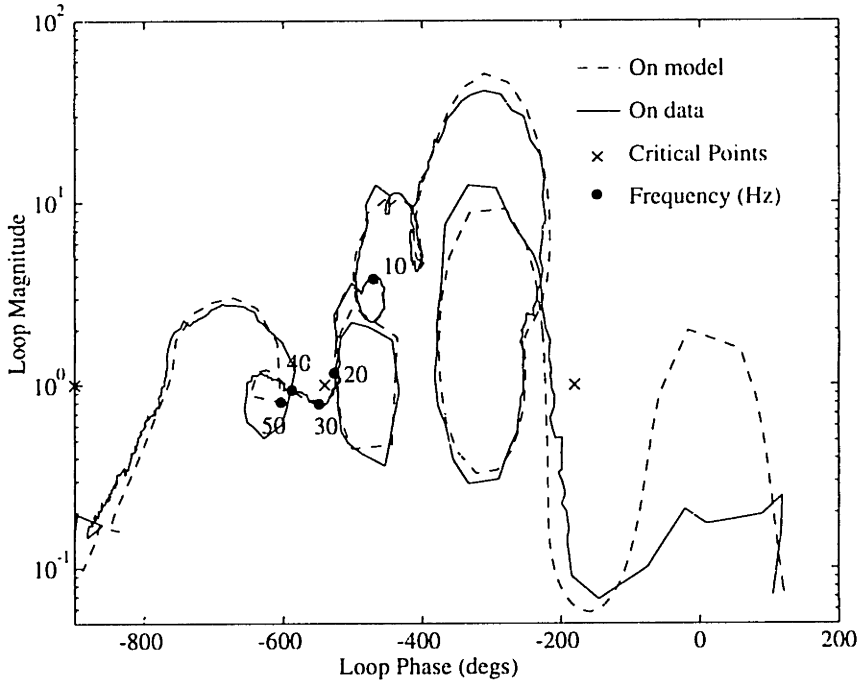

Figure 4.1: Nichols Plot

passes underneath all of the critical points. This indicates that this system is predicted to be stable by both the measured open loop data and the frequency response of the design model.

While the locus of the Nyquist function indicates whether or not the system is stable, in the multivariable case it does not provide any indication of how sensitive the system is to perturbations. This results because of the determinant operator in the Multivariable Nyquist function. The Nyquist criterion tests when $\det(I + G_{yu}(j\omega)K(j\omega)) = 0$. If $I + G_{yu}(j\omega)K(j\omega)$ is singular at some frequency, ω_0, *i.e.* the matrix is rank deficient at ω_0, then $\det(I + G_{yu}(j\omega_0)K(j\omega_0)) = 0$ and the closed-loop system is is on the verge of stability. However, the system can be nearly singular without the determinant being close to zero. Consider the following simple system,

$$X = \begin{bmatrix} \alpha & 0 \\ 0 & \frac{1}{\alpha} \end{bmatrix}. \tag{4.4}$$

Then $\det(X)$=1 for all values of α. However, for large values of α the matrix is nearly singular, since $\underline{\sigma}(X) = 1/\alpha$. A small perturbation $(-1/\alpha)$ to the (2,2) element

of X is sufficient to make the matrix singular. Thus the $\det(I + G_{yu}(j\omega)K(j\omega))$ in the Nyquist function may be large while only a very small perturbation in G_{yu} is necessary to make the determinant equal to zero, and the system unstable.

To provide information on sensitivity of a system, the singular values of the sensitivity transfer function, $(I + G_{yu}(j\omega)K(j\omega))^{-1}$, are calculated. A large maximum singular value at any frequency indicates that the system is very sensitive to perturbations at that frequency. Since the singular values of $I + G_{yu}(j\omega)K(j\omega)$ are the inverse of the singular values of the sensitivity transfer function, inverting $I + G_{yu}(j\omega)K(j\omega)$ is not necessary to determine the sensitivity. Instead, a small minimum singular value of $I + G_{yu}(j\omega)K(j\omega)$ also indicates sensitivity. The minimum singular value is equal to the magnitude of the smallest complex perturbation which will destabilize the system. While this is not of particular interest in itself, a large difference between $\underline{\sigma}(I + G_{yu}(j\omega)K(j\omega))$ calculated using the frequency response of the model, and calculated using the open loop data, can be indicative of modelling errors which make the system very sensitive to possible plant perturbations.

The singular values, however, give no indication of stability itself so they must be used in conjunction with plotting the Nyquist function. As an example, consider the Nichols plot in Figure 4.1 and the plot of the singular values of $I + G_{yu}(j\omega)K(j\omega)$ for the same system shown in Figure 4.2. The Nichols plot predicts that the closed loop system will be stable. When tested experimentally, the closed loop system was unstable, with an instability at approximately 50 Hz. The difference between the Nyquist functions at 50 Hz based on the model and the data indicate that modelling errors do exist at this frequency. However, there is no indication that the error is potentially destabilizing. The Nyquist function in the 20–30 Hz range passes much closer to a critical point than in the 50 Hz region. Figure 4.2 shows that, indeed, the system is sensitive in the 20–30 Hz range, but there is close agreement between the prediction from the model and from the data indicating that modelling error is not a factor in this frequency range. However, at 50 Hz there is a very large difference between the minimum singular values calculated from the model and from the open loop data, indicating that significant modelling error is present. At the same time,

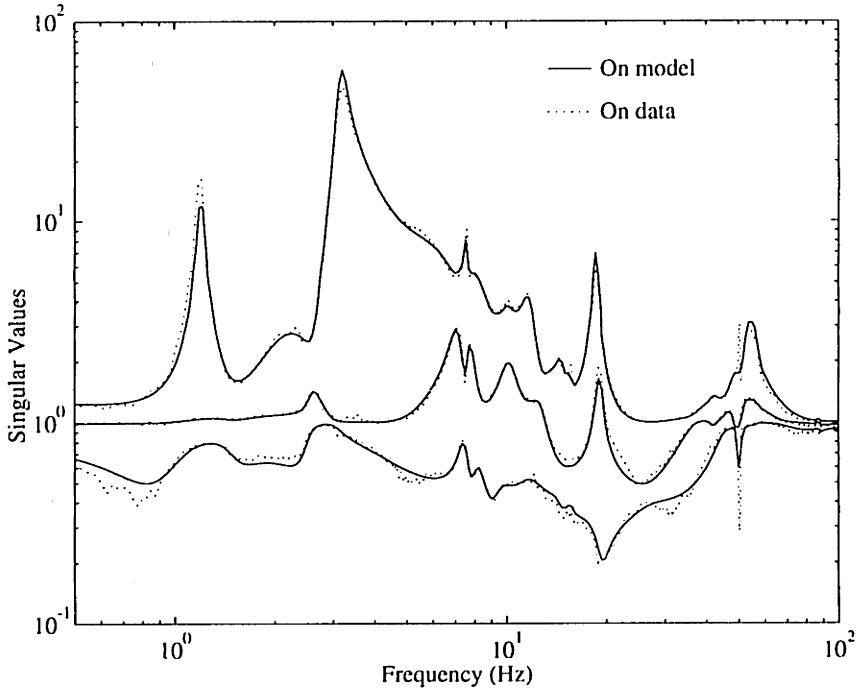

Figure 4.2: Singular value Plot

the singular value plot based on the open loop data indicates that because of the modelling errors, the system is very sensitive at this frequency. Due to a lightly damped pole near this frequency, large perturbations in the frequency response are possible. When experimentally tested, the presence of a perturbation in this pole destabilized the system. Thus, this example shows the utility of plotting the singular values of $I + G_{yu}(j\omega)K(j\omega)$ as well as checking the Nyquist criterion.

The Nichols and singular values plots provide information about the stability and sensitivity of the closed loop system. They do not give any indication of what performance can be expected. This information can be obtained by plotting the state cost as a function of frequency. The state cost can be written as,

$$J_{xx} = \int_{-\infty}^{+\infty} \mathrm{tr}\left\{G_{cl}^{*}(j\omega)R_{zz}G_{cl}(j\omega)\right\} \mathrm{d}\omega, \tag{4.5}$$

where R_{zz} is a matrix which applies a relative weighting to the outputs, and $G_{cl}(s)$ is a frequency domain representation of the closed-loop system. The square root of the integrand of this cost is then plotted versus frequency. With uncorrelated disturbances

of equal intensity, this plot is analogous to the transfer function from the disturbance source to the performance metric in the SISO case. A comparison of open and closed-loop performance using the design model reveals predicted performance and frequency regimes where more control effort might be focused. The same comparison when the frequency response of the compensator is applied to the measured open-loop data provides a prediction of the performance that can be expected during experimental implementation.

Significant deviation between closed loop performance predictions based on the model and open loop data can indicate the presence of modelling error which causes performance degradation. An example of this can be seen in Figures 4.3 and 4.4. The first figure shows the open and closed loop frequency response of a system as predicted by the design model. The second figure shows the same as predicted using the measured open loop data. In the upper right hand corner of each figure is the predicted performance improvement in dB. It can be seen that in the 1–2 Hz range, the 3–4 Hz range, and at 17 Hz that the prediction using the open loop data indicates degraded performance when compared to the model prediction. The degradation in performance indicates that important modelling errors are present in these frequency ranges.

Thus using these three analysis techniques on both the model of the system and measured open loop data provides the control designer a great deal of information about the stability and performance of the system. This information can be used to assist the designer in choosing parameters for control design. For example, it can be used to determine which modes to treat as uncertain in robust control techniques, or which actuator/sensor pairs to emphasize in multivariable control design.

Having discussed the synthesis and analysis techniques that will be used in this thesis. The comparison of robust control techniques begins in the following chapter with the study of a low order sample problem.

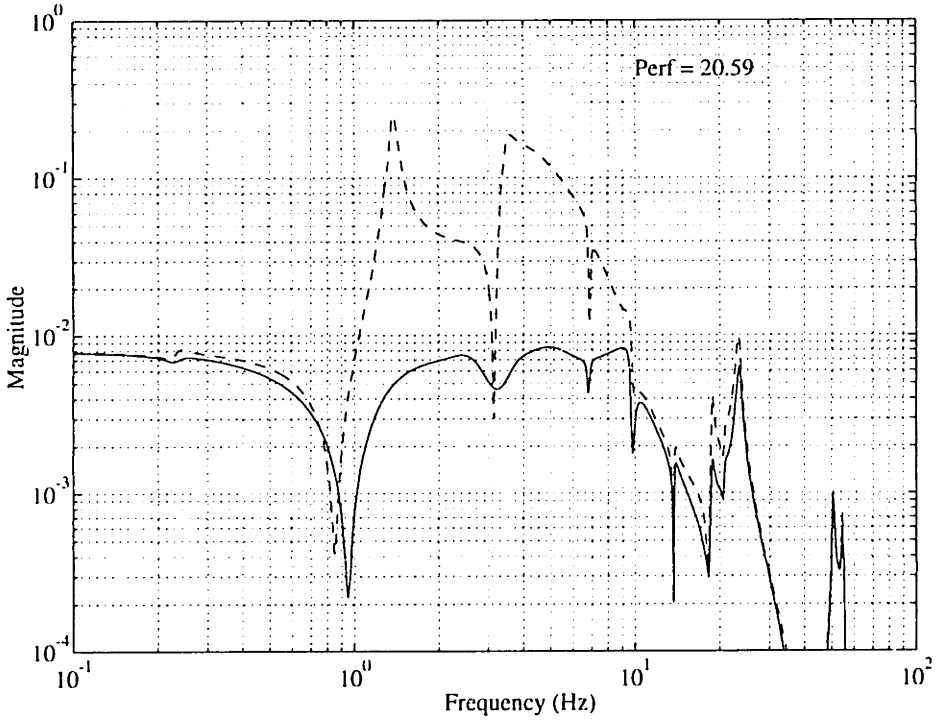

Figure 4.3: Prediction of performance using model.

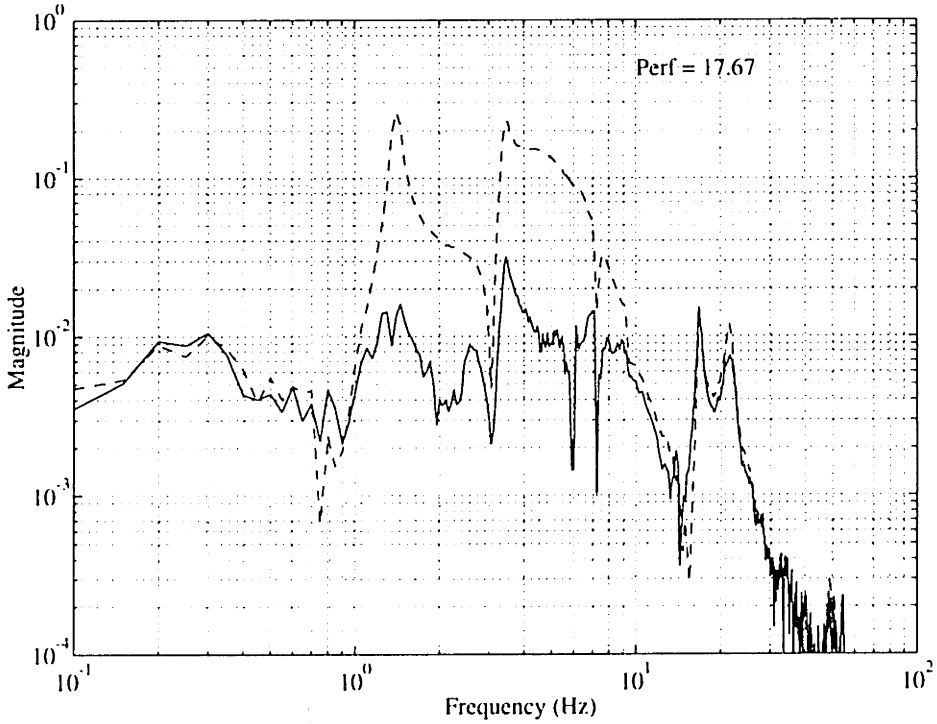

Figure 4.4: Prediction of performance using open loop data.

Chapter 5

Sample Problem

In this chapter, the robust control techniques are compared a low order sample problem. In the first section, a general sample problem representative of structural control applications is presented. In the sections that follow, compensators designed for two different input-output configurations of the sample problem are presented so that comparison of the robust control techniques can be made on a more genereal level.

5.1 Problem Definition

To study and compare the robust control techniques selected in the preceding chapter, a low order sample problem has been devised. The system is a cantilevered Bernoulli-Euler (BE) beam, Figure 5.1, with length and mass density of unity in arbitrary units, and stiffness scaled such that the fundamental frequency is 1 rad/sec. The infinite order dynamics of the beam were truncated at four modes to yield an 8 state sample problem. There are four force inputs located 1/4, 1/2, and 3/4 of the distance along the beam as well as at the tip of the beam. These can be used as disturbance or control inputs. The inputs are denoted u_1, u_2, u_3, and u_4, respectively. Collocated with the force inputs are displacement outputs which can be used as feedback sensors or performance measurements. These outputs are denoted y_1, y_2, y_3, and y_4.

A state space representation of the system dynamics can be written as

$$\dot{x} = Ax + Bu\,, \tag{5.1}$$

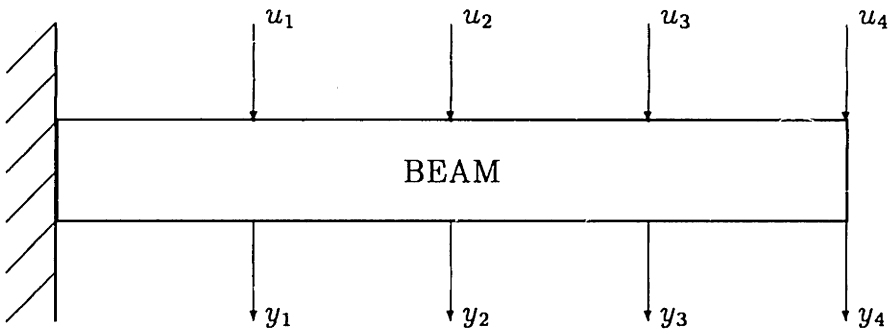

Figure 5.1: Schematic drawing of BE beam for sample problem.

$$y = Cx\,, \tag{5.2}$$

where,

$$A = \text{diag}\left\{ \begin{bmatrix} 0 & 1 \\ -\omega_i^2 & -2\zeta\omega_i \end{bmatrix} \right\}, \qquad i = 1,2,3,4\,, \tag{5.3}$$

$$B = \begin{bmatrix} B_1 & B_2 & B_3 & B_4 \end{bmatrix} \tag{5.4}$$

$$B_j = \begin{bmatrix} 0 & \phi_1(j) & 0 & \phi_2(j) & 0 & \phi_3(j) & 0 & \phi_4(j) \end{bmatrix}^T \tag{5.5}$$

$$C = \begin{bmatrix} C_1 & C_2 & C_3 & C_4 \end{bmatrix}^T \tag{5.6}$$

$$C_j = \begin{bmatrix} \phi_1(j) & 0 & \phi_2(j) & 0 & \phi_3(j) & 0 & \phi_4(j) & 0 \end{bmatrix}, \tag{5.7}$$

For each mode, $\zeta = 0.01$, ω_i is the natural frequency, and $\phi_i(j)$ is the modeshape at the j^{th} location. The values for ω_i and $\phi_i(j)$ were obtained from Ref. [41].

In Ref. [42], it is demonstrated that the input-output topology (the choice of sensors and actuators) affects the nature of compensation required to maximize performance. For this reason, topologies using different combinations of these actuators and sensors will be analyzed. The first sample problem, Section 5.2, uses an input-output degenerate [43] system in which the disturbance and control input are identical, *i.e.* input degenerate, and the performance and sensor output are identical, *i.e.* output degenerate. For an input-output degenerate topology, the performance can be maximized by using high gain. The second sample problem, Section 5.3, uses a non-degenerate system in which the disturbance and control input not collocated, and

the performance and sensor output are not collocated. However, the feedback sensor and control input are collocated. For a non-degerenate topology, the performance is not necessarily maximized by using high gain. The differences in compensation for these topologies will become apparent in a later section.

A second issue that affects the nature of compensation is the number of actuators and sensors that are used in control. Therefore both MIMO and SISO systems will be considered in this thesis. However, MIMO systems are much more difficult to analyze and interpret. Because the comparison procedures used in the sample problem require a more detailed study of changes in the compensator, while the next chapter focuses more on the performance that can be achieved by the different robust control techniques, MIMO systems will be studied only in the Chapter 6. Therefore, to aid in interpretation, only SISO control loops will be considered for the sample problem.

5.1.1 Uncertainty

Throughout this thesis, uncertainty in the magnitude of the frequencies of the modes of the system will be considered. This choice of uncertainty is motivated by the uncertainty that has been noted in the MACE test article. Karlov [44, 45] provides estimates of the frequencies and 3σ uncertainty bounds on some of the frequencies using an Extended Kalman Filter routine. The results are computed on a preliminary version of the MACE test article, and thus do not apply to this thesis directly. However, based on these results, and the errors in frequency of the MACE FEM that were noted in Chapter 2, frequency uncertainty is used exclusively in this thesis. Uncertainty modelling itself is beyond the scope of this thesis and grounds for future research.

Two forms of frequency uncertainty will be used in the following sections. For the first, consider the A matrix in the real modal form, Equation 3.51. Then with uncertainty this can be respresented as

$$A = A_0 + \Delta A = (1 + \delta_\omega) \begin{bmatrix} -\zeta\omega & \omega\sqrt{1-\zeta^2} \\ -\omega\sqrt{1-\zeta^2} & -\zeta\omega \end{bmatrix}, \tag{5.8}$$

where $\underline{\delta_\omega} \leq \delta_\omega \leq \overline{\delta_\omega}$, and $\underline{(\cdot)}$ and $\overline{(\cdot)}$ indicate the minimum and maximum percentage uncertainty in the frequency. Note that rank $\{\triangle A\} = 2$ which implies that an internal feedback loop representation of the uncertainty , $\triangle A = B_0 \Delta C_0$ with $\Delta = \delta I$; has B_0, Δ, and C_0 matrices that have rank=2. This form of the uncertainty is an exact representation of the change in the system.

A second representation of the uncertainty can be made which is approximate. For systems with very light damping, $\omega^2 \gg \zeta\omega$,

$$A = A_0 + \triangle A = \begin{bmatrix} 0 & 1 \\ -(\omega + \delta_\omega \omega)^2 & -2\zeta\omega \end{bmatrix}. \tag{5.9}$$

Further, for $\delta_\omega \ll 1$, the quadratic term in δ_ω can be dropped to yield

$$\triangle A = \begin{bmatrix} 0 & 0 \\ 2\delta_\omega \omega^2 & 0 \end{bmatrix}. \tag{5.10}$$

In this representation, $\triangle A$ is a rank 1 matrix. Therefore, an internal feedback loop representation, $\triangle A = B_0 \delta C_0$, has B_0, δ, and C_0 matrices that are rank 1.

For all analysis of stability bounds for the system in this chapter, the rank 2 representation, Equation 5.8, will be used. As well, this form of uncertainty is used for control synthesis using SWLQG and MM. A slightly modified version of this uncertainty, which ignores the damping of the mode, is used for control synthesis using ME (refer to Section 3.2.4).

$\mathcal{H}_\infty$ analysis does not distinguish between structured and unstructured Δ blocks. The rank 2 uncertainty would be treated as two independent rank 1 uncertainties Therefore, to reduce conservatism caused by this, the rank 1 uncertainty is used in $\mathcal{H}_\infty$ synthesis. Note that the $\mathcal{H}_\infty$ synthesis will still be conservative since $\mathcal{H}_\infty$ considers the uncertainty δ_ω to be a complex number when it is, in fact, real valued. Also, the internal feedback loop representation is not unique. Because $(\beta B_0)(1/\beta C_0) = B_0 C_0$, an arbitrary scaling parameter β is present. As a result, the controller synthesis is potentially conservative [46].

For μ-synthesis, the rank 1 uncertainty representation will be used as well. The presence of the D-scales in this technique removes the arbitrary scaling parameter

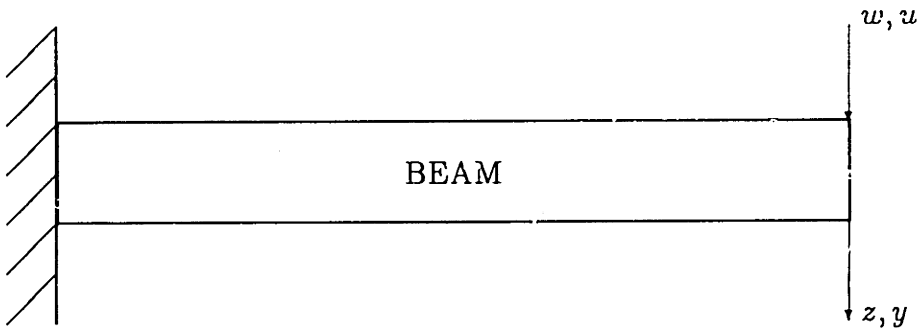

Figure 5.2: Schematic drawing of BE beam for input-output degenerate system.

β from the uncertainty loop. However, μ-synthesis is still conservative because it considers the uncertainty δ_ω to be complex.

For the remainder of this chapter, the frequency of the third mode of the system, located at approximately 17 rad/sec, is considered uncertain. This mode was selected so that the system uncertainty is located in a region of closely spaced modes within the bandwidth of the controller. This choice of uncertainty is motivated by the type of uncertainty that is seen in MACE.

5.2 Sample Problem #1

In the first sample problem (Figure 5.2) the disturbance input, control input, sensor output and performance output are all collocated at the tip of the beam. In the notation of the standard system, Equation 3.1,

$$C_y = C_4,\ C_z = C_4,\ B_u = B_4,\ B_w = B_4\,. \tag{5.11}$$

Thus, the topology is input-output degenerate. As mentioned previously, the frequency of the third mode of the system will be considered uncertain. Figure 5.3 shows the frequency response for the beam through the control input and sensor output, for the nominal system, and for the system with perturbations of $\pm 5\%$ in the frequency of the third mode. The system has a series of alternating complex poles

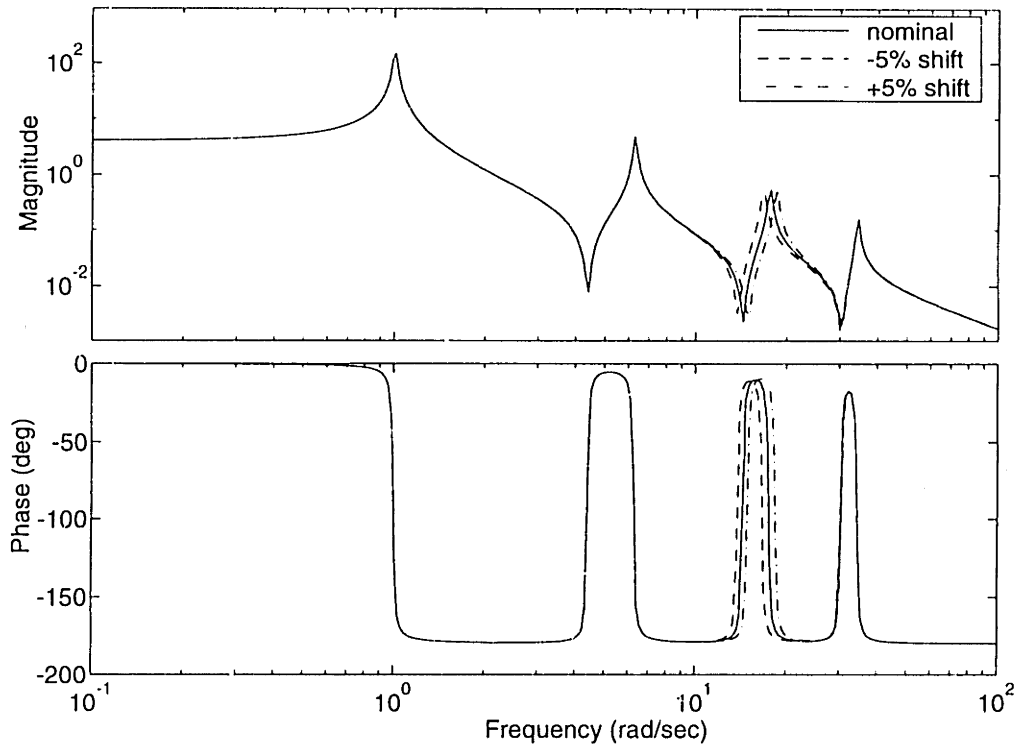

Figure 5.3: Transfer function for nominal system, and system with $\pm 5\%$ perturbation in the frequency of the uncertain (third) mode of the system.

and zeros, which results in the phase being bounded by 0 and -180 degrees even under the perturbations.

Note that the changes to the transfer function caused by the frequency perturbation are mostly localized. There is a small effect on the overall gain of the system, as well as on the first and third zero of the transfer function. However, the transfer function is altered primarily in the 10–25 rad/sec range. This region will therefore be denoted the uncertain region. The zero in the uncertain region shifts in the same direction as the uncertain pole, resulting in substantial changes in the gain and phase of the system.

In this section, compensators designed for this system using the LQG, SWLQG, Maximum Entropy, Multiple Model, $\mathcal{H}_\infty$, and μ-synthesis techniques are presented and compared. LQG compensators are discussed first to present a "reference" compensator to which the compensators developed using the robust techniques can be compared. The robust control techniques are separated into two groups: $\mathcal{H}_2$ based

methods, SWLQG, ME and MM; and $\mathcal{H}_\infty$ based methods, $\mathcal{H}_\infty$ and μ-synthesis. These groups will be discussed separately due to the similarities within them.

5.2.1 LQG controllers

Before proceeding with robust control design, it is useful to investigate the nature of LQG compensators for this system. These compensators contain the basic structure of compensation which is used by all of the techniques. They provide the means by which robust controllers may be compared to compensators which optimize the performance without regard to the parameter uncertainty.

In this section, the general structure of the LQG compensators for this system will be discussed. This will be done by showing the trends in the compensator as the sensor noise and control weighting are decreased. At the end of this section, an LQG compensator is presented which will be taken as the "reference" compensator for this system. The perturbations from the "reference" compensator will then be used to demonstrate the effects of the robust control techniques.

The general structure of LQG controllers for this system consists of three parts. Figure 5.4 shows the transfer function of the system from input to output scaled up by a factor of 60, along with a series of LQG compensators which have the same control weighting, but different sensor noise intensities. The first is a real zero which provides phase lead. The frequency of this zero is governed by the control weighting and sensor noise. As either of these decreases, the frequency of the real zero increases, shifting the introduction of phase lead to increasingly high frequencies. The second feature is a pair of heavily damped complex poles at high frequency which roll off the compensator. The third is a network of complex poles and zeros clustered around the poles and zeros of the plant. This includes a pair of complex poles and zeros in the uncertain region. The network of complex poles and zeros for each of these compensators has an alternating pole-zero pattern similar to that of the plant. These poles and zeros are positioned such that the loop transfer function to have an alternating pole-zero structure in which each plant zero is followed by a compensator pole, compensator zero and then plant pole.

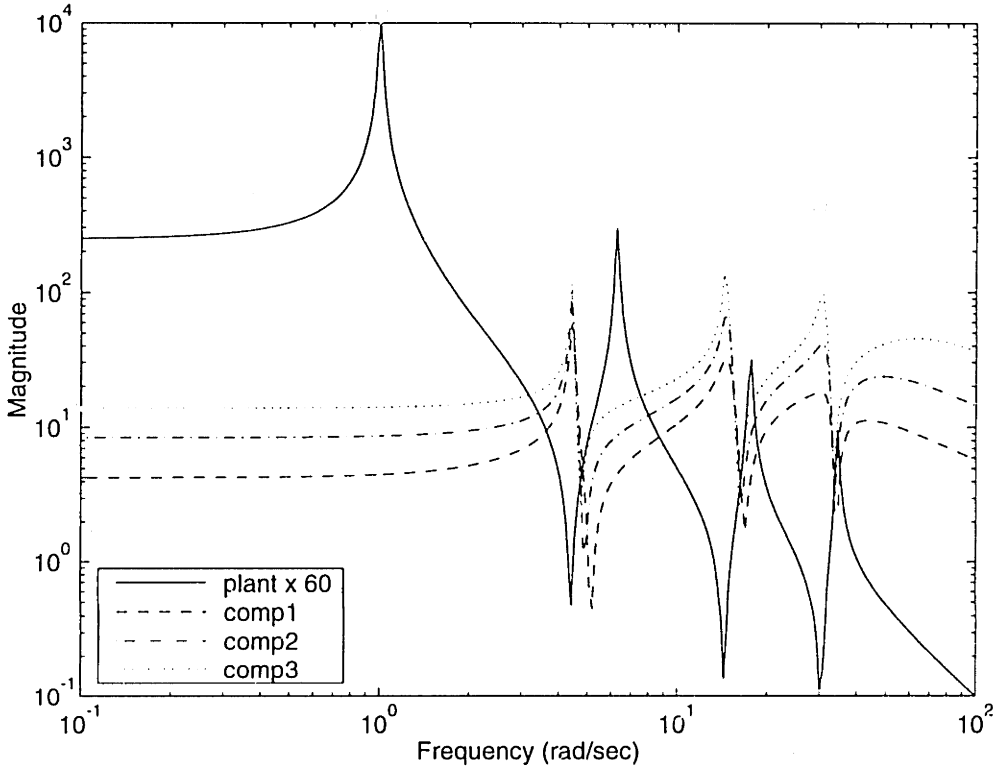

Figure 5.4: Transfer function for the nominal plant scaled by 60, with a series of LQG compensators with the same control weighting but different sensor noise intensities. Comp1 has the highest noise, comp3 the lowest.

The actual position of the compensator poles and zeros relative to the plant poles and zeros in each of these regions is governed by the sensor noise and control weighting. For constant control weighting, as the sensor noise is decreased, the compensator zeros shift lower in frequency and the compensator poles shift lower in frequency and become less damped. This can be seen in Figure 5.4. In the limit as both the sensor noise and the control weighting go to zero, the compensator poles and zeros are placed at the same frequency and damping as the plant zeros. This asymptotic pole-zero cancellation behavior was shown in Ref. [42].

To design the "reference" compensator, a series of LQG designs was made by varying both the control weighting and the sensor noise intensity. Because the input-output loop is phase bounded, a compensator with sufficiently high gain to raise the loop gain above unity for frequencies extending past the highest frequency of the model will be stable for perturbations of the uncertain pole greater than 100%. With

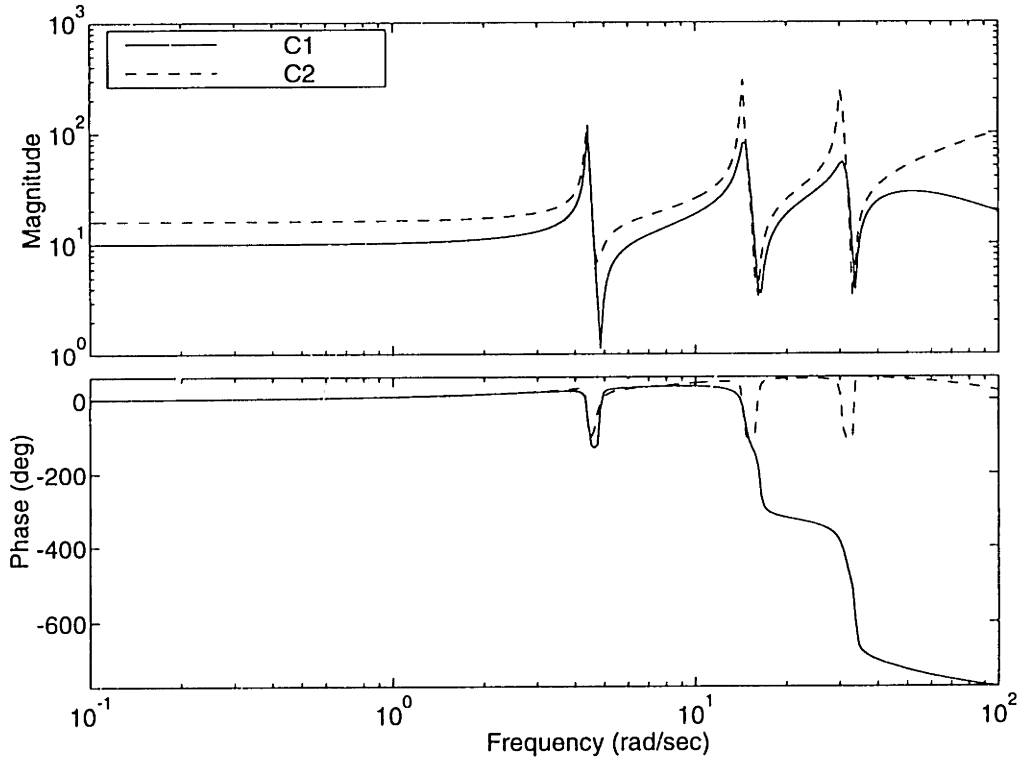

Figure 5.5: Transfer function of compensators designed using LQG with high sensor noise (C1) and low sensor noise (C2).

low noise and control weightings, LQG produces such a controller. This controller could not be implemented in practice because of phase lag in sensors, and unmodelled dynamics. Therefore, to introduce a practical limitation on the compensators, a constraint that the bandwidth of the compensator be approximately 40 rad/sec was imposed.

With this constraint in place, another series of compensators was designed. Figure 5.5 shows two compensators from this series. The first has a control weighting of $\rho = 1 \times 10^{-3}$, a sensor noise intensity of $\theta = 5 \times 10^{-4}$, and is denoted C1. The second was designed using a lower sensor noise intensity, but higher control weighting to keep the bandwidth approximately the same. It has a control weighting of $\rho = 2.5 \times 10^{-3}$, a sensor noise intensity of $\theta = 1 \times 10^{-6}$, and is denoted C2. Note that compensator C1 has two pairs of nonminimum phase zeros while C2 has all minimum phase zeros.

It has been observed that robust control techniques often contain minimum phase dynamics rather than nonminimum phase dynamics [47]. This has been interpreted

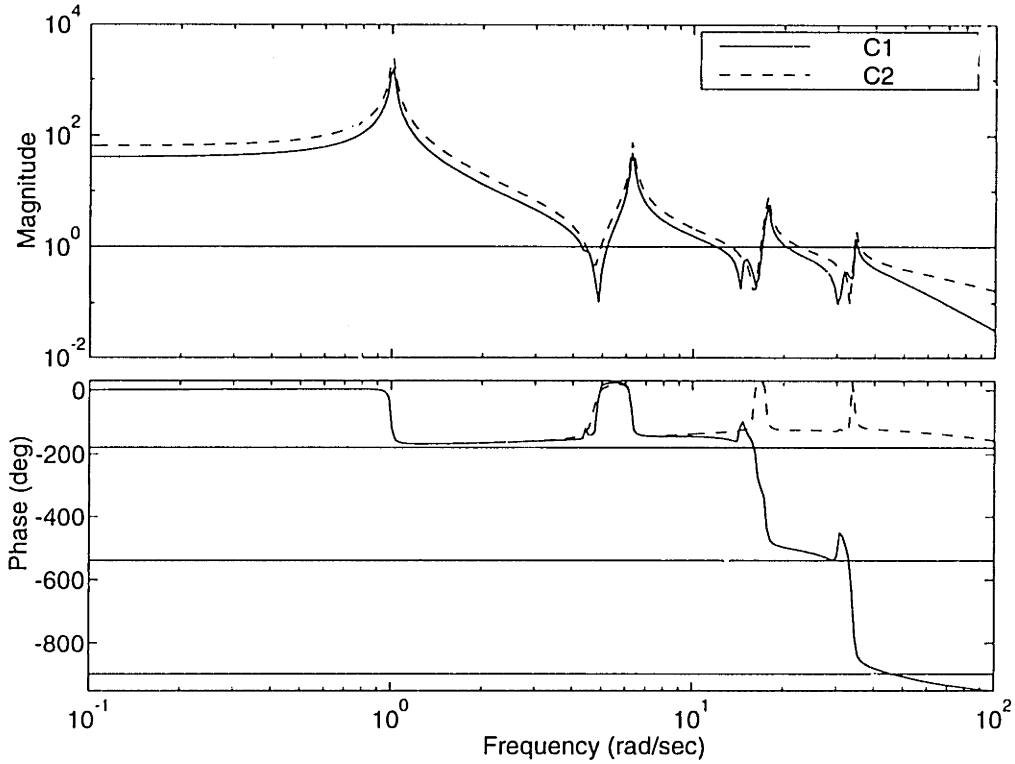

Figure 5.6: Loop transfer function for compensators C1 and C2 with nominal plant.

in Neo-Classical control [42] to mean that nonminimum phase zeros are inherently non-robust and minimum phase zeros are robust. This is not always the case. In Figure 5.6, the loop transfer function for the plant cascaded with each of the two compensators is shown. Observe that the phase for the C2 loop is bounded by $\pm 180°$ below 100 rad/sec (above 100 rad/sec which is not shown, the phase crosses $-180°$). This implies that the gain margin for this system is determined from the last crossover which is governed by the roll-off dynamics, not the dynamics in the range of parametric uncertainty. The loop transfer function for C1 does not have the phase bounded in the same way, and thus the gain margin within the frequency range of uncertainty is an issue.

Figures 5.7 and 5.8 show a close-up of the 10–20 rad/sec range of the loop transfer function in which the plant is perturbed by shifting the frequency of the uncertain mode by -5% and $+5\%$, respectively. Note that for a shift of -5%, the alternating pole-zero pattern of the loop has not been disturbed. Stability of the system with

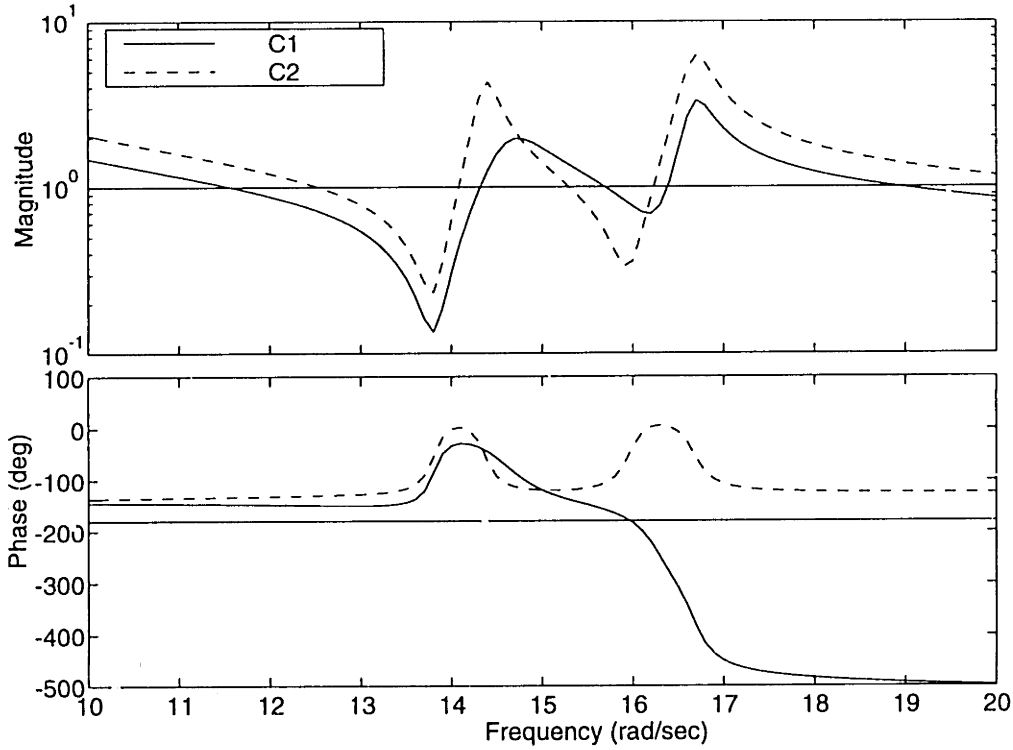

Figure 5.7: Loop transfer function for C1 and C2 on plant with third mode frequency shifted -5%.

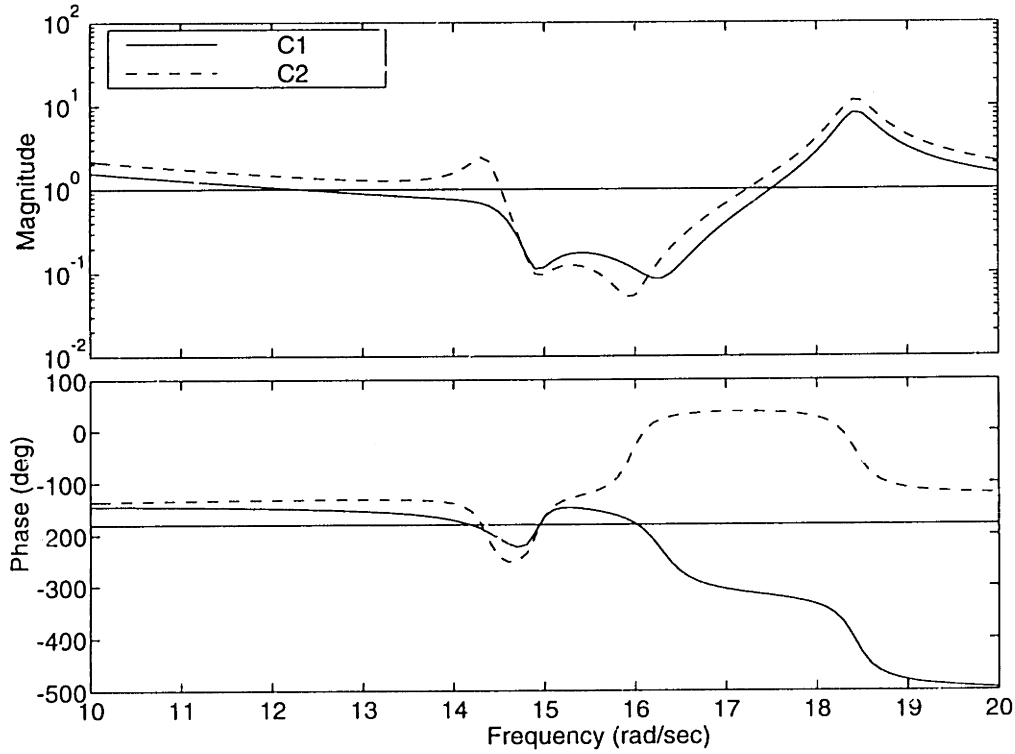

Figure 5.8: Loop transfer function for compensators C1 and C2 on plant with third mode frequency shifted +5%.

compensator C2 is seen from the fact that the phase does not cross $-180°$. It can also be seen that the C1 system is stable, though with low gain and phase margins. However, for a perturbation of $+5\%$ in the frequency of the third mode, the alternating pole-zero pattern of each loop is destroyed. The C2 loop phase is no longer bounded by $\pm 180°$, and a close inspection will show that the phase crosses $-180°$ before the gain crosses below unity so that this system will be unstable. By contrast, compensator C1, which contains nonminimum phase zeros, has a much more heavily damped pole which does not cause as high a gain as the lightly damped pole in C2. Because of the higher damping, the loop gain in the 13–15 rad/sec range is less than unity, and therefore it is acceptable that the phase crosses $-180°$ in this range.

Thus, it can be seen that simply using minimum phase dynamics to phase stabilize the nominal plant is not necessarily sufficient for robust stability to perturbations in the frequency of a mode. To use phase stabilization it is necessary to consider the perturbations which occur in the phase of the system, so that unlike compensator C2 in Figure 5.8 the phase boundedness of the loop is not destroyed by the perturbation in the plant.

Compensator C1 permitted the broadest worst case bound of all the LQG designs considered. Henceforth, it will be considered as the "reference" compensator.

5.2.2 $\mathcal{H}_2$-based robust methods

The $\mathcal{H}_2$-based methods (SWLQG, ME and MM) provide robustness to the uncertain mode in a very similar way. To illustrate the approach these methods take, compensators designed using the SWLQG technique will be presented first in some detail. The primary effects which occur in the compensator as a result of sensitivity weighting will be presented followed by a discussion of the consequences of these changes on the robustness range of the compensator. The secondary effects of providing greater robustness will then be discussed. Next, the differences between the SWLQG and the ME and MM controllers will be shown with a discussion of how these affect the closed loop properties. Finally, the issue of conservatism in the MM technique, which provides some robustness guarantees, will be considered.

As with all the $\mathcal{H}_2$ methods, the basic structure of the SWLQG controller is the same as that of the "reference" compensator. With zero sensitivity weighting, the compensators are identical. With sensitivity weighting on the third frequency of the system, the largest changes in the compensator occur in the uncertain region. Figure 5.9 compares the poles and zeros of a series of SWLQG compensators with increasing sensitivity weights. The frequency response of four of these compensators are compared in Figure 5.10.

In Figure 5.9 it can be seen that the compensator pole in the uncertain region becomes more heavily damped, as the sensitivity weights are increased, while maintaining approximately the same frequency. The compensator zero in this region, which is nonminimum phase in the LQG compensator, migrates into the left half plane, then becomes more heavily damped (though always less damped than the pole) while its frequency is reduced. Figure 5.10 shows that in the region around the pole, the gain of the compensator is reduced as a result of the increased damping in the pole. As well, above the nominal frequency of the compensator zero, the gain is increased. With the exception of the first SWLQG design in which the compensator zero in the process of migrating into the left half plane is located very close to the $j\omega$-axis, the gain and the phase of the compensator undergo smaller transitions due to the increased damping of both the pole and zero. These changes to the compensator represent the primary effects of increased robustness

To understand how these primary effects increase the robustness of the compensator, recall that for the "reference" compensator in the uncertainty region, the plant zero is followed by a compensator pole, compensator zero, and finally a plant pole. For positive perturbations in the uncertain pole, stability is governed by the compensator pole because an increase in the frequency of the plant zero can rise above the frequency of the compensator pole destroying the alternating pole zero pattern. For negative perturbations, the behavior of the compensator zero dominates stability issues since a sufficiently large perturbation results in the frequency of the plant pole passing below the frequency of the compensator zero.

The reduction in gain around the compensator pole results in gain stabilization

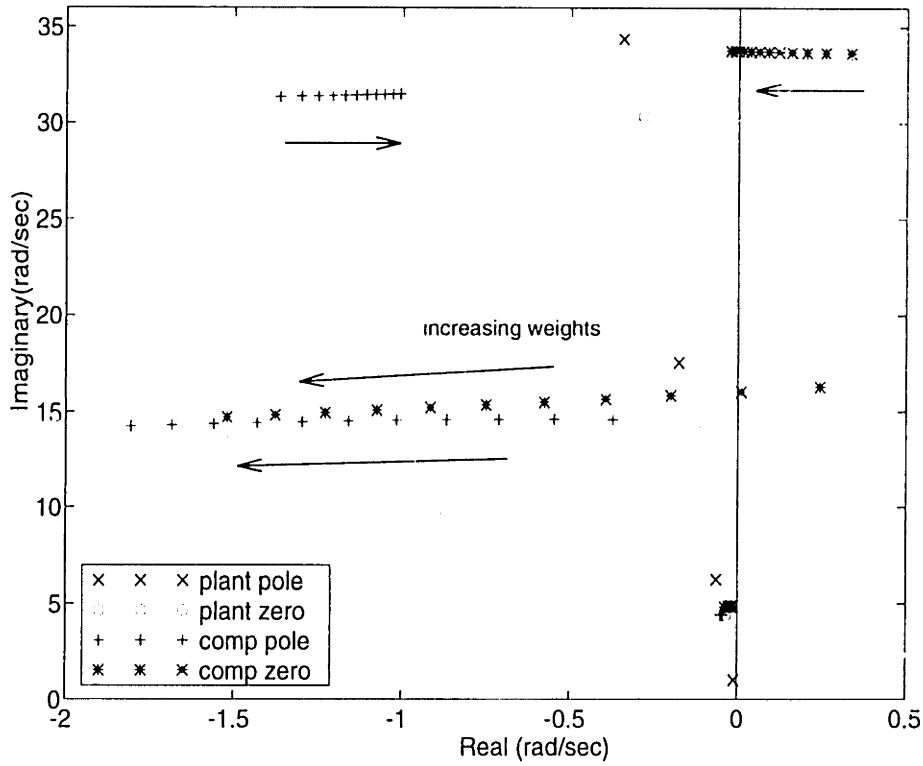

Figure 5.9: Poles and zeros of SWLQG compensators with increasing robustness. Closeup of the region near the imaginary axis. Note that the locus of poles and zeros begins with zero sensitivity weights, *i.e.* LQG.

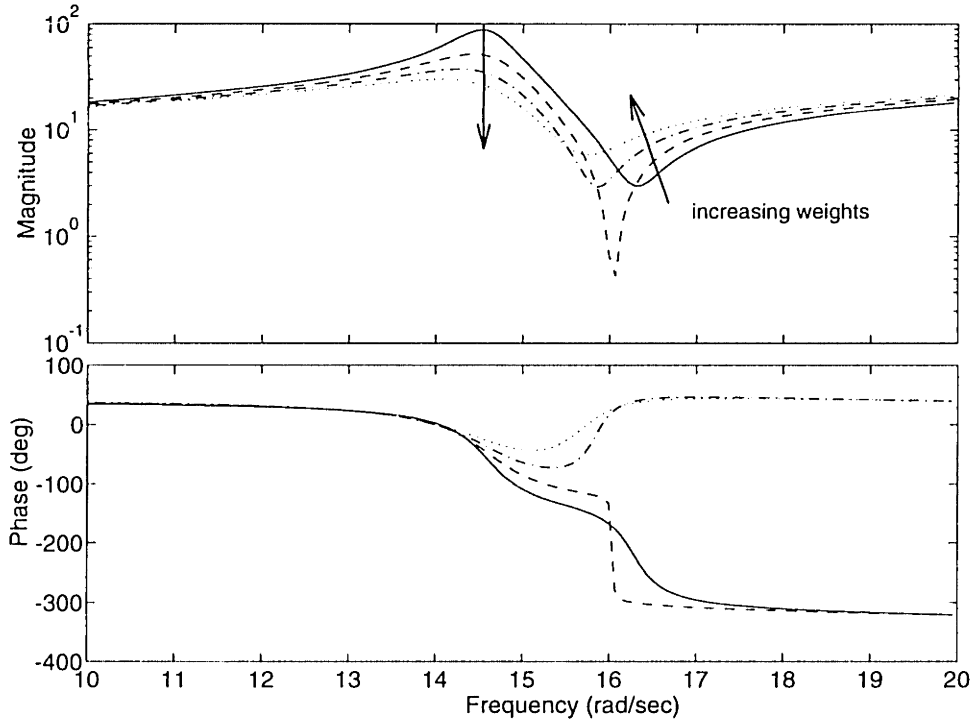

Figure 5.10: Compensator transfer functions for LQG controller (solid), and three SWLQG controllers with increasing sensitivity weights.

of the system for positive perturbations in the uncertain frequency. Recall that Figure 5.8 shows that a positive shift in the frequency of the uncertain plant pole can destroy the alternating pole-zero pattern of the LQG loop. The same is true for the SWLQG compensators. In the preceding section it was shown that lower gain in the "reference" compensator, C1, maintained stability for larger perturbations than compensator, C2. Similarly, the SWLQG compensators remain stable for larger perturbations than the "reference" compensator due to the reduction in gain caused by the damping of the compensator pole.

For negative perturbations in the uncertain pole, the compensator zero is more important than the compensator pole. In Figure 5.9, it can be seen that there is a large separation between the compensator zero and plant pole. This separation permits a -20% shift in the uncertain pole before the alternating pole-zero pattern of the loop is destroyed. With an increased sensitivity weight, the compensator zero moved into the left half plane which resulted in the phase of the loop being bounded by $\pm 180^\circ$ for perturbations which do not destroy the alternating pole-zero structure. Note that the C1 compensator of the preceding section also had a minimum phase zero in the uncertain region, however light damping in the compensator pole led to poor robustness for positive perturbations in the uncertain frequency.

Next consider the secondary effects of increased robustness. Two important secondary effects occur. The first is an increase in the compensator gain at high frequencies and the second is a decrease in the gain of the compensator at low frequencies. These effects can be seen in Figure 5.11. While the changes appear small, it will be seen later that they are significant.

There are three changes in the compensator that lead to these effects. The first is a reduction in the frequency of the real compensator zero. The second is the reduction in the frequency of the complex compensator zero pair in the uncertain region which has already been noted. Third, with increased sensitivity weighting the high frequency roll-off poles of the compensator increase in frequency. These shifts in location of poles and zeros can be seen in Figure 5.12.

For a better understanding of how the shifts in these poles and zeros cause the

noted changes in the frequency response, consider the poles and zeros in two groups. Combining the real zero with the roll-off poles creates a lead compensator which rolls off at high frequency. If the DC gain of this system is held constant, then a decrease in the frequency of the real zero will cause an increase in the gain at high frequency. Similarly, an increase in the frequency of the roll-off poles results in increased gain at high frequency. Next, consider the compensator pole and zero in the uncertain region as a lag-lead network. The frequency response of this network is:

$$G_{ll}(s) = \frac{s^2 + 2\zeta_z\omega_z s + \omega_z^2}{s^2 + 2\zeta_p\omega_p s + \omega_p^2} \tag{5.12}$$

At DC the gain is the ratio of the square of the frequency of the zeros and poles, and is greater than unity. The gain at high frequency is unity. Reducing the frequency of the compensator zero reduces the low frequency gain. Therefore, the effect of both of these groups of poles and zeros is to reduce the low frequency gain relative to the high frequency gain.

The overall gain is not determined strictly by the poles and zeros of the compensator. But the increase in the differential gain between high and low frequency has resulted in both a reduction of the low frequency gain and an increase in the high frequency gain shown in Figure 5.11.

Compensators designed using Maximum Entropy and Multiple Model are very similar to the SWLQG compensators. Figure 5.13 shows the degree of similarity in the frequency responses of ME, MM and SWLQG compensators which are robust to $\pm 20\%$ perturbations in the frequency of the uncertain pole. However, some important differences do exist. The first is the primary effect on the compensator zero in the uncertain region. Comparing Figures 5.9, 5.14, and 5.15, it can be seen that the zero in the uncertain region exhibits similar damping in the MM, ME and SWLQG compensators, but the frequency of the zero is not altered as much by MM and ME as it is by SWLQG. The result is that the differential gain in the lag-lead network in the uncertain region is not altered as significantly. As a result, the difference in gain between high and low frequencies is not as large in MM and ME as it is in SWLQG.

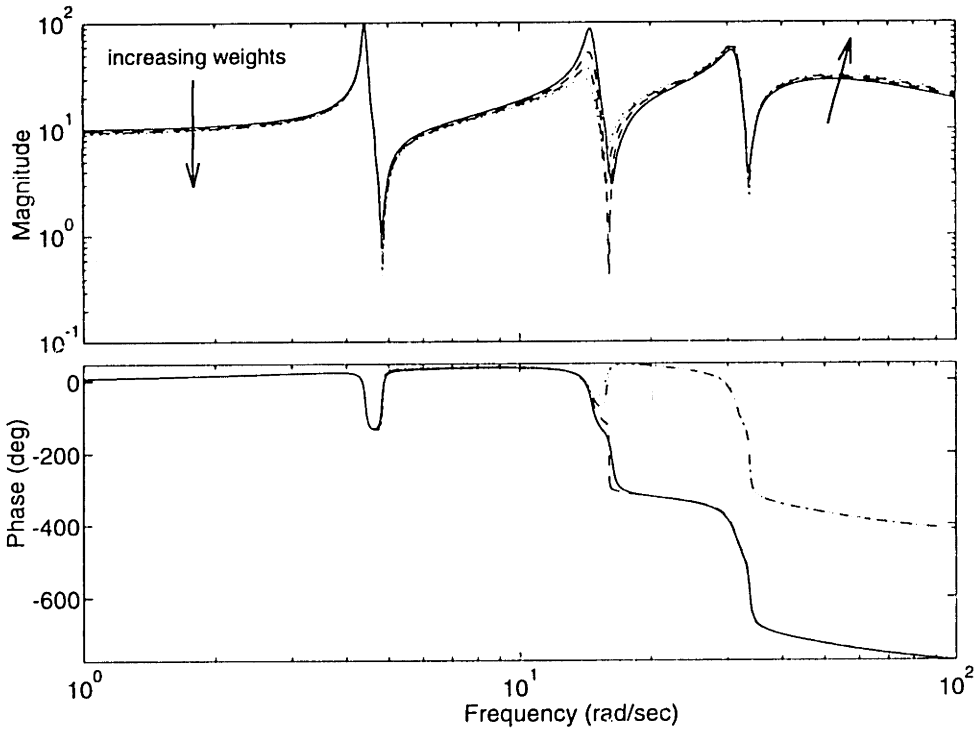

Figure 5.11: Compensator transfer functions for LQG controller (solid), and three SWLQG controllers with increasing sensitivity weighting.

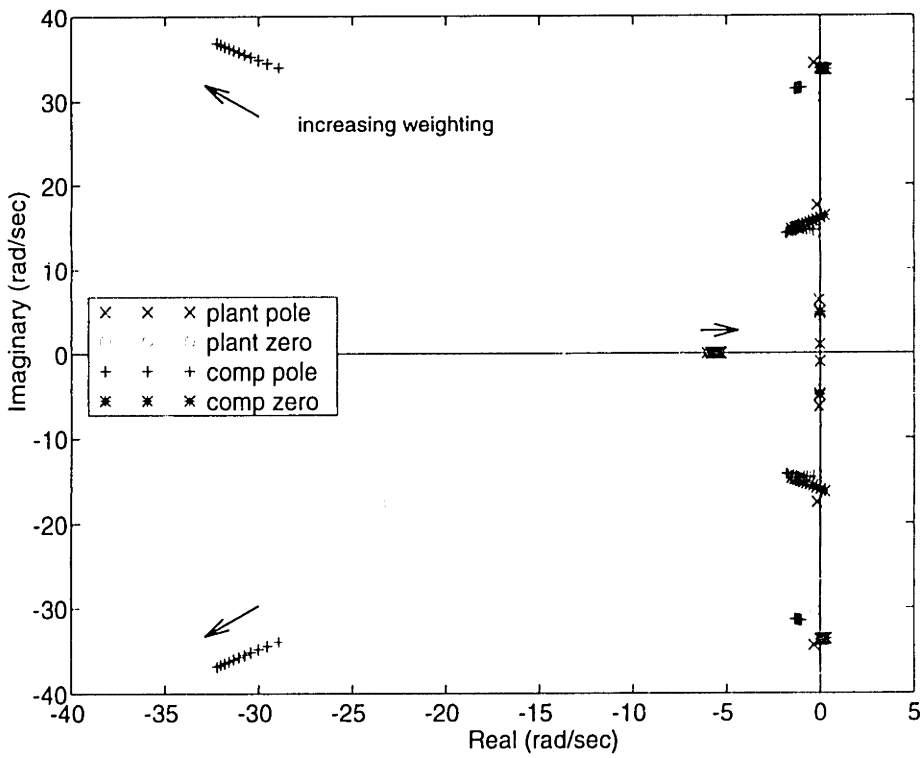

Figure 5.12: Poles and zeros of SWLQG compensators with increasing robustness.

This effect can clearly be seen in the frequency response of the compensators in Figure 5.13.

In addition, the real zero of the MM compensators is not altered as much by increased uncertainty. This can be seen by comparing Figures 5.12 and 5.16. A smaller shift in the real zero also results in a smaller gain differential between high and low frequency. Figure 5.13, shows that the high frequency gain for the MM compensator is the lowest of the robust techniques, while the low frequency gain is the highest.

It is possible to draw conclusions about the effects of the changes in the compensator on closed loop properties. Increased high frequency gain results in a higher cross-over frequency and thus a larger bandwidth for the system. Figure 5.17 shows the complementary sensitivity transfer function for the compensators in Figure 5.13. The results indicate that the bandwidth of the SWLQG compensator is higher than both the other techniques, and that the MM compensator is closest to the "reference" compensator in bandwidth. Performance effects will be shown in Section 5.2.4 with the remainder of the robust control techniques.

Finally, because the MM technique provides guarantees of stability at each of the design points, the conservatism of the technique can be addressed. Herein, the design approach uses three plant models: the nominal, which receives a weighting of 90% in the performance metric, and two models with the uncertain pole shifted by plus or minus some percentage, each weighted 5%. The compensator is guaranteed to stabilize the nominal system and the systems with the uncertain frequency shifted.

Figure 5.18 shows the closed loop state cost of the nominal plant as a function of the stability bounds for a series of MM compensators designed with increasing uncertainty. It can be seen that the achieved bounds are close to the guaranteed points which shows that the conservatism of the multiple model technique is not large. This conservatism may be further reduced if the nominal model is weighted 100%. The technique in some respect relies on conservatism since it is tacitly assumed that the space between guaranteed points represents a guaranteed stability region. There are in fact no guarantees at intermediate points. However, the results shown

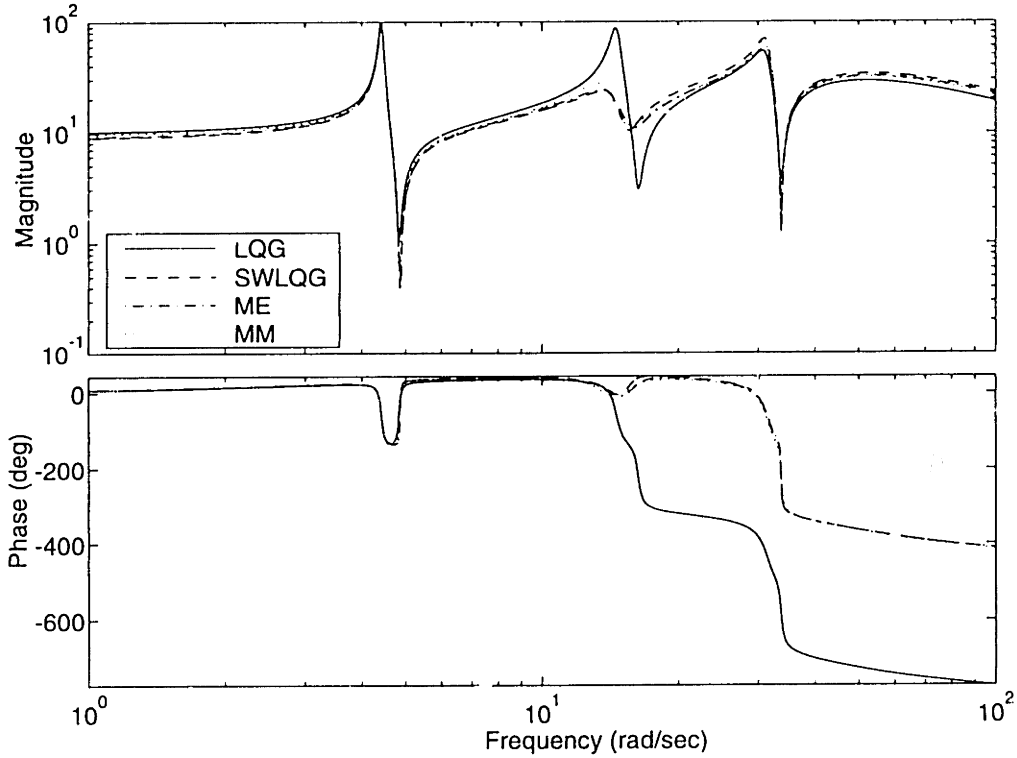

Figure 5.13: Compensator transfer functions for LQG controller along with SWLQG, ME and MM controllers which each are robust to ±20% shifts in the frequency of the third mode.

here indicate that it is not a bad assumption in the case of a single uncertainty.

5.2.3 $\mathcal{H}_\infty$-based methods

In addition to the $\mathcal{H}_2$ methods of the preceding section, two $\mathcal{H}_\infty$-based methods, $\mathcal{H}_\infty$ and μ-synthesis, have been investigated. These methods are presented separately because they lack the degree of similarity that exists between the $\mathcal{H}_2$-based compensators.

Comparing compensators designed using $\mathcal{H}_\infty$ and $\mathcal{H}_2$ methods is complicated by the fact that the two methods optimize inherently different properties. $\mathcal{H}_2$ compensators minimize the variance of a combination of inputs and outputs while $\mathcal{H}_\infty$ compensators minimize the worst case amplification from the system input to output. The experiment in Chapter 6 has an RMS ($\mathcal{H}_2$) performance metric. Therefore,

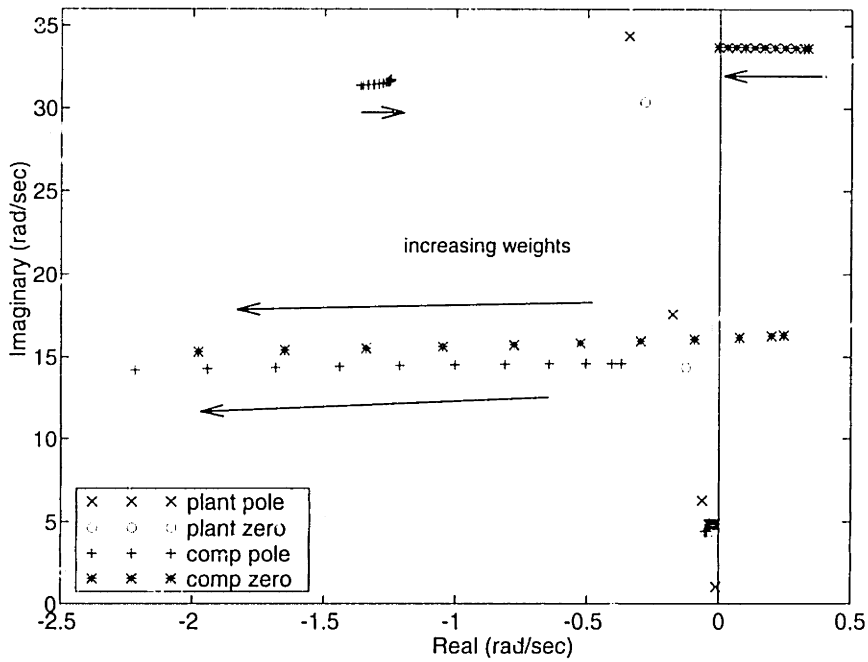

Figure 5.14: Poles and zeros of ME compensators with increasing robustness. Closeup of the region near the imaginary axis.

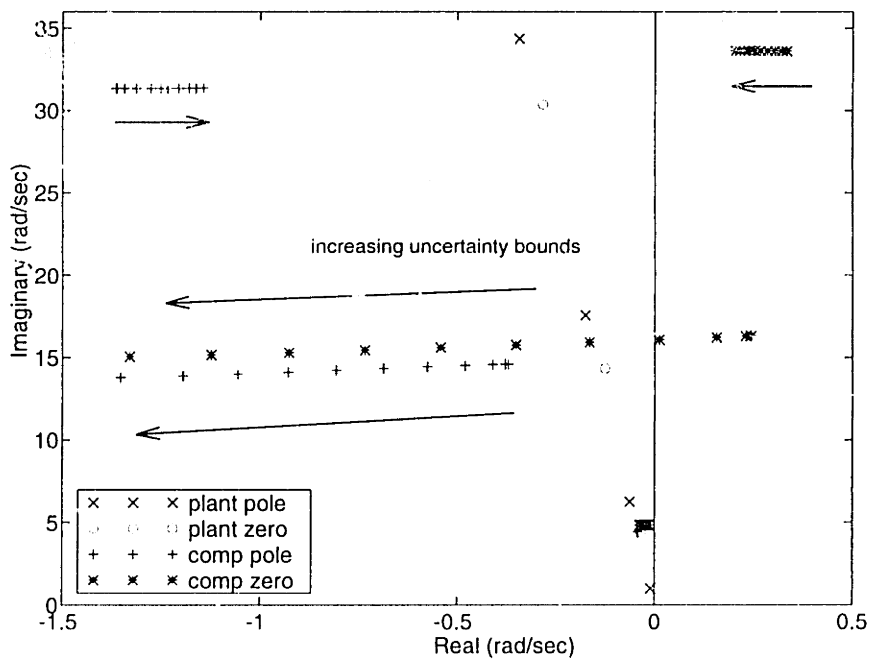

Figure 5.15: Poles and zeros of MM compensators with increasing robustness. Closeup of the region near the imaginary axis.

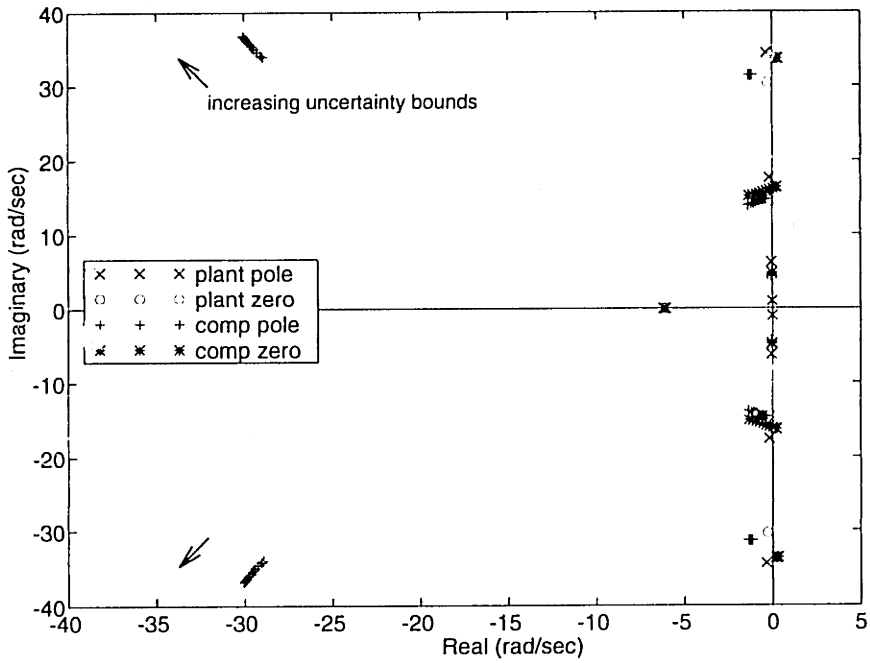

Figure 5.16: Poles and zeros of MM compensators with increasing robustness.

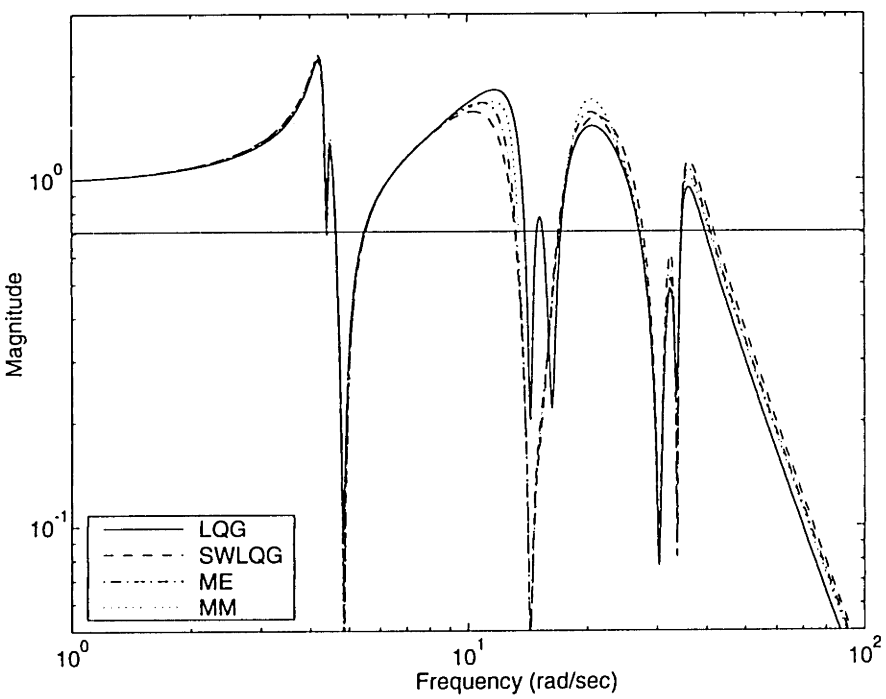

Figure 5.17: Complementary sensitivity transfer function for LQG controller along with SWLQG, ME and MM controllers which each are robust to $\pm 20\%$ shifts in the frequency of the third mode.

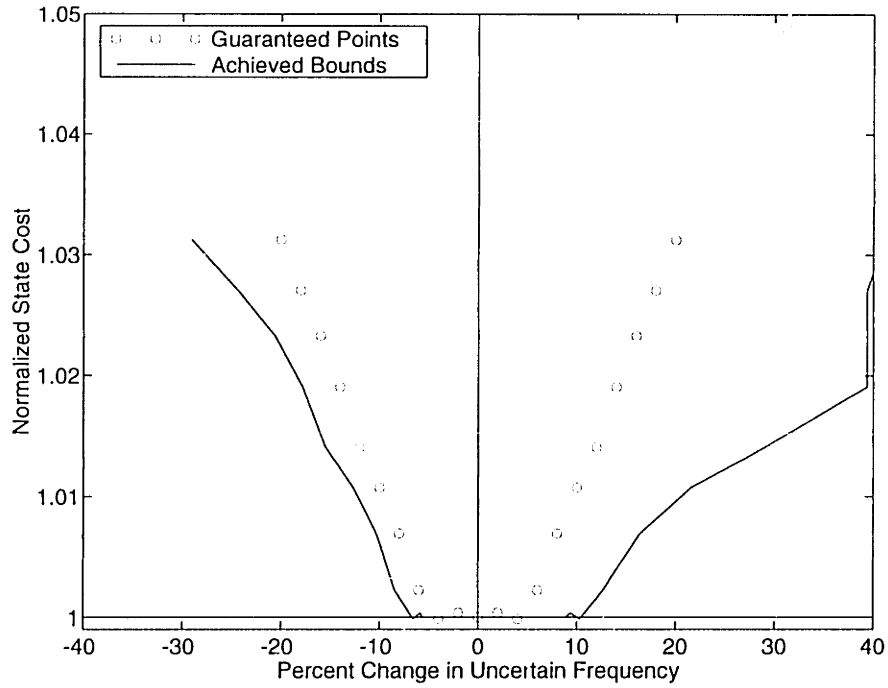

Figure 5.18: Closed loop cost of the nominal system as a function of the achieved bounds and guaranteed points to perturbations in the frequency of the third mode of the system for Multiple Model compensators.

because of this physical motivation, all of the robustness techniques are compared on the basis of an $\mathcal{H}_2$ performance metric.

In order to better perform an $\mathcal{H}_2$ minimization in an $\mathcal{H}_\infty$ framework, a frequency dependent weighting function was placed on the disturbance to performance loop. The weighting function has a real zero at 40 rad/s, a real pole at 400 rad/s and a DC gain of 10. The disturbance to performance transfer function is guaranteed to lie below the inverse of this weighting function scaled by the $\mathcal{H}_\infty$ norm of the design. therefore, an $\mathcal{H}_\infty$ minimization with this weighting function will prevent high frequency amplification. If a design with an $\mathcal{H}_\infty$ norm less than unity is achieved, the disturbance to performance transfer function will have a magnitude less than 0.1 at all frequencies with a one pole roll off at 40 rad/sec. This weighting function was selected iteratively in an attempt to match the performance levels achieved by the $\mathcal{H}_2$ based designs and the desire to have a bandwidth of approximately 40 rad/sec.

In the following two sections the $\mathcal{H}_\infty$ compensators will be presented separately

from the μ compensators. One reason the techniques are presented separately is that the compensators address robustness quite differently. Another reason is that some additional manipulation of design parameters is necessary that is unique to each technique.

$\mathcal{H}_\infty$ designs

This section begins with a brief discussion of the parameters used in the $\mathcal{H}_\infty$ designs. This is followed by a description of the basic structure of the $\mathcal{H}_\infty$ compensators. Finally, the effects on the compensator and closed loop system of adding uncertainty to the $\mathcal{H}_\infty$ design will be discussed.

In order to have a well-posed $\mathcal{H}_\infty$ design problem, it is necessary to have a direct feedthrough from the disturbances to the sensor output and from the control input to the performance. In the notation of the standard problem, Equation 3.1, this means $D_{yw} \neq 0$ and $D_{zu} \neq 0$. This is similar to the constraint in LQG of non-zero sensor noise intensity and non-zero control weighting. As with the LQG designs, these parameters were varied until a satisfactory design resulted. With $D_{yw} = [0 \;\; 0.7]$ and $D_{zu} = [0 \;\; 7 \times 10^{-4}]^T$, a compensator which achieves robustness bounds of $+11\%$ and -4%, calculated as described in Section 4.2, was designed. This compensator yielded an $\mathcal{H}_2$ cost on the nominal plant roughly equal to that of the "reference" LQG compensator. In addition, this compensator resulted in a 41 rad/sec bandwidth; only marginally wider than that of the "reference" compensator. These similarities make comparison with the designs in the preceding section possible. Uncertainty was added to the problem using the form in Equation 5.10.

Figure 5.19 shows that the LQG and $\mathcal{H}_\infty$ compensators have a similar structure. Note that the compensator pole and zero located in the uncertain region are located at higher frequency for $\mathcal{H}_\infty$ than LQG. Recalling that robustness to positive perturbations is governed by the compensator pole, and negative perturbations by the compensator zero, provides an explanation why the $\mathcal{H}_\infty$ compensator can tolerate larger positive perturbations and smaller negative perturbations. Another notable difference occurs in the dynamics at high frequency. The LQG design has a set of

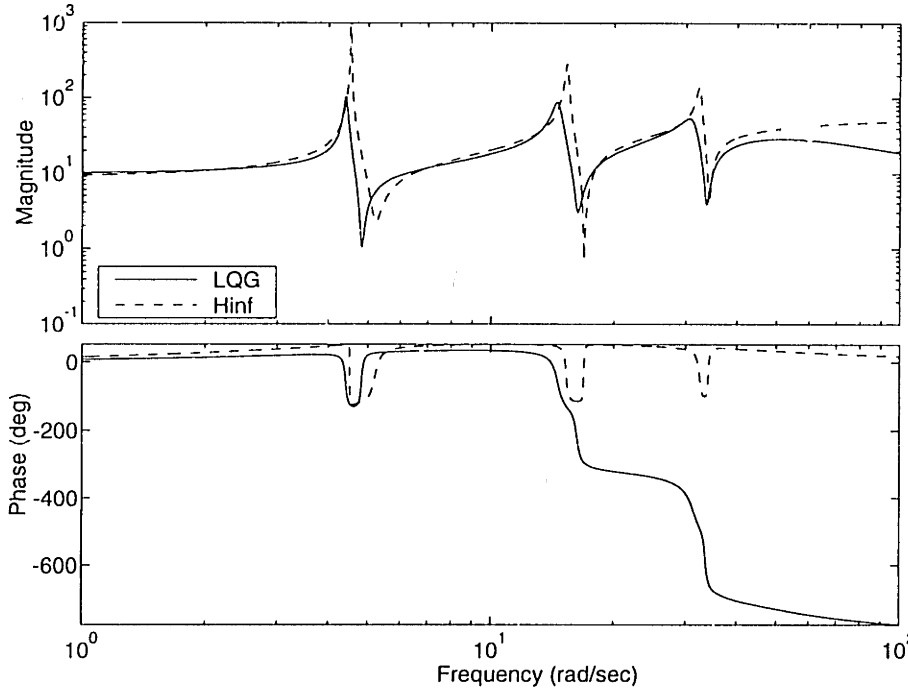

Figure 5.19: Frequency response of "reference" LQG and $\mathcal{H}_\infty$ compensator with no uncertainty guarantees.

complex poles for roll-off while the $\mathcal{H}_\infty$ design has two real poles spaced two decades apart. The second real pole is in fact an artifact of the $\mathcal{H}_\infty$ design process. State space methods for calculating the $\mathcal{H}_\infty$ controller yield only a suboptimal compensator [11]. As the design approaches optimality, the frequency of the highest compensator pole approaches infinity. At the same time, the problem becomes poorly conditioned. It has been shown that the optimal $\mathcal{H}_\infty$ compensator is all-pass [48]. The $\mathcal{H}_\infty$ designs in this section have an $\mathcal{H}_\infty$ norm within 0.1% of the optimal $\mathcal{H}_\infty$ compensator.

The effects on the compensator of adding uncertainty to this $\mathcal{H}_\infty$ problem can be characterized in two stages. In the first stage, small changes in the compensator result in a small increase in the robustness bound to negative perturbations and a large increase for positive perturbations. Little change in the bandwidth or nominal cost of the compensator occurs. In the second stage, the compensator is radically different. It contains unstable poles and achieves large bounds to both negative and positive perturbations. However, the bandwidth and nominal $\mathcal{H}_2$ cost are significantly increased.

In the first stage, robustness is achieved primarily by changes to the compensator within the uncertain region (10–20 Hz). Thus primary effects dominate. As greater uncertainty is added to the control problem, the damping and frequency of the compensator pole in the uncertainty region increases. As well, both the damping and the frequency of the compensator zero in this region are reduced. These changes can be seen in Figure 5.20.

Reducing the frequency of the compensator zero increases the distance between the plant pole and compensator zero. This permits a larger negative perturbation in the uncertain pole before the alternating pole-zero structure is destroyed. This modification of the compensator translates into a small increase in robustness to negative perturbations. Increasing the damping of the compensator pole reduces the gain of the compensator in a narrow frequency range. For positive perturbations, the reduction in gain is sufficient to gain stabilize even for perturbations large enough to destroy the alternating pole-zero pattern of the loop. Thus larger positive perturbations can be tolerated in these $\mathcal{H}_\infty$ designs.

Figure 5.21 shows the closed loop cost as a function of the perturbed frequency for compensators in this first stage. The figure clearly shows the small increase in the stability region for negative perturbations and the large increase in the stability region for positive perturbations. The figure also demonstrates that there is little change in the nominal cost for these designs.

In the second stage, the placement of the compensator pole and zero in the uncertainty range is dramatically different. Figure 5.22 shows that while in the first stage the compensator pole is moved higher in frequency and damping, in the second stage it is moved lower in frequency while its real part increases. For large uncertainty, the pole is located in the right half plane. The compensator zero is placed differently in this stage as well. It is nonminimum phase and lower in frequency with increasing uncertainty. For large uncertainty the zero is placed at a lower frequency than the compensator pole. In fact, both the pole and zero are placed low enough to be outside the uncertainty range. Thus, perturbations in the frequency of the third mode have little interaction with the compensator, and the system is stable for broad ranges of

uncertainty.

As one might expect, the consequences of this dramatic change are great. Shifting the compensator zero below the frequency of the compensator pole results in a lead-lag network which increases the gain differential between high and low frequency. Another change that increases the gain differential is the placement of the real compensator zero. In the $\mathcal{H}_2$ designs, as uncertainty increased, the real zero was placed at lower frequency. The same behavior is noted in the $\mathcal{H}_\infty$ compensators and can be seen in Figure 5.22. The consequences of the increased gain differential are a reduction in performance (Figure 5.23) and an increase in bandwidth (Figure 5.24) for the $\mathcal{H}_\infty$ compensators.

$\mathcal{H}_\infty$ synthesis is a bounding method and therefore provides robust stability guarantees. Figure 5.23 illustrates the closed loop cost on the nominal plant as a function of both the achieved and the guaranteed bounds. It is evident from the figure that the guarantees provided are not very useful. The huge difference between the guaranteed and the achieved stability bounds show the excessive conservatism of this procedure. This figure also shows the large increase in cost which is incurred as stability bounds are broadened.

μ-synthesis

In this section, compensators designed using μ-synthesis will be presented. It is necessary first to discuss how the problem is set up in the μ framework. This is followed by a discussion of the changes that occur in compensators designed using μ-synthesis with different amounts of uncertainty. A brief discussion of the conservativeness of μ synthesis as a bounding technique will follow.

Recall from Section 3.3.4 that the objective of μ-synthesis is to find a compensator which reduces the structured singular value (μ) of the interconnection of the plant and a delta block formulated to represent the robustness and performance requirements of the system. Figure 5.25 shows the system interconnection structure which was used for this sample problem. Four delta blocks exist. The block Δ_0 represents the frequency uncertainty. The input-output structure of the uncertainty loop is

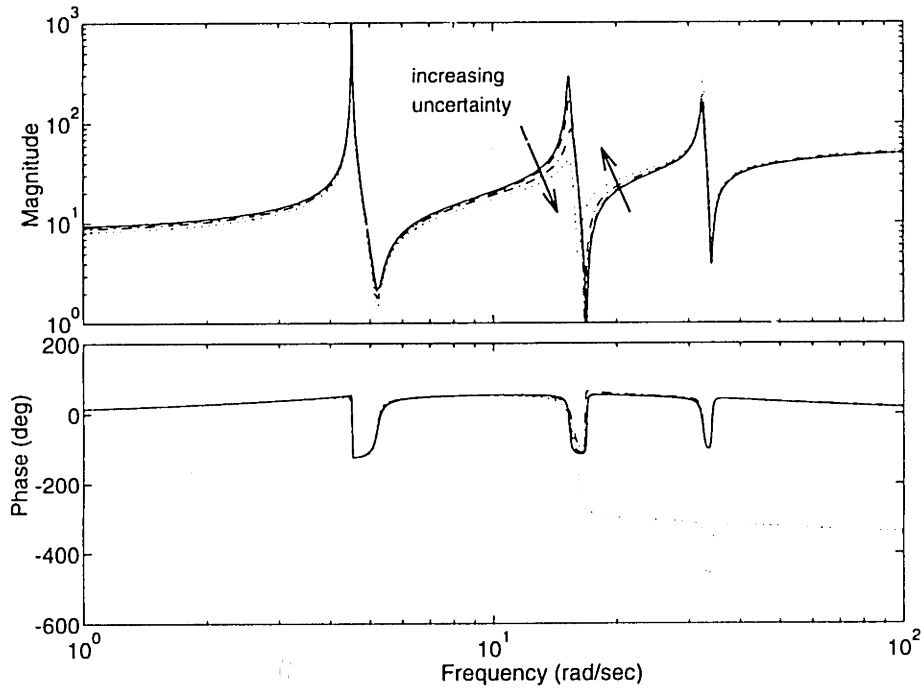

Figure 5.20: Compensator transfer functions for nominal $\mathcal{H}_\infty$ controller along with $\mathcal{H}_\infty$ designs with small but increasing robustness to uncertainty in the frequency of the third mode.

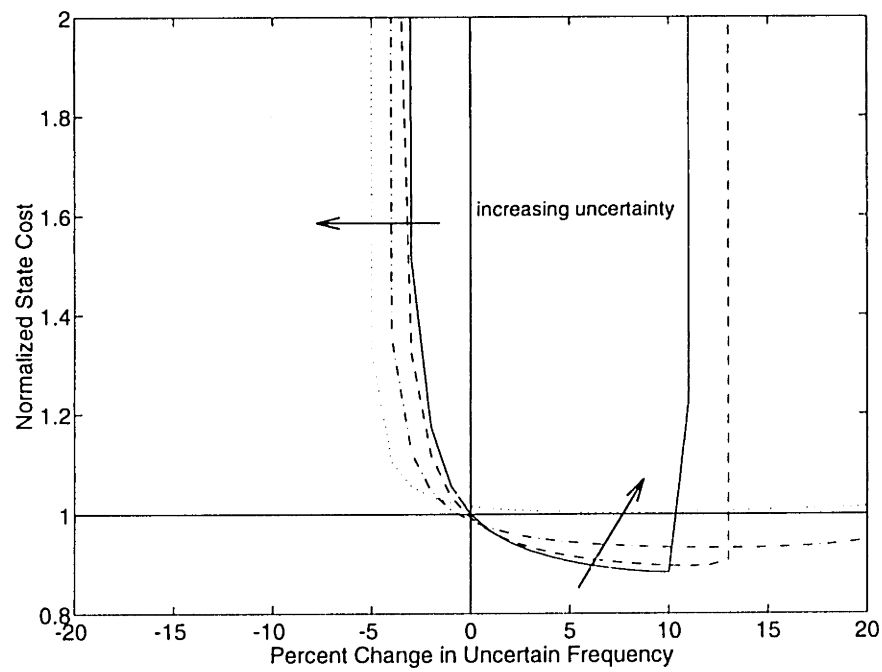

Figure 5.21: Closed loop cost of the system as a function of the frequency of the third mode of the system for a series of $\mathcal{H}_\infty$ controllers.

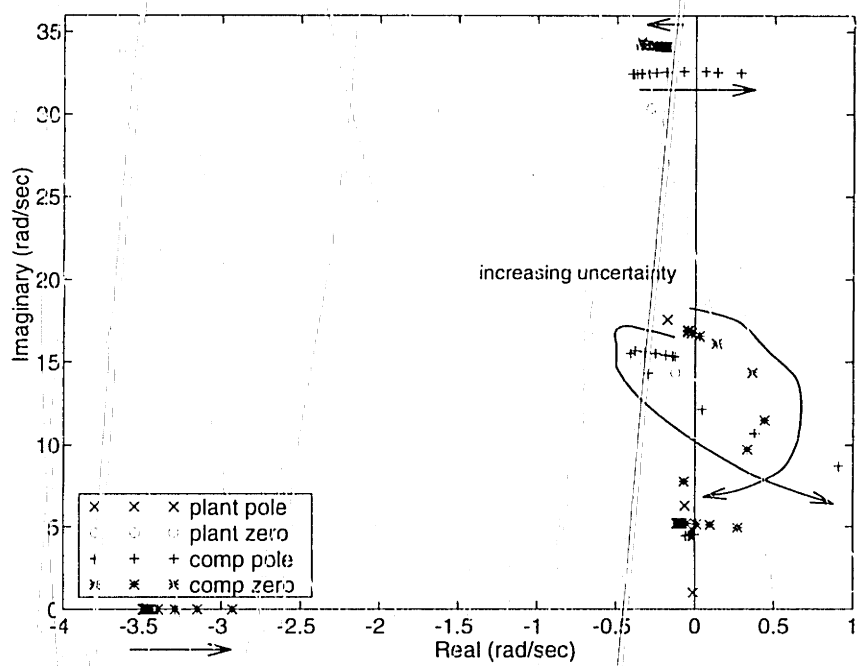

Figure 5.22: Poles and zeros of $\mathcal{H}_\infty$ compensators with increasing robustness. Closeup of the region near the $j\omega$ axis.

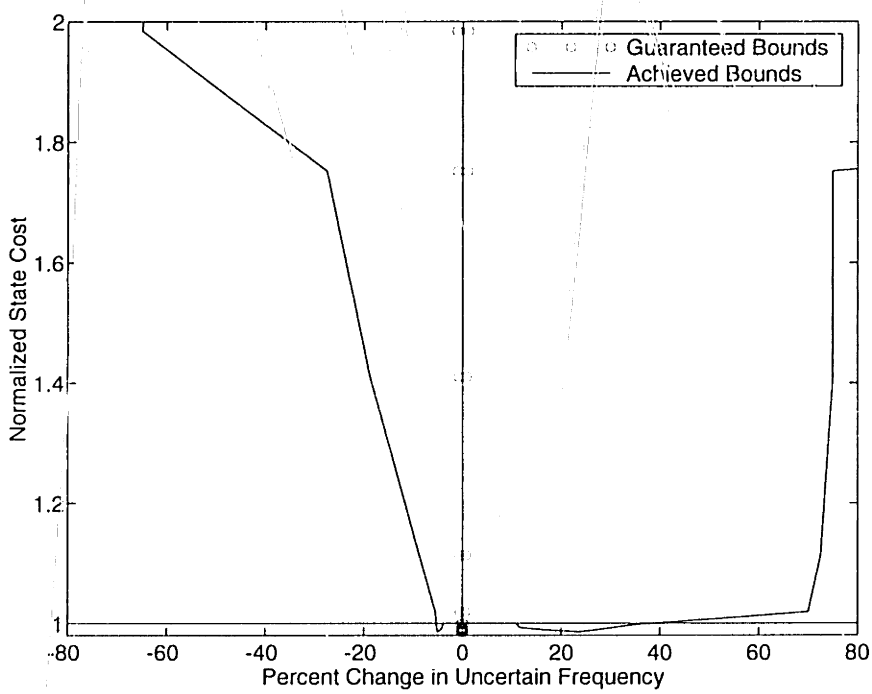

Figure 5.23: Closed loop cost on the nominal plant as a function of stability bounds.

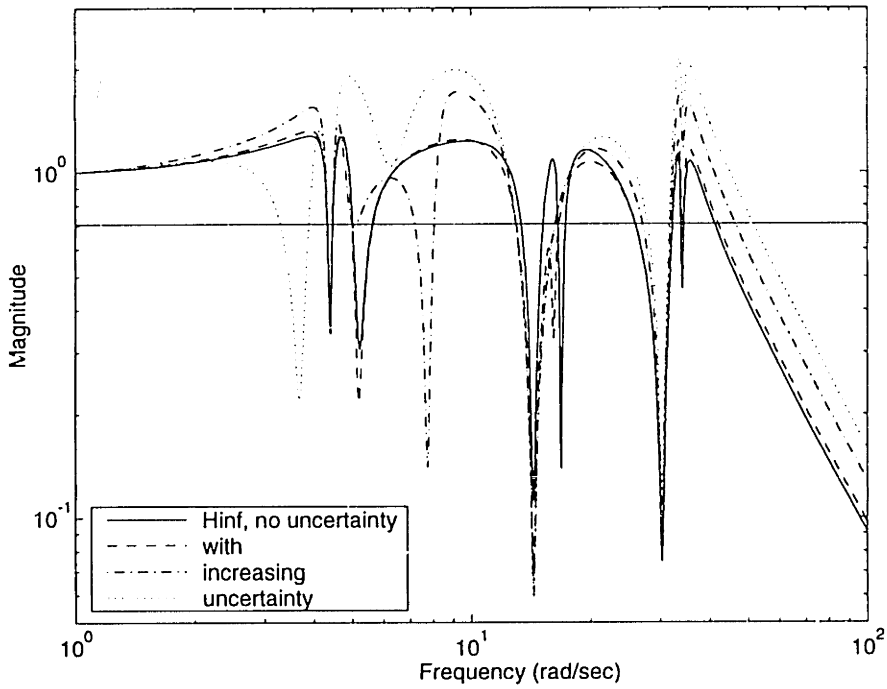

Figure 5.24: Complementary sensitivity transfer function for $\mathcal{H}_\infty$ compensators with various amounts of uncertainty.

represented in Equation 5.10. The matrices B_0 and C_0 were scaled in each design so that $|\Delta_0| \leq 1$.

The performance loop has input w_1 and output z_1. The function $W_1(s)$ is a frequency weighting function on the performance, and is identical to the weighting used in the $\mathcal{H}_\infty$ designs. The block Δ_1 represents a fictitious uncertainty and is included such that if stability is guaranteed for this loop, then the performance requirement is met.

Inputs w_2 and w_3, outputs z_2 and z_3, and the corresponding delta blocks and weighting functions are necessary to have a well-posed problem. The K step of the $D-K$ iteration is an $\mathcal{H}_\infty$ minimization. As in the preceding section, it is required that there be a feedthrough from the disturbance to the output and from the control input to the performance. The feedthrough from disturbance to output is supplied by the fictitious input w_2. The feedthrough from control input to performance is provided by the fictitious output z_3.

The blocks Δ_2 and Δ_3 represent multiplicative errors at the input and output

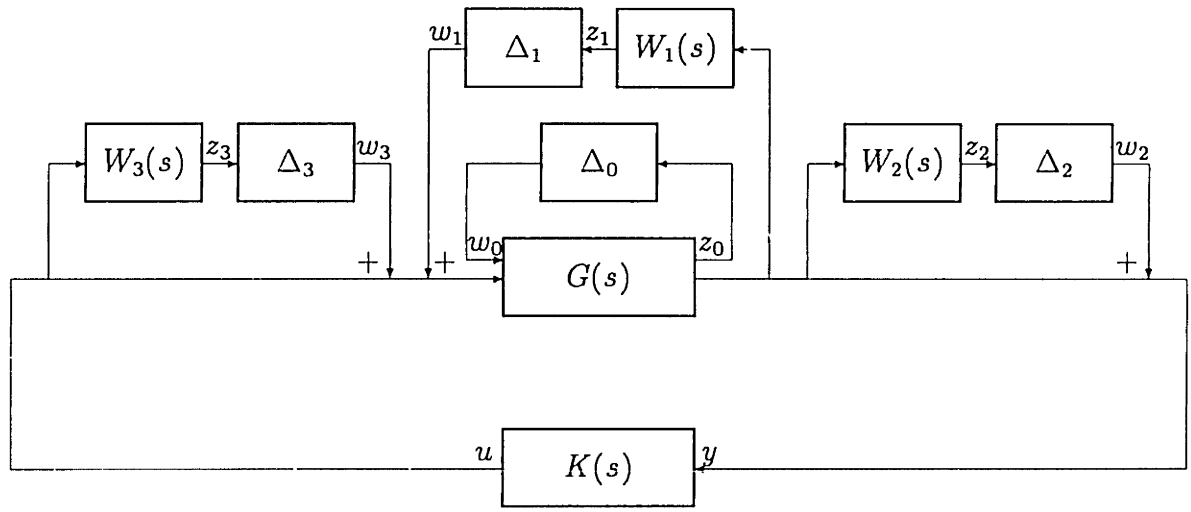

Figure 5.25: System interconnection for μ-synthesis problem.

of the system. Therefore the functions W_2 and W_3 can be used to place bandwidth limitations on the system. However, because a design which achieves a structured singular value of $\mu < 1$ ensures robust performance to the uncertainties represented by all of the delta blocks, the compensator will not only have a bandwidth constraint, but will also be constrained to be robust to all perturbations in the associated delta block. This can place much stiffer constraints on the μ compensators than were imposed on any of the compensators from the previous techniques. This makes it difficult to provide a fair comparison. Therefore, the weighting functions were set to constrain the problem as little as possible. The function W_3 was set after trial and error to a constant value of $\sqrt{0.1}$, which forces the complementary sensitivity to be less than $\sqrt{10}$ at all frequencies. Judging from the complementary sensitivities in Figure 5.17, this is a very mild constraint. The function W_2 is frequency dependent with a single zero at 9 rad/sec, a single pole at 90 rad/sec, and a DC gain of 0.2. The magnitude of the complementary sensitivity must be less than the inverse of W_2 which sets the mild constraint of a bandwidth less than about 90 rad/sec.

Four compensators were designed using μ-synthesis, corresponding to uncertainties of ± 1, 2, 4 and 6% in the frequency of the third mode. As noted in Section 3.3.4, the use of D-scales results in compensators which have a much greater number of

states than the system. Therefore, a balanced reduction technique was used to reduce the compensators to the minimum size for which the structured singular value remained less than unity. The compensators which guaranteed stability for 1 and 2% uncertainty were reduced to 15 states. The 4% compensator was reduced to 7 states. The 6% compensator was reduced to 21 states.

The structure of these four compensators is very similar despite the difference in the number of states and is also similar to that of the $\mathcal{H}_\infty$ compensators in the preceding section (see Figure 5.26). This is not surprising since the K iteration is an $\mathcal{H}_\infty$ minimization.

The differences between these four compensators can be characterized in two stages. A different approach is taken to ensure stability for small and large perturbations in the uncertain frequency (Figure 5.26). In the first stage, the frequency and damping of the compensator pole in the uncertain region is successively increased. The increases are similar to the changes that occurred in the $\mathcal{H}_\infty$ designs. However, the compensator zero is placed in the left half plane, similar to $\mathcal{H}_2$ designs. In the second stage, the compensator dynamics are completely removed from the uncertainty region by pole-zero cancellation.

For the $\pm 4\%$ and $\pm 6\%$ compensators, the consequence of cancelling the dynamics in the uncertain region are significant. Because of the cancellation, the differential gain between high and low frequency is increased. For these compensators, this results in an increase in gain at high frequency rather than a drop in gain at low frequency. Consequently, performance is not sacrificed (see Figure 5.27). However, because the gain at high frequencies is large, the bandwidth for these compensators increases to 46.7 and 47.6 rad/sec, respectively, from 43.5 rad/sec in the $\pm 1\%$ compensator. It is likely that the mild bandwidth constraint in combination with the stringent performance requirement is the reason that the bandwidth increased rather than performance decreased. In fact, the performance of the $\pm 4\%$ compensator is better than that of the 1% compensator.

Like $\mathcal{H}_\infty$ and Multiple-Model, μ-synthesis provides guarantees of robustness. Figure 5.27 shows the closed loop cost of the system with perturbed values of the un-

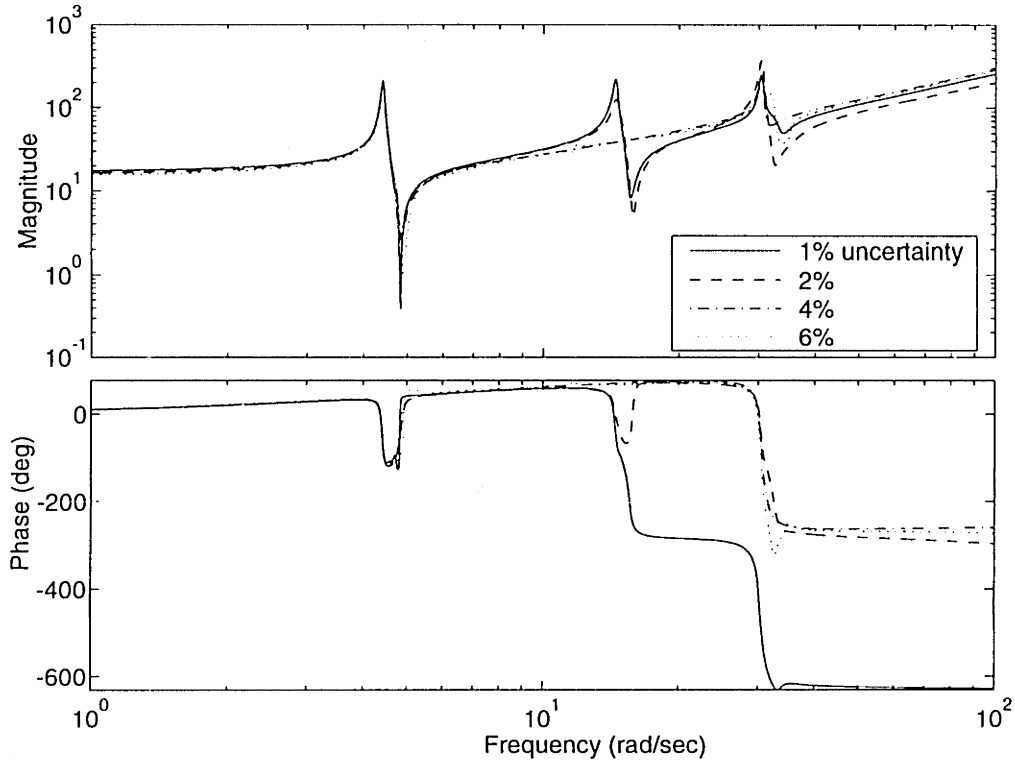

Figure 5.26: Compensator transfer function for μ synthesis compensators.

certain frequency for each of the four compensators. the guaranteed bounds are also shown. The figure demonstrates that the achieved robustness bounds for these compensators are substantially larger than the guaranteed bounds. This shows that μ-synthesis can be very conservative. In fact, designs for $\pm 8\%$ uncertainty could not achieve a structured singular value less than unity, *i.e.* could not guarantee robustness, even when the performance and bandwidth constraints were weakened. Thus the conservatism has limited μ-synthesis to guaranteeing $\pm 6\%$ uncertainty while it is clear from the $\mathcal{H}_2$ techniques that robustness can be achieved to greater than $\pm 20\%$ uncertainty. However, μ-synthesis is considerably less conservative than $\mathcal{H}_\infty$ which could only guarantee $\pm 2\%$ uncertainty with severe performance degradation.

5.2.4 Conclusions of the First Sample Problem

It has been shown in the preceding sections that all of the control techniques presented are effective at increasing robustness to uncertainty. However, the real distinction

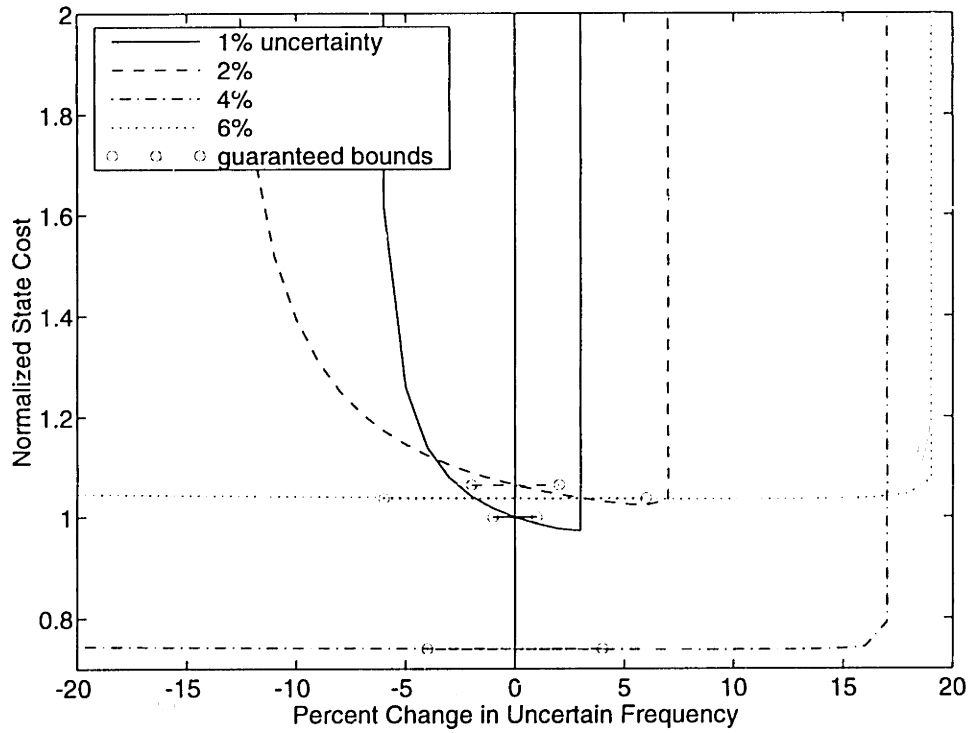

Figure 5.27: Closed loop cost of the system as a function of the frequency of the third mode of the system for four μ compensators.

between the techniques arises from how the effects of adding robustness change the bandwidth and performance of the system. For techniques which provide guarantees, conservatism also distinguishes the techniques.

The bandwidth increase and performance sacrificed as a result of increasing robustness were tracked for each of the techniques. It was shown in the preceding section that for the $\mathcal{H}_\infty$ based methods, $\mathcal{H}_\infty$ and μ-synthesis, robustness was accompanied by substantial increases in bandwidth of the compensators. The $\mathcal{H}_2$-based methods incurred much smaller bandwidth increases, with Multiple Model compensators sustaining the smallest increase. Bandwidth is an important quantity because of unmodelled dynamics. For robust stability, unmodelled dynamics place a real bandwidth constraint on a control system. Therefore, the level of control authority is limited. This implies that for a control technique which results in a small bandwidth increase as robustness increases, a higher level of control authority can be used than for a technique which incurs a large bandwidth increase when a real bandwidth

limit exists. Thus higher performance may be possible because a higher authority controller can be implemented within the same bandwidth limitation. Recall that for the μ-synthesis compensators, due to mild bandwidth constraints and stringent performance constraints, the performance did not vary significantly. However, substantial bandwidth increases resulted as the robustness was increased.

The performance/robustness trade-off can clearly be seen for the SWLQG, ME, MM, and $\mathcal{H}_\infty$ techniques in Figure 5.28. This figure shows the nominal closed loop cost of the system as a function of the achieved stability bounds. The performance/robustness trade-off can be seen by the fact that the closed loop cost increases as wider robustness bounds are achieved. For a given cost, all of the techniques can tolerate a larger positive than negative perturbation. Therefore, the negative perturbation is the worst case perturbation. It is clear from the figure that in comparison to any of the three $\mathcal{H}_2$ techniques, $\mathcal{H}_\infty$ sacrifices much more performance for equivalent worst case bounds. The $\mathcal{H}_2$ based methods sacrifice only a small amount of performance. For this sample problem there appears to be very little difference in performance sacrifice between these methods. However, it should be noted that Multiple Model compensators sustain the least performance loss for equivalent worst case bounds. It should also be noted that while the SWLQG compensators sacrifice only slightly more performance, they do so with a wider bandwidth.

For the techniques that provide some guarantees to robustness, the conservatism can be compared. Conservatism is an important quantity for the same reason that bandwidth is important. If a technique is overly conservative, then in providing robustness guarantees to a particular amount of uncertainty, it actually achieves much wider uncertainty bounds. But at the same time, it sacrifices the performance that attaining these achieved bounds requires. If the technique were less conservative, less performance would be sacrificed in guaranteeing equivalent bounds. In addition, it may not be possible for a compensator to guarantee robustness to a particular uncertainty, even if it actually achieves robustness. This was true for μ-synthesis which could not guarantee robustness to 8% uncertainty despite achieving robustness to 18%. It was also true for $\mathcal{H}_\infty$ compensators which achieved uncertainty bounds

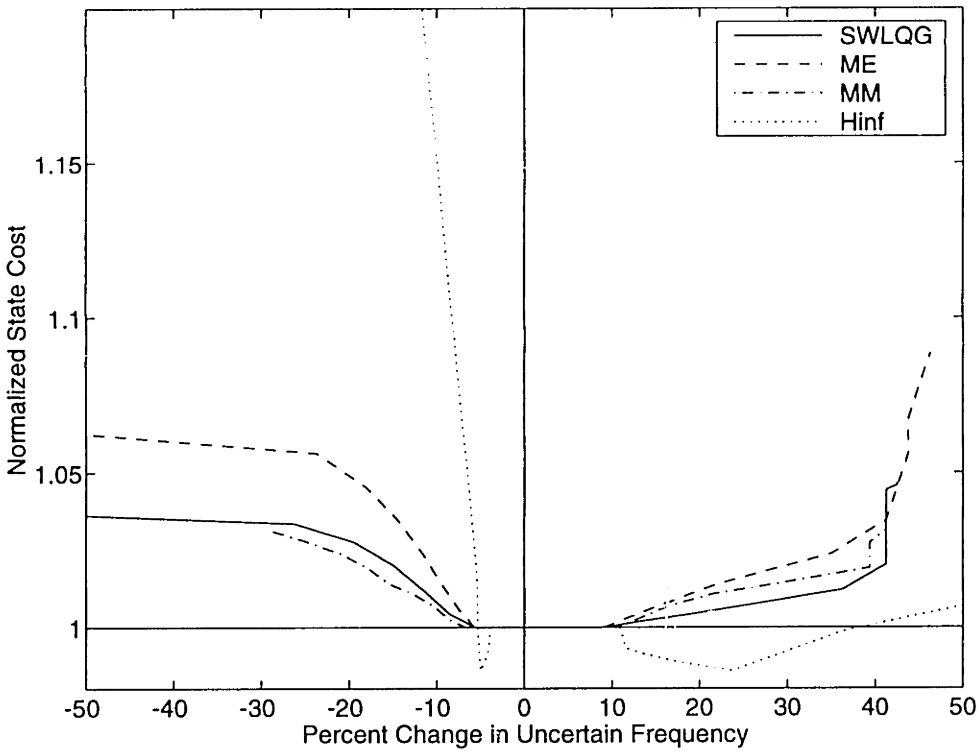

Figure 5.28: Closed loop cost on the nominal plant as a function of achieved stability bounds for SWLQG, ME, MM and $\mathcal{H}_\infty$ compensators.

greater than 50% but guaranteed to only 2% uncertainty (Figure 5.23).

Comparing the achieved and guaranteed bounds in Figures 5.18, 5.23, and 5.27, which show the achieved robustness bounds and the guaranteed robustness bounds for MM, $\mathcal{H}_\infty$ and μ compensators, it can be clearly seen that the achieved guaranteed robustness bounds are closest together for the Multiple Model technique. Thus the Multiple Model technique is the least conservative of these methods. However, this statement must be qualified by the fact that Multiple Model guarantees stability only at the points indicated in Figure 5.18. It does not guarantee stability for intermediate values of the uncertain parameter. From Figure 5.23 it can be seen that the robustness guarantees provided by $\mathcal{H}_\infty$ are almost negligible. μ-synthesis designs, while much less conservative than $\mathcal{H}_\infty$, encountered significant conservatism. Robustness could not be guaranteed for uncertainties greater than 6% despite weakening of the performance and bandwidth constraints.

Because of the conservatism in the μ approach, and the problems with compen-

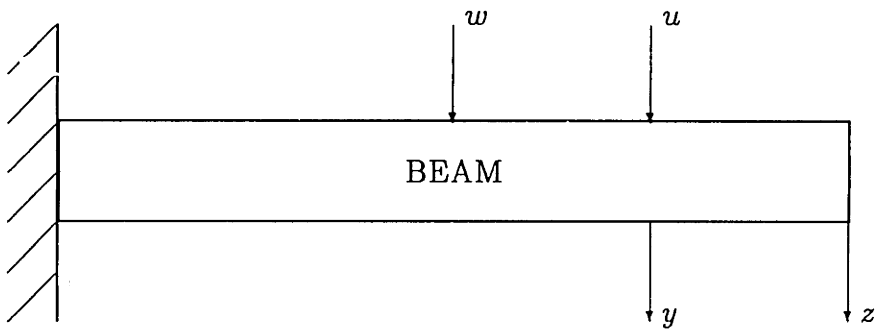

Figure 5.29: Schematic drawing of BE beam with non-degenerate inputs and outputs.

sator and system order in dealing with a large number of uncertainties for practical examples (such as the experiment in Chapter 6), the μ-synthesis technique will not be investigated further. Similarly, because of the extreme conservatism of the $\mathcal{H}_\infty$ designs, and the large decrease in performance for achieved bounds compared to the $\mathcal{H}_2$ methods, the $\mathcal{H}_\infty$ synthesis technique will not be investigated further. Further comparison of the $\mathcal{H}_2$ methods will be made in the following section, by comparing compensators designed for the same system with a different input-output configuration.

5.3 Sample Problem #2

In this sample problem, the control input and sensor output are collocated at the 3/4 point of the beam, while the disturbance input is located at the midpoint of the beam, and the performance output is located at the tip of the beam (Figure 5.29). In the notation of the standard system, Equation 3.1,

$$C_y = C_3,\ C_z = C_4,\ B_u = B_3,\ B_w = B_2\,. \tag{5.13}$$

Thus the topology is non-degenerate.

Figure 5.30 shows the transfer function from each of the two inputs to each output. Notice that the third mode is not very observable in the performance loop, but is important in the control loop. In contrast, the second mode of the system is nearly

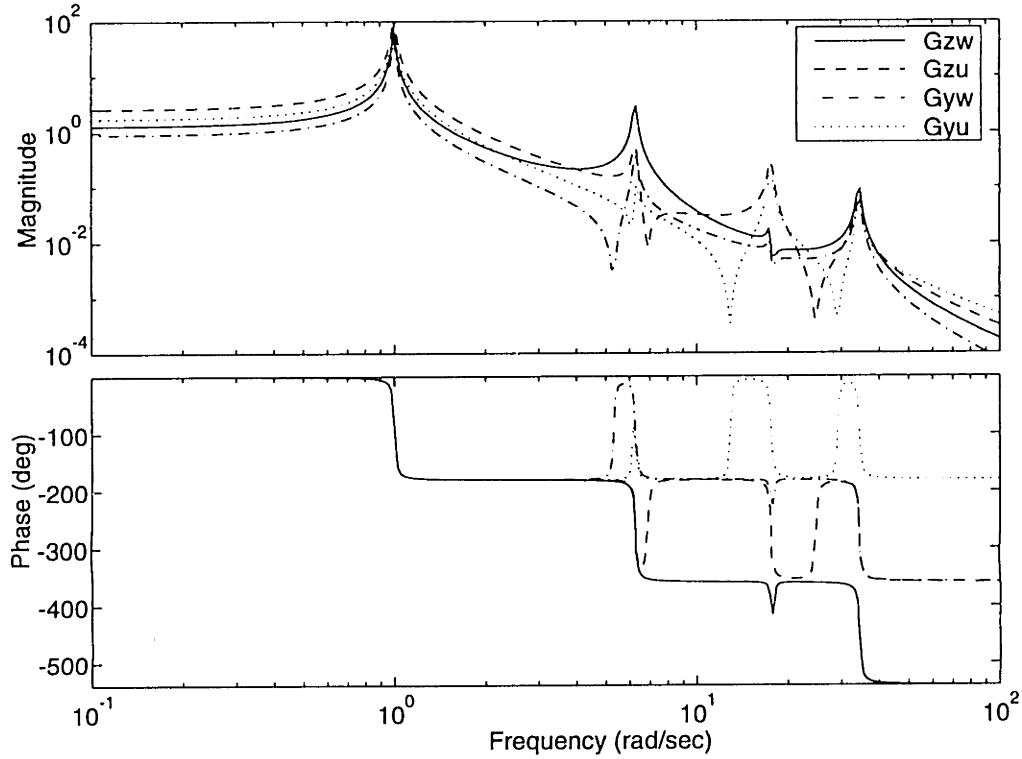

Figure 5.30: Four transfer functions for input output loops.

unobservable in the control loop but important in the performance loop. Also, note the position of zeros near the second mode in the off-diagonal transfer functions (G_{zu} and G_{yw}). These transfer functions are important because control for a non-degenerate problem is fundamentally quite different from control for a problem with either input degeneracy, output degeneracy or both. For the general control problem, the closed loop transfer function is

$$G_{cl} = G_{zw} - G_{zu}K(I + G_{yu}K)^{-1}G_{yw} \,. \tag{5.14}$$

If any degeneracy occurs, the expression for the closed loop transfer function can be reduced to $G_{cl} = (I + G_{yu}K)^{-1}G_{zw}$, for which a large K tends to make the output small. This is not necessarily true in the non-degenerate case . G_{cl} can be minimized by a subtraction of the two terms, which does not require that K be large. As will be shown in the next section, the zeros of the off-diagonal transfer functions play an important role in the subtraction, and limit how well it can be performed.

As with the preceding problem, the third mode of the system is considered un-

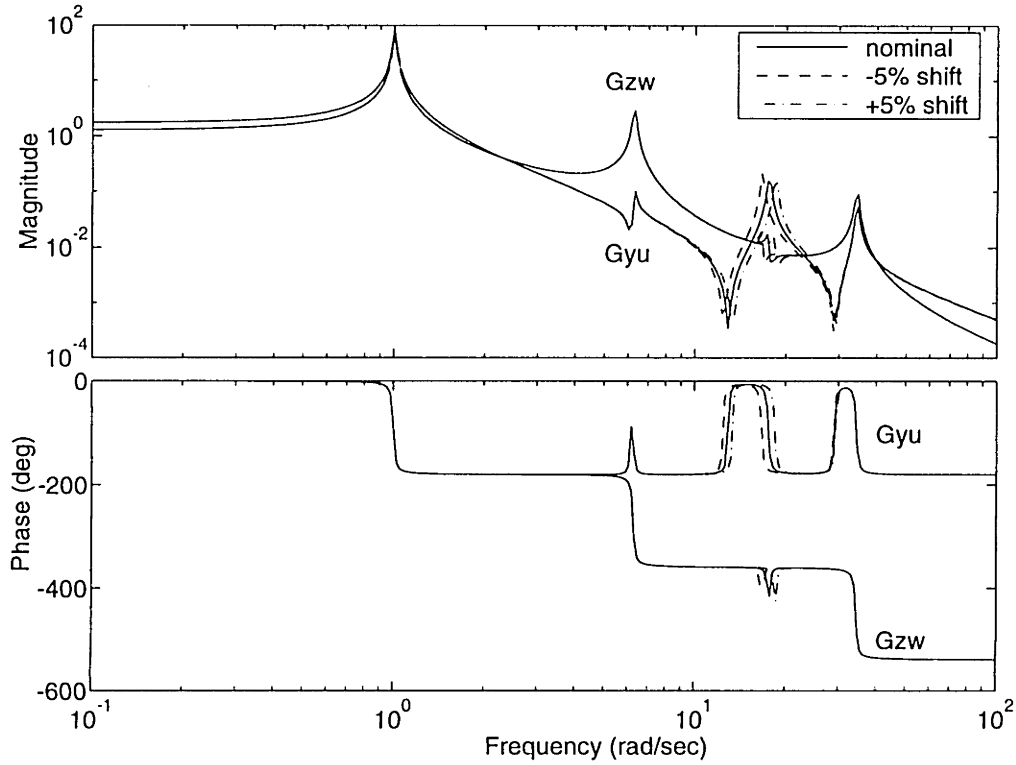

Figure 5.31: G_{zw} and G_{yu} for the nominal plant and plants with $\pm 5\%$ perturbations in the frequency of the third mode.

certain. Figure 5.31 shows the disturbance to performance transfer function, G_{zw}, and the input to output transfer function, G_{yu}, for the nominal plant and for the plant with $\pm 5\%$ perturbations in the uncertain mode. In the 10–30 rad/sec range significant differences between the nominal and perturbed plants exist. Therefore, this region is denoted the uncertain region.

In this section, the results of designing compensators for this system will be presented, and will be compared using the criteria in Chapter 4. As in Section 5.2, first an LQG compensator is presented for later comparison with controllers designed using SWLQG, Maximum Entropy and Multiple Model. The $\mathcal{H}_\infty$ and μ-synthesis techniques will not be investigated on this problem. The compensators designed using SWLQG, ME , and MM for this problem do not share the same degree of similarity as in the preceding problem, and will therefore be presented in separate sections.

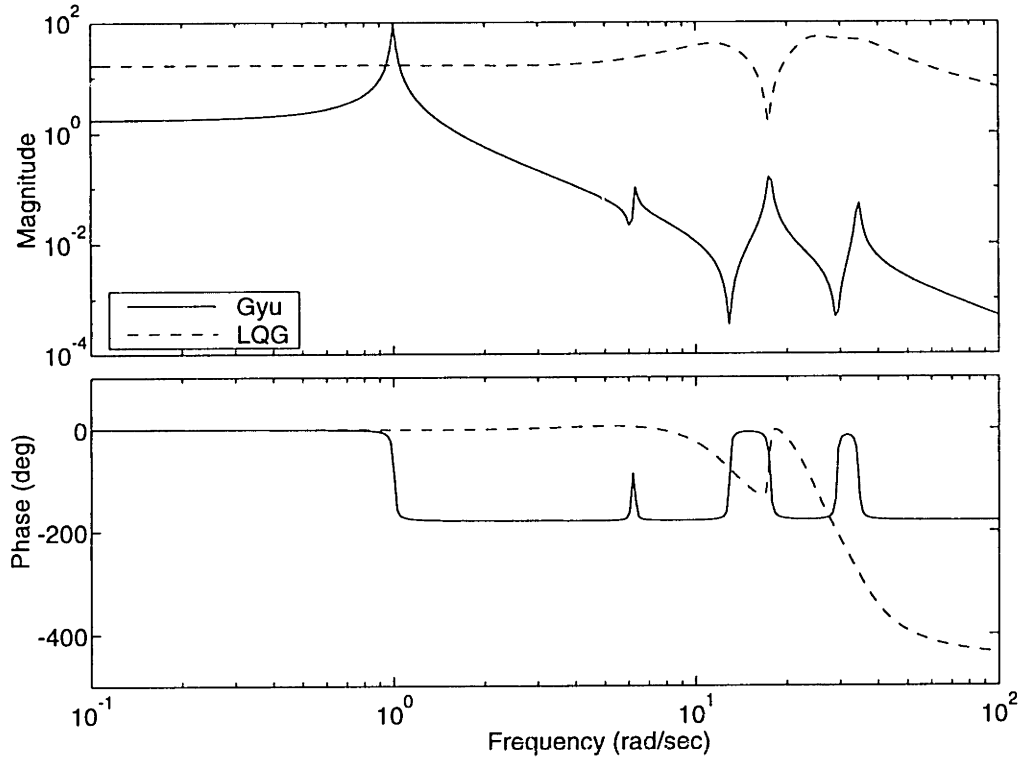

Figure 5.32: Frequency responses of control loop, G_{yu}, and LQG compensator.

5.3.1 LQG

Using the same procedure as in Section 5.2.1, a series of LQG controllers with a bandwidth of approximately 40 rad/sec was designed. Again, the most robust of these was selected for comparison with compensators designed using robust control techniques. Designed with sensor noise intensity $\theta = 10^{-4}$ and control weighting $\rho = 10^{-4}$, the selected compensator achieves stability robustness bounds of -4% and $+8\%$ for perturbations in the uncertain mode.

The frequency response of this compensator and the control loop (G_{yu}) are shown in Figure 5.32. A robustness problem is encountered due to the very lightly damped zero at 17 rad/sec, and its proximity to the uncertain mode. This compensator zero is present at all but the lowest levels of control authority. Because the third mode has little effect on the cost of the system, a notch has been placed near it in order to gain stabilize in the region around the third mode. Because the zero is placed slightly

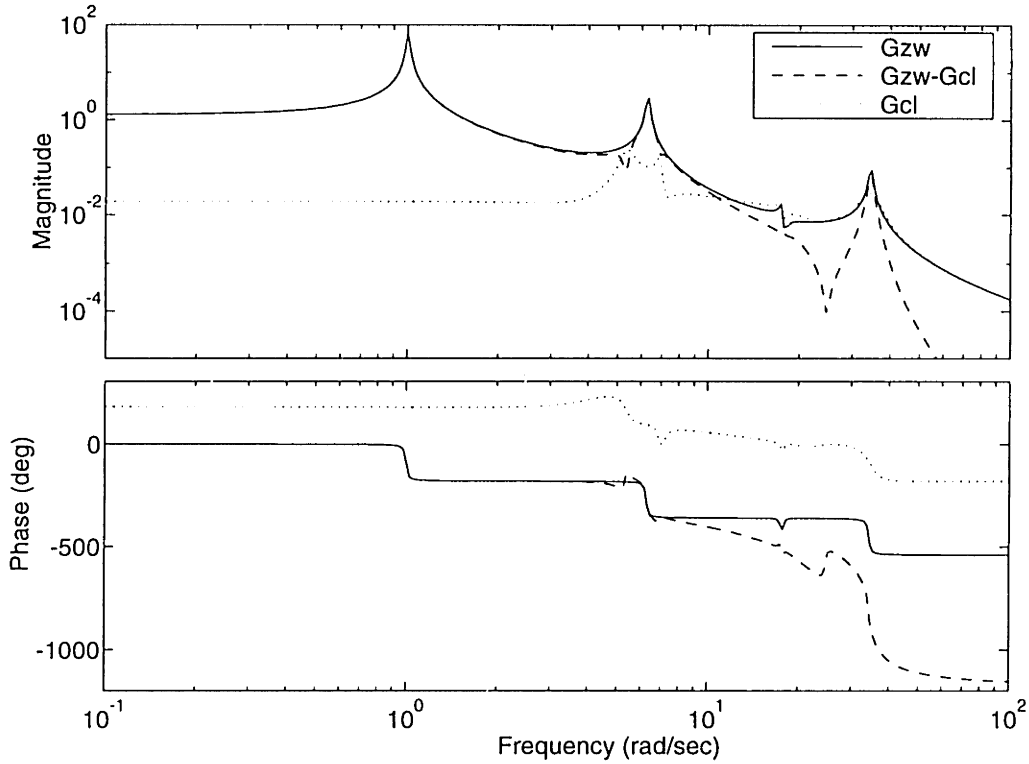

Figure 5.33: G_{zw}, $G_{zu}K(I+G_{yu}K)^{-1}G_{yw} = G_{zw} - G_{cl}$, and G_{cl} for the LQG controller applied to the nominal model.

above the nominal frequency of the plant pole, it requires a smaller negative than positive perturbation of the uncertain pole to destabilize the system. In both cases, instability occurs when the plant pole shifts sufficiently such that the notch no longer gain stabilizes the system.

Recalling the expression for the closed loop performance, Equation 5.14, Figure 5.33 shows G_{zw}, $G_{zw} - G_{cl} = G_{zu}K(I + G_{yu}K)^{-1}G_{yw}$ and G_{cl} for this compensator. Note that the subtraction is poor in the 4–8 rad/sec range around the second mode. The frequency response of this region contributes 90% of the closed loop cost. The two peaks which occur in the closed loop frequency response, G_{cl}, are due to the zeros of the off-diagonal terms of the transfer function matrix, G_{zu} and G_{yw}.

The three robust control techniques (SWLQG, ME, and MM) each approach providing robustness to the uncertain mode in a different way. Therefore, each will be discussed separately beginning with SWLQG.

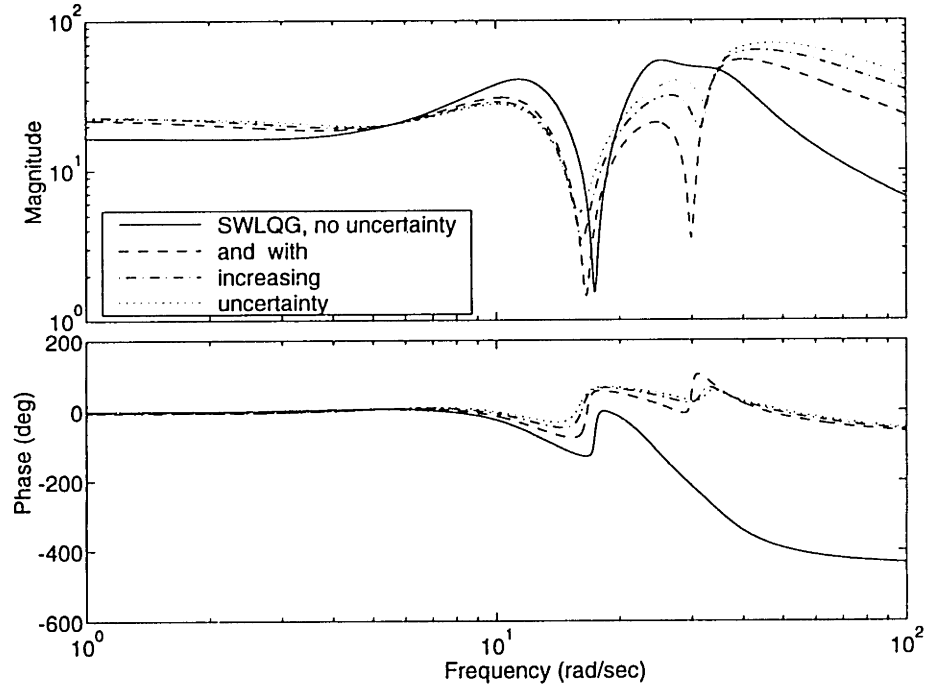

Figure 5.34: Compensator transfer functions for a series of SWLQG controllers.

5.3.2 Sensitivity Weighted LQG (SWLQG)

This section begins with a discussion of the primary effects of adding robustness to SWLQG compensators. This will be followed by a discussion of the secondary effects of these compensators. While the primary effects are quite different for the different robust control techniques, the secondary effects are similar.

The SWLQG approach for this problem is primarily to phase stabilize the uncertain region. To do so, three significant changes occur in the compensator. Figure 5.34 shows the frequency response for a series of SWLQG compensators with increasing sensitivity weights. Figure 5.35 shows the poles and zeros of the compensator plotted in the complex plane. The first figure is useful for observing changes in the frequency response due to the changes in location of the complex poles and zeros of the compensator. The second makes changes to the real poles and zeros more evident than a frequency response function.

The first of the three significant changes concerns the notch that LQG places at 17 rad/sec. As sensitivity weighting is increased, the zero in this notch is placed at a

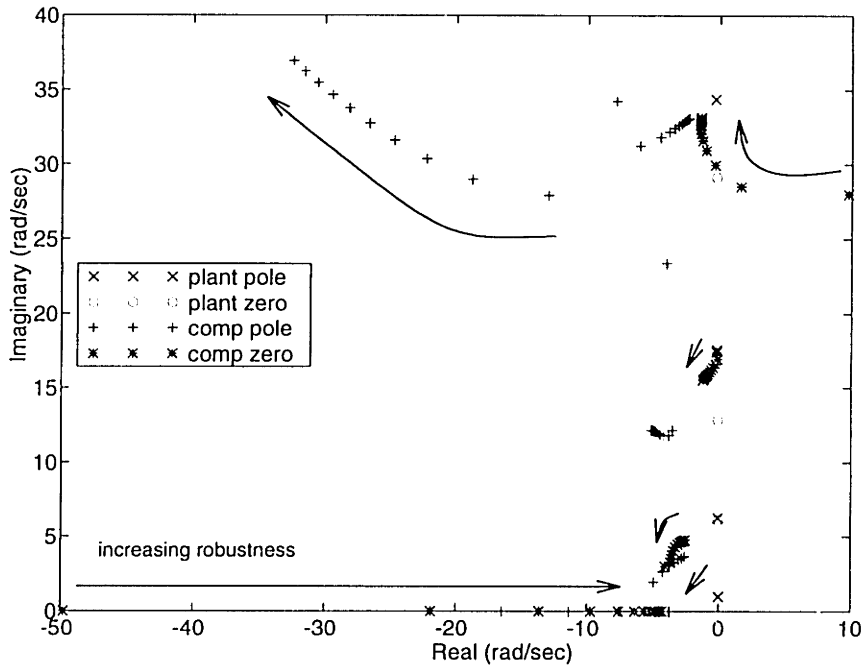

Figure 5.35: Poles and zeros of SWLQG compensators with increasing robustness.

lower frequency and is damped. The second change concerns a complex nonminimum phase zero that LQG has placed near 33 rad/sec. SWLQG places this zero at higher frequency and in the left half plane. The third change is a shift in the frequency of the real zero which LQG has placed at 50 rad/sec. The frequency of this zero is reduced by nearly a decade to the 5–10 rad/sec range as sensitivity weighting is increased. This creates a significant amount of lead in the uncertain region which can be seen by comparing the phase in the LQG compensator (SWLQG with no uncertainty) and the SWLQG compensators in Figure 5.34. The effect of these changes is to phase stabilize in the uncertain range. This can be seen in Figure 5.36 which shows the loop transfer function for the LQG and an SWLQG compensator on the nominal plant.

The most important secondary effect involves the frequency response of the compensator in the 4–8 rad/sec region that is critical to performance. Figure 5.34 shows that the slope of the magnitude of the frequency response in this region is lower as sensitivity weighting is increased. This is caused by the heavily damped low frequency poles and zeros that can be seen in Figure 5.35. As sensitivity weighting is increased,

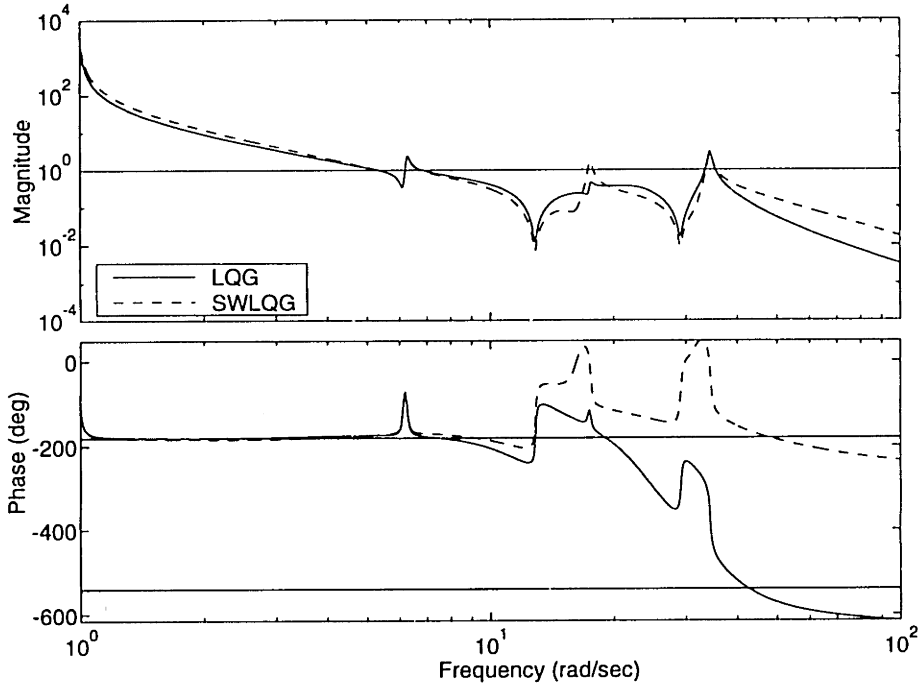

Figure 5.36: Loop transfer functions for LQG and SWLQG compensators on nominal plant.

these poles and zeros become more heavily damped. These changes have little effect on the robustness, and are therefore secondary effects. While the change seems to be relatively small, it has dire consequences. Figure 5.37 shows $G_{zu}K(I+G_{yu}K)^{-1}G_{yw}$, G_{zw}, and G_{cl} from 1–10 rad/sec for both the LQG and an SWLQG controller. It can be seen that the effect of the change in slope has caused the subtraction in this region to be less exact. As a result, the closed loop response G_{cl} is higher for SWLQG than LQG and the performance is decreased.

5.3.3 Maximum Entropy (ME)

For this sample problem, Maximum Entropy relies on providing phase margin so that the loop gain can cross unity over a broad range of frequencies. It does so in a manner that is quite different from the SWLQG compensators of the preceding section. Rather than providing lead and using minimum phase zeros to maintain the loop phase between $\pm 180°$, ME uses a combination of lag and lead in different frequency ranges to drop the loop phase below $-180°$ at a frequency well below the

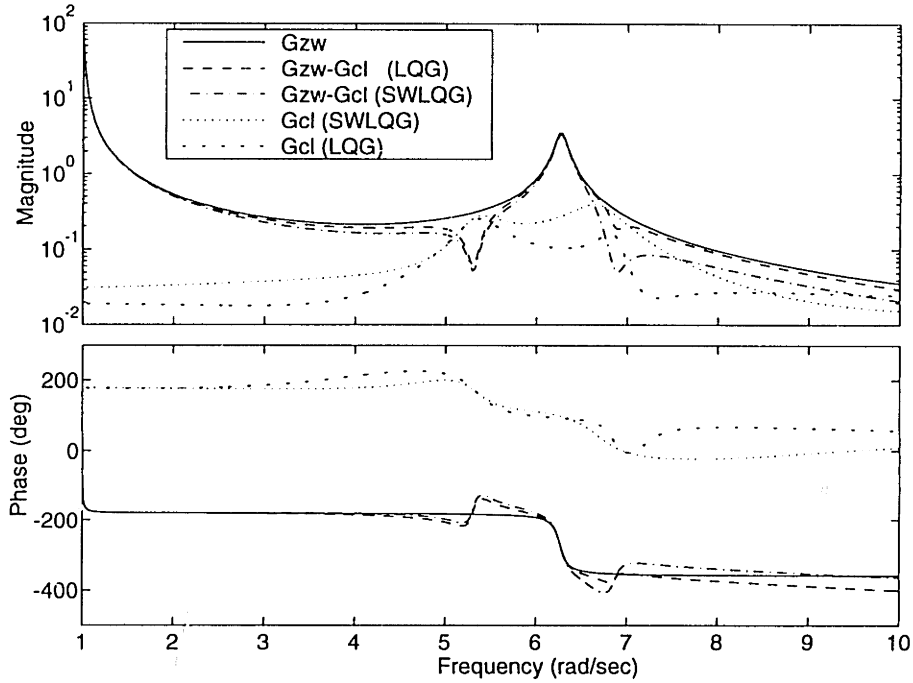

Figure 5.37: G_{zw}, $G_{zu}K(I+G_{yu}K)^{-1}G_{yw} = G_{zw} - G_{cl}$, and G_{cl} for SWLQG and LQG controllers.

uncertain pole and then maintain the loop phase above $-540°$ until a frequency well above the uncertain pole.

This combination of lag and lead is evident in Figure 5.38 in which an ME loop is compared with the LQG loop. To drop the loop phase below $-180°$ at a frequency well below the frequency of the uncertain pole, the ME compensators provide lag at frequencies below the nominal frequency of the uncertain pole. Using this lag, the 180° phase drop caused by the uncertain pole is located well between the $-180°$ and $-540°$ marks. Lead is used at frequencies above the uncertain pole to push the $-540°$ phase crossing higher in frequency. By not cancelling the uncertain pole with a compensator zero, the ME compensator ensures that only small changes occur in the loop phase. Changes caused by a shift in the frequency of the uncertain pole merely change the frequency of the 180° phase drop which is already plainly seen.

The means by which the ME compensators provide lag and lead in the appropriate region becomes evident by comparing ME compensators with varying degrees of robustness. Figure 5.39 shows the compensator transfer function for a series of

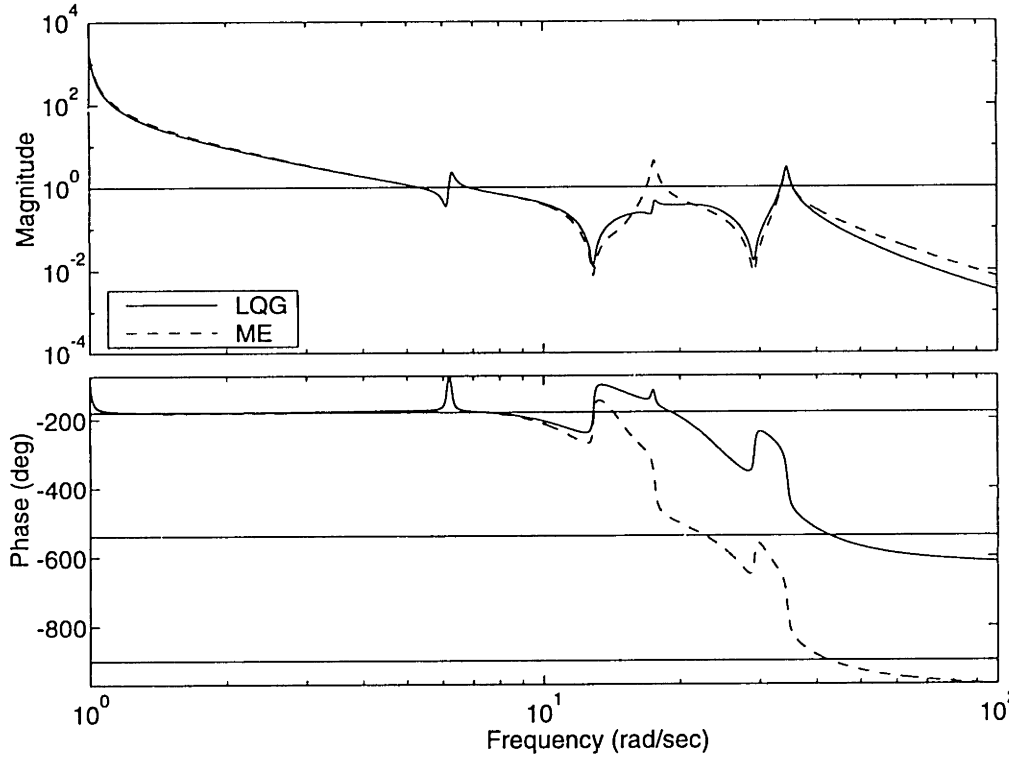

Figure 5.38: Loop transfer function for the nominal plant with an ME and LQG controller.

ME compensators which achieve progressively more robustness. Note that in the region from 10–20 rad/sec, the lightly damped minimum phase zero has been replaced by a more heavily damped nonminimum phase zero which has been placed at a lower frequency. In addition, the heavily damped compensator pole located at about 11 rad/sec is shifted down in frequency. The shifting of this pole results in phase lag which, along with the lag contributed by the nonminimum phase zero, allows the loop phase to cross $-180°$ at a frequency well below that of the nominal uncertain pole location. These changes permit large negative perturbations in the uncertain pole frequency.

At frequencies above the now heavily damped nonminimum phase zero, additional phase permits an increase in the range of positive perturbations that can occur. Lead is provided by two of the compensator changes that are shown in Figure 5.40. As uncertainty weighting is increased, the location of the real zero (nominally at 50 rad/sec) shifts to the 18-20 rad/sec range. In addition, the compensator pole that

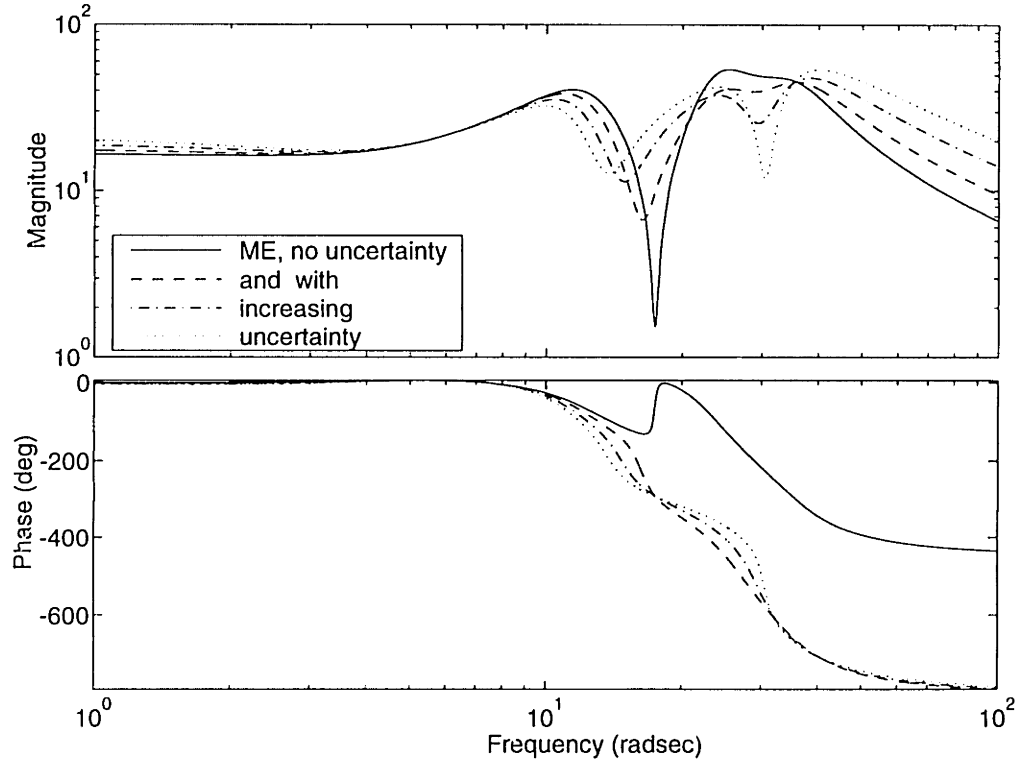

Figure 5.39: Compensator transfer functions for a series of ME controllers.

is nominally located at approximately 25 rad/sec is shifted higher in frequency. This change shifts the phase lag associated with the pole to higher frequency thus creating a net lead at frequencies below the pole. Associated with the increase in lead is an increase in gain at high frequency which causes a small increase in the bandwidth of the ME compensators.

An important secondary effect again affects the frequency response in the 4–8 rad/sec range. As uncertainty weighting is increased, the heavily damped low frequency poles shown in Figure 5.40 remain at the same damped frequency, however the damping in these poles increases. Also, the real zero which is nominally located near 3 rad/sec shifts up in frequency. The result is again a change in slope in the frequency response of the compensator in the 4–8 rad/sec range that can be seen in Figure 5.39. In comparison to the SWLQG compensators, the effect is very small, however, it is present and results in a decrease in performance for the ME compensators.

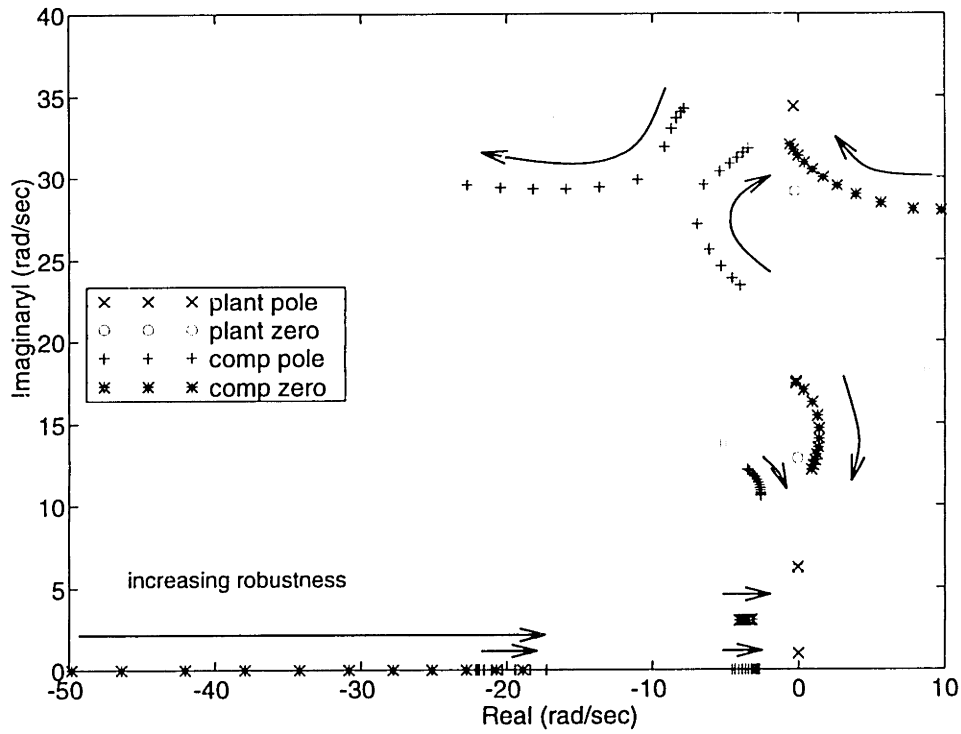

Figure 5.40: Poles and zeros of ME compensators with increasing robustness.

5.3.4 Multiple Model (MM)

The Multiple Model technique uses a different approach to increase robustness. It relies on gain stabilization in the uncertain region rather than phase stabilization. Figures 5.41 and 5.42 show two ways by which gain stabilization is achieved. First, notice that the lightly damped zero which LQG used to cancel the uncertain pole is also present in the MM compensators. The zero is in the left half plane for some compensators and the right half plane for others. However, the frequency of this zero is reduced as greater uncertainty is considered and robustness increases. For negative perturbations in the uncertain pole, the notch is more effective than in LQG.

As shown in Figure 5.41, above 18 rad/sec the compensator gain is reduced as greater uncertainty is included in the formulation of the MM problem. The reduction in gain is primarily the result of decreased damping in the nonminimum phase zero nominally located at 30 rad/sec. As it becomes more lightly damped, a notch is generated. The gain in the compensator between the very deep notch below 17 rad/sec,

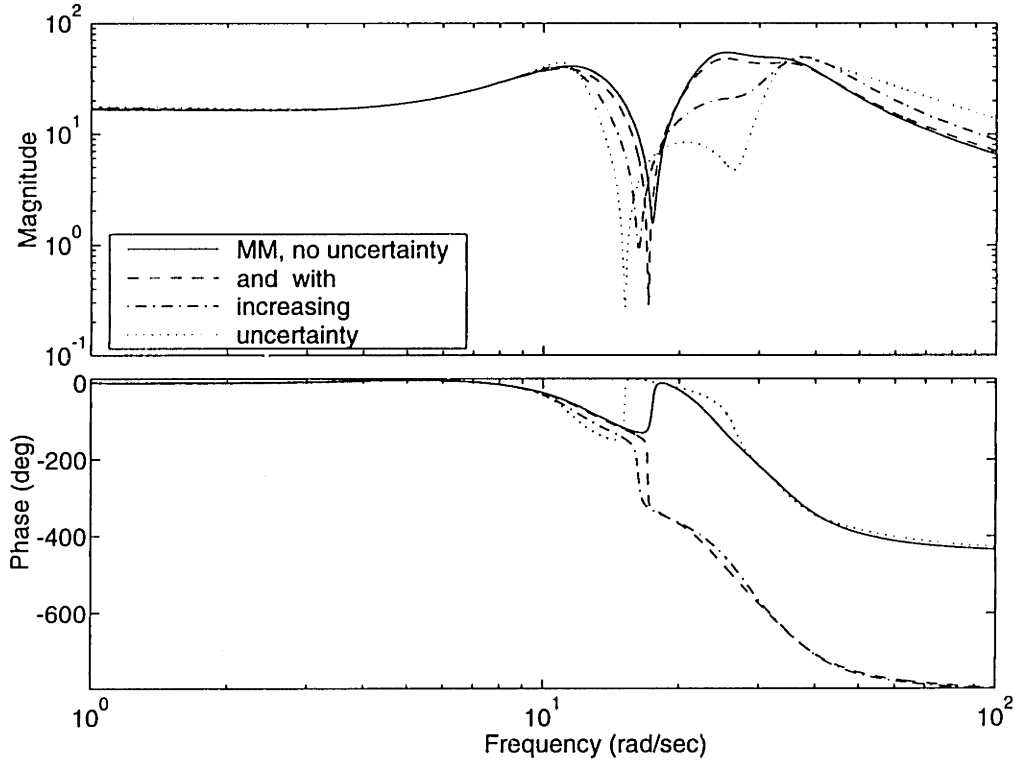

Figure 5.41: Compensator transfer functions for a series of MM controllers.

and the notch at 30 rad/sec, is much lower than the gain in the LQG controllers. This results in gain stabilization for large positive perturbations.

Some secondary effects occur as well. Note that Figure 5.42 shows that the real zero nominally located at 50 rad/sec has been shifted lower in frequency. For the SWLQG and ME techniques this was one of the primary effects because it resulted in phase lead which permitted phase stabilization. This shift has very little effect on the gain stabilization by which MM increases robustness, therefore it is a secondary effect. As uncertainty is increased, this real zero is placed at a lower frequency. This causes the gain at high frequencies to rise and a small increase occurs in the bandwidth of the MM compensators. Figure 5.41 shows that in the 4–8 rad/sec range, the MM compensators have nearly an identical frequency response as the LQG compensator. The secondary effect which dominated the ME and SWLQG approaches is not present in the MM approach.

Recall that Multiple Model provides some guarantees of robustness. Therefore,

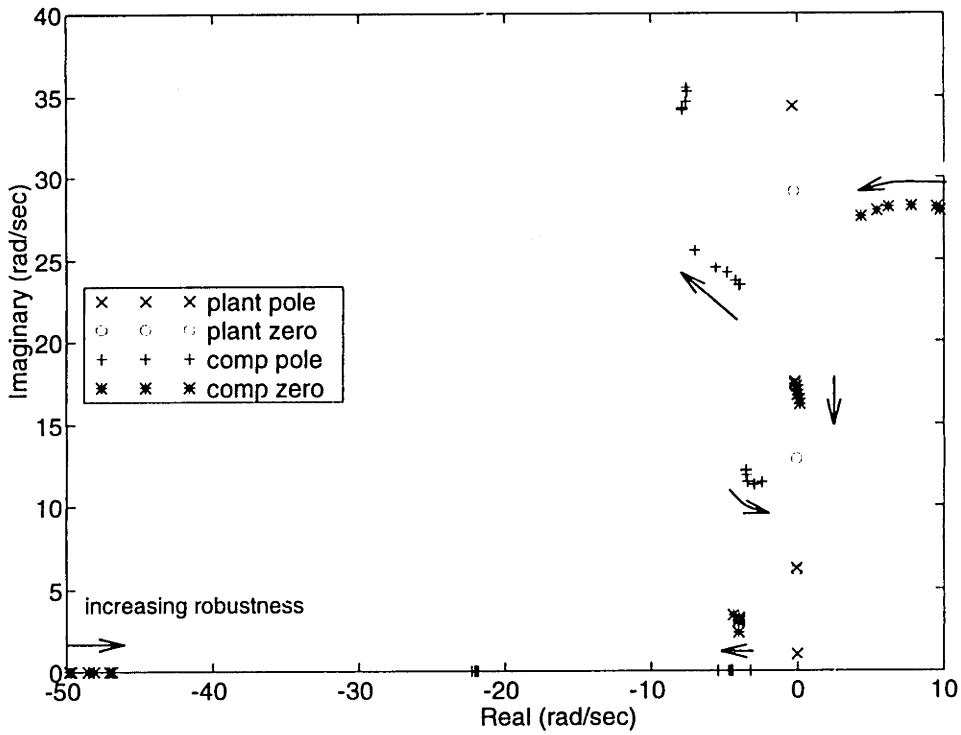

Figure 5.42: Poles and zeros of MM compensators with increasing robustness.

the conservatism of the technique must be addressed. Figure 5.43 shows the nominal closed loop cost plotted as a function of the achieved uncertainty bounds and the points at which MM guarantees stability. Note that the guaranteed points for negative perturbations are almost the same as the achieved bounds. This indicates that for this problem the Multiple Model approach has very little conservatism.

5.3.5 Conclusions

Once again, all of the control techniques presented are effective at increasing robustness to uncertainty. For this problem, however, the performance degradation that results from increased robustness leads to a much clearer distinction between the control techniques.

Figure 5.44 shows the frequency response of the nominal LQG compensator and SWLQG, ME and MM compensators that achieve robustness to 18% perturbations in the uncertain modal frequency. The figure shows that the SWLQG compensator has

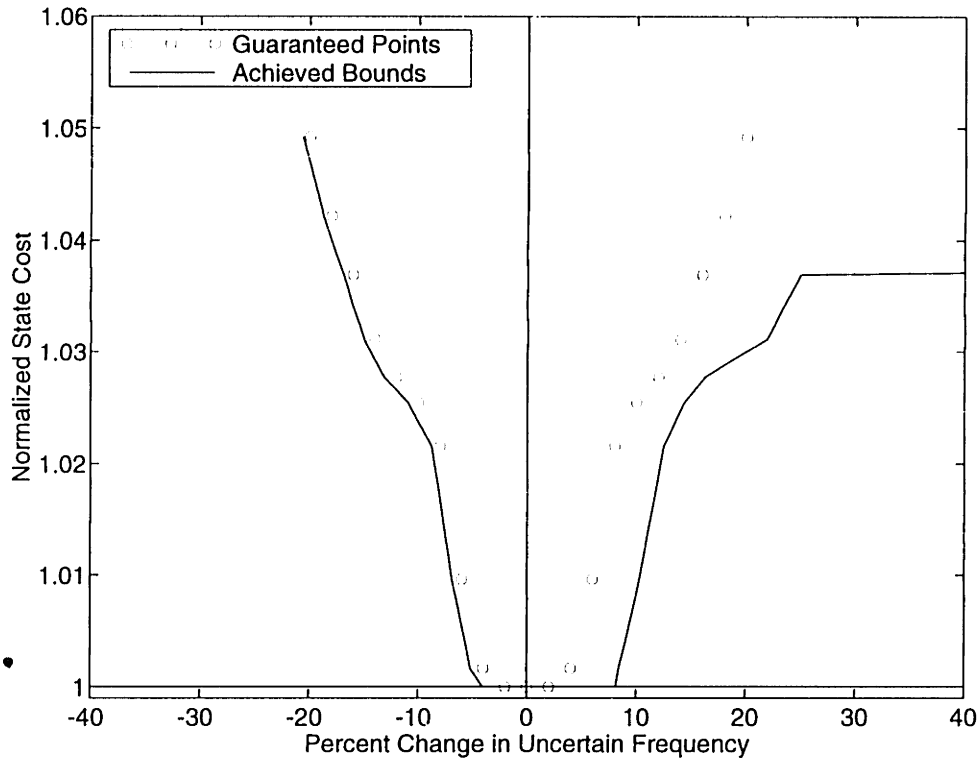

Figure 5.43: Closed loop cost on the nominal plant as a function of stability bounds for MM compensators.

a much higher gain at high frequency than either the MM or ME compensators. The consequences of higher gain do not affect the performance in this sample problem. However, if sensor noise were present, it would reduce the closed loop performance to a greater extent for the SWLQG compensators then for the MM or ME compensators. Note that below 10 Hz, and particularly in the 4–8 Hz region that is critical for performance, that the frequency response of the MM compensator is the closest to that of the optimal LQG compensator. Figure 5.45, which plots the closed loop frequency response of the system, shows that the performance loss occurs mostly in this 4–8 rad/sec range. As discussed earlier, this region contributes most to the closed loop cost because of zeros in the off-diagonal terms in the transfer function matrix. The secondary effects of robustification which were noted in the preceding sections, cause the subtraction of G_{zw} and $G_{zu}K(I+G_{yu}K)^{-1}G_{yw}$ to be less accurate. Therefore, because the MM compensators had the smallest secondary effects, it had the least performance loss.

The performance robustness trade-off can be seen more directly in Figure 5.46. In this figure, the nominal closed loop cost of the SWLQG, ME, and MM compensators is plotted as a function of the achieved robustness bounds. As in the first sample problem, the worst case bound is on the negative perturbations of the uncertain frequency. For a given closed loop cost, the compensators maintain stability for larger positive perturbations than negative perturbations. The figure clearly shows that the SWLQG compensators have sacrificed much more performance to achieve equivalent robustness bounds than is sacrificed with the ME and MM compensators. Also, ME sacrifices significantly more performance than the Multiple Model compensators.

A more direct secondary effect is the performance reduction on this sample problem. Figure 5.46 shows the closed loop cost on the nominal plant of SWLQG, ME, and MM compensators as a function of the achieved robustness bounds. The figure clearly shows that the SWLQG compensators sacrifice much more performance to achieve robustness than either the ME or the MM techniques. Also, the ME compensators sacrifice a great deal more performance than the MM compensators.

Combining the results of the two sample problems, the Multiple-Model compensators consistently perform better than the rest. These compensators sacrifice less performance, have smaller high frequency gain increases, and thus have smaller bandwidth increases than the other robust control techniques. The distinction between SWLQG and ME is more difficult to make. In both problems, SWLQG tended to have the largest secondary effects. Bandwidth increase and gain at high frequency were substantially larger for SWLQG than for either ME or MM. In the first problem, the performance sacrificed by SWLQG was smaller than that of ME, but the bandwidth increase was more substantial. With equivalent bandwidths, the performance difference would be much smaller. In the second problem, ME compensators clearly performed better than the SWLQG compensators.

Within the uncertain region, it is difficult to draw conclusions about how one technique performs compared to another. All the techniques addressed are successful in providing robustness to the uncertainty, despite taking completely different approaches. But, outside of the uncertain region, it appears that the smaller the changes

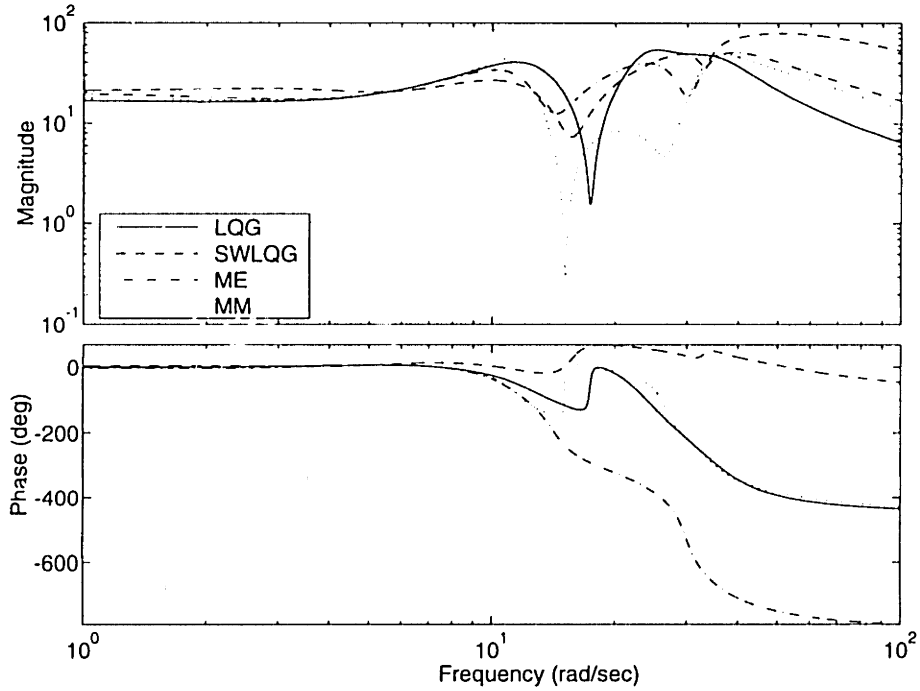

Figure 5.44: Transfer function for SWLQG, ME and MM compensators robust to perturbations of 18%, with nominal LQG compensator.

made to the optimal LQG compensator, the better the technique performs. Multiple Model compensators in both examples maintained a frequency response which most closely matched that of the LQG controllers outside of the uncertain region. As a result, it had smaller secondary effects than any of the other techniques.

These sample problems are only an idealized view of real structural systems. To extend the conclusions made here to real systems which are complicated by sensor noise, phase lags, time delays, and multiple uncertainties, the robust control techniques are compared in the next chapteron the basis of performance on the MACE test article.

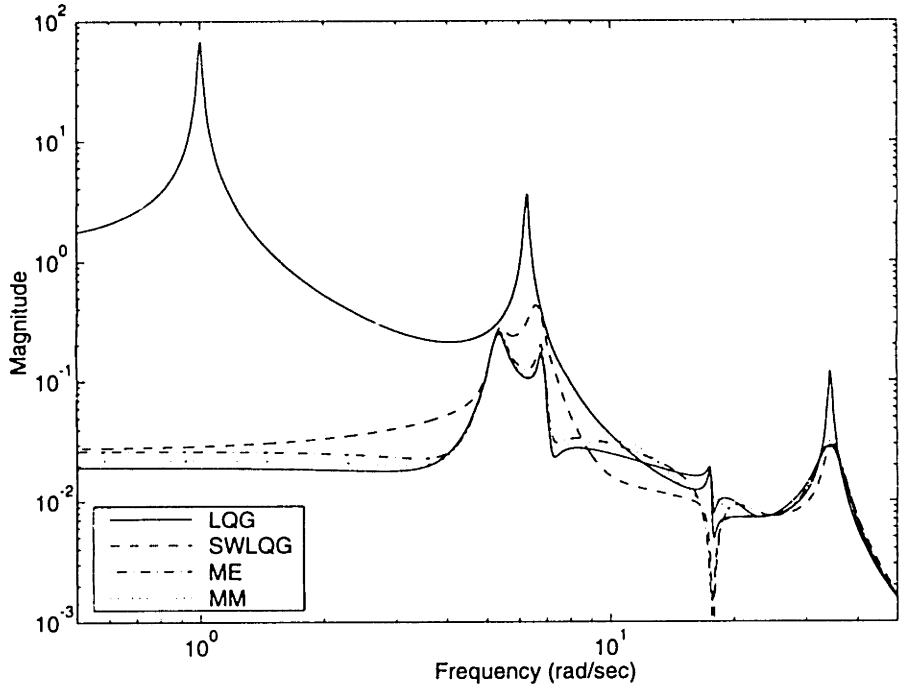

Figure 5.45: Performance transfer function for SWLQG, ME and MM compensators robust to perturbations of 18%, with open loop and LQG performance.

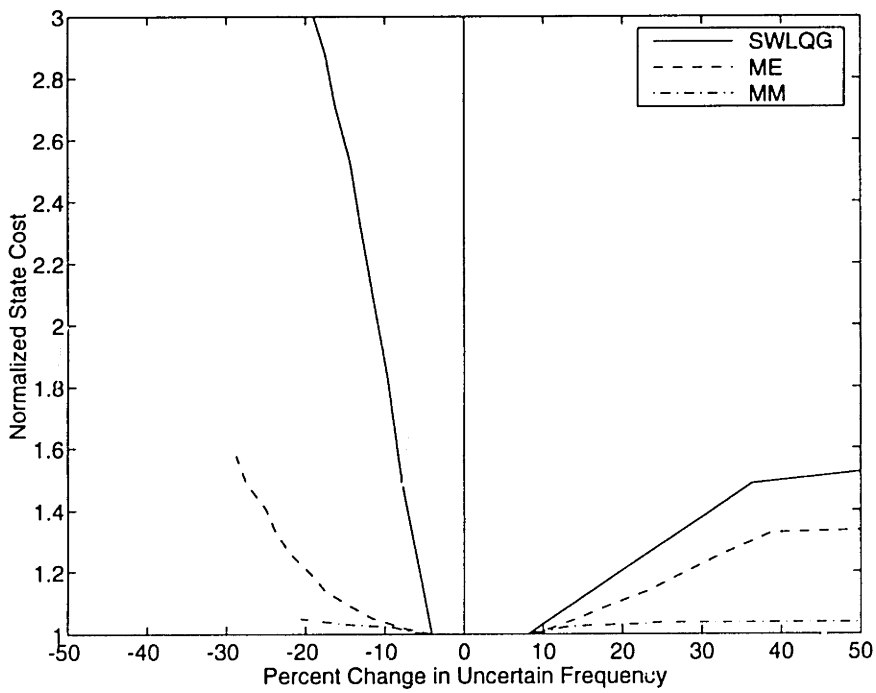

Figure 5.46: Closed loop cost on the nominal plant as a function of stability bounds for SWLQG, ME, and MM.

Chapter 6

MACE Experiments

Designing compensators for an experimental system using each of the robust control techniques provides a complementary axis on which a comparison of these techniques can be made. In the sample problem, the performance/robustness trade off was studied for a particular level of control authority. The performance decrease was measured with respect to the performance that was achieved by an optimal (non-robust) compensator. On experimental systems, optimal techniques often generate compensators that are not sufficiently robust to stabilize the system. Therefore a performance decrease is not observed when robust controllers are implemented. Instead, a performance increase is observed. The increase occurs because higher authority robust compensators can be implemented. Therefore it is useful to compare the robust control techniques on the basis of the maximum performance that can be achieved using each.

In this chapter, the results of SISO and MIMO experiments on the MACE test article are presented. The objective of the control experiments is to compare the remaining robust control design techniques (SWLQG, ME, and MM) on the basis of the maximum performance that is obtainable. For the SISO experiments, the compensators are compared directly as in the sample problem to observe the primary and secondary effects of robustification and their consequences. With multiple uncertainties, it is more difficult to distinguish primary effects. Where possible, these effects are shown. Due to the multivariable nature of the MIMO problem, it is difficult to

make conclusive statements about the primary and secondary effects of robustification. Therefore, only the maximum performance is used to compare the techniques.

6.1 SISO Control Designs

The control objective for this problem is to minimize the RMS inertial angular displacement of the primary gimbal payload about the X-axis when disturbed by a white noise, relative angle command input to the X-axis secondary gimbal (refer to Figure 2.1). The frequency response of the disturbance to the performance loop, Figure 6.1, shows that the largest contributions to the performance are from the X-axis rotation mode of the system at 1.4 Hz and the first horizontal bending mode at 3.4 Hz (refer to Table 2.1).

The control input for this problem is the primary gimbal X-axis relative angle command, and the feedback sensor output is the primary payload X-axis rate gyro. Figure 6.2 shows the control input to feedback sensor output transfer function. This control topology is output degenerate because both the performance output and the sensor output come from the X-axis rate gyro measurements. However, note that there is an integrator on the rate gyro measurement for the performance output since inertial angular displacement is the performance variable, not angular rate.

From Figures 6.1 and 6.2 it is quite apparent that modelling errors exist. It can also be seen that the error in the frequency of some of the modes represents a large part of that error. Figure 6.1 shows that the frequencies of the third and fourth Y-axis bending modes (refer to Table 2.1), located at 18.7 and 22.8 Hz in the control design model, are in error by about 10%. In addition, small errors can be seen in the frequencies of the X-axis rotation mode (1.4 Hz), the first Y-axis bending mode (3.4 Hz) and the second Y-axis bending mode (9.4 Hz). At high frequency there is a gain error. However, the error is primarily due to the reduction of the control model from the original 127 states to 37 states. It can be seen in Figure 6.2 that in addition to these errors, the second Y-axis bending mode (9.4 Hz), at least one of the first suspension cable violin modes (6.8 Hz) and one of the second violin modes (13.7

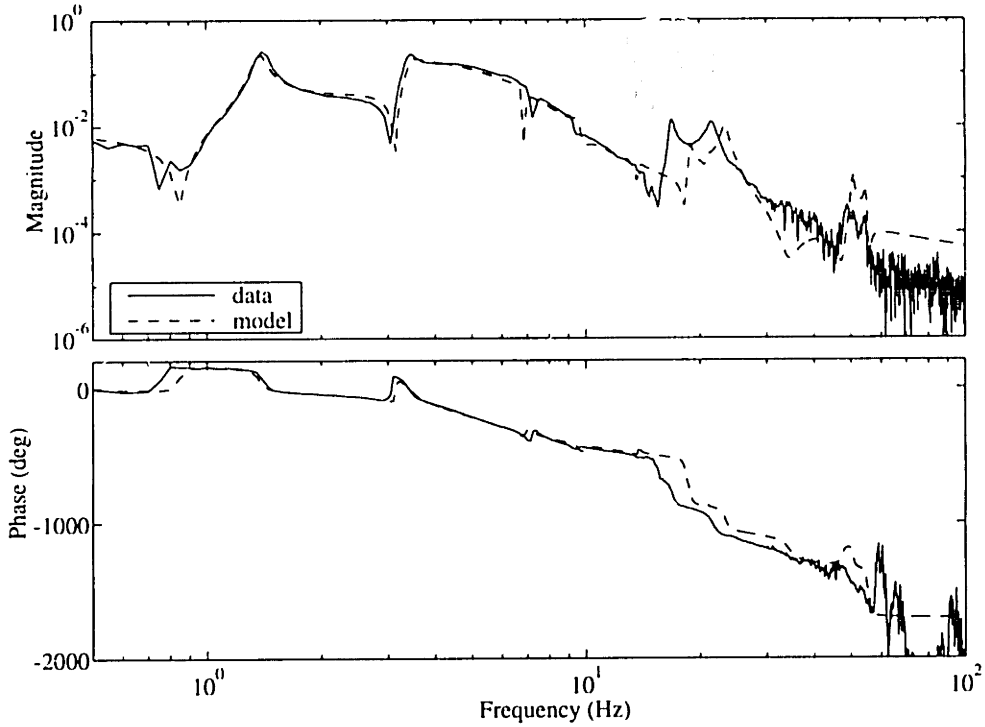

Figure 6.1: Disturbance to Performance transfer function.

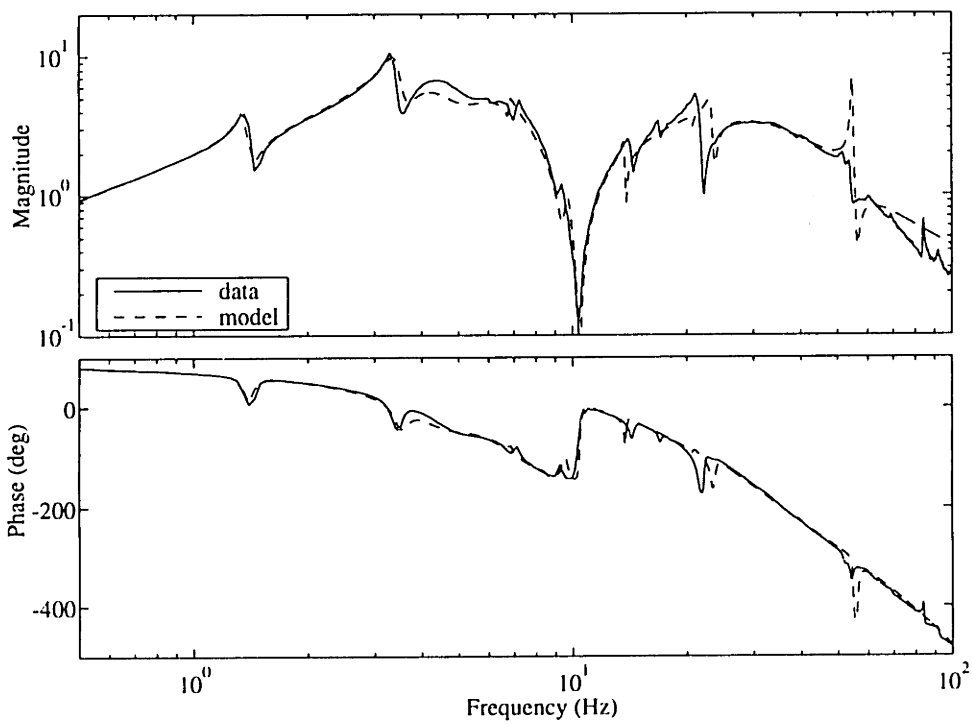

Figure 6.2: Control input to sensor output transfer function.

Hz) are modelled incorrectly. Also, the damping in the fifth Y-axis bending mode (50.4 Hz) is clearly erroneous. These errors point to modes which may be considered uncertain in the control design.

6.1.1 Design Approach

In this section, the approach used to design compensators using the LQG, SWLQG, ME and MM techniques is discussed. The approach relies on the analysis tools outlined in Chapter 4 to provide predictions of robustness problems which can then be addressed using robust control design.

The general approach was to design a series of compensators with different bandwidths (*i.e.* different control authority) and include uncertainties only when necessary. To begin the process, several LQG controllers which achieved roughly equal performance were designed with different ratios of control weighting (ρ) and sensor noise intensity (θ). The most robust had a ratio of 1 to 5 (ρ to θ). This ratio was held constant for all subsequent designs. Control authority was increased by reducing ρ and θ by the same factor.

As control authority increased, LQG compensators began to encounter robustness problems that were identified using the procedures from Section 4.3. Guided by the modelling errors that were noted in the preceding section, particular modal frequencies were then included in the uncertainty set used in each of the robust control formulations. Robust controllers were then designed, and the process of increasing control authority continued. When robustness problems again arose, the uncertainty set was expanded as necessary. In this way, only the uncertainties that were important for robust control wer retained in the uncertainty set.

This procedure was followed for the SWLQG and ME control designs. Due to the longer iteration time of the MM technique, the uncertainties identified for the LQG and ME compensators were used in all MM designs. The uncertainty sets that were used for each of the robust control designs are summarized in Table 6.1.

At the first two levels of authority, LQG compensators were sufficiently robust, so that no compensators were designed using the robust techniques. At the third

level, however, performance degradation and high sensitivity in the 7 Hz range indicated that errors in the sixth mode (6.8 Hz) in the design model caused stability and performance problems for the LQG controller. Thus the initial member of each uncertainty set was this mode. The magnitude of weighting on this mode for the ME and SWLQG techniques was determined iteratively in an attempt to maximize the predicted performance. This procedure was then followed for each additional mode that entered the uncertainty set. Notice in Table 6.1 the incremental build up of the uncertainty sets for the SWLQG and ME techniques as the control authority increases.

Due to the length of time required to calculate a multiple model compensator, the same iterative technique of adjusting the weights (uncertainty bounds for MM) was not feasible. Based on the ME and SWLQG controllers, it was decided to consider the same modes uncertain (note that the third violin mode at 20.7 Hz was left out of the MM uncertainty set, as in the highest authority ME designs). In Chapter 3, it was stated that selecting a set of models which contain a low estimate and high estimate of the frequency that is uncertain results in a combinatorial set of models when multiple uncorrelated uncertainties are considered. Limiting the set to one model with low estimates for all of the uncertainties, and one with high estimates for all of the uncertainties reduces the computational burden at the cost of correlating the uncertainties. In Ref. [47], it was shown that MM is effective when these two models alone are considered. For this work then, the nominal model is included as well making three models which are equally weighted for all MM control designs. The two perturbed models therefore have the uncertain modes changed in frequency. For all but the 18.8 and 23 Hz modes, the two models had the frequencies of the uncertain modes shifted by $\pm 3\%$. From comparing the data and the model transfer functions, it was clear that the frequencies of the other two modes were predicted to be about 10% higher than measured. Therefore, the 18.8 Hz mode was shifted by -12% and -6%, and the 23 Hz mode by -10% and -5%.

A second issue that has been considered in these designs is compensator stability. Many of the high authority LQG compensators contained unstable poles. Therefore

Control Authority	Modes in Uncertainty Set†			
	SWLQG	ME	MM	stable MM
$\rho = 0.04$, $\theta = 0.2$	ND	ND	ND	ND
$\rho = 0.02$, $\theta = 0.1$	ND	ND	ND	ND
$\rho = 0.01$, $\theta = 0.05$	6	6	2, 6, 7, 8, 9, 11, 14	ND
$\rho = 5 \cdot e^{-3}$, $\theta = 2.5 \cdot e^{-2}$	6, 9	2, 6	as above	ND
$\rho = 2.5 \cdot e^{-3}$, $\theta = 1.25 \cdot e^{-2}$	2, 6, 8, 9, 11, 14	2, 6, 8, 9, 11, 14	as above*	ND
$\rho = 1 \cdot e^{-3}$, $\theta = 5 \cdot e^{-3}$	as above	2, 6, 8, 9, 10, 11, 14	as above*	2, 6, 7, 8, 9, 11, 14
$\rho = 5 \cdot e^{-4}$, $\theta = 2.5 \cdot e^{-3}$	2, 6, 7, 8, 9, 11, 14*	2, 6, 7, 8, 9, 10, 11 ,14	as above*	as above
$\rho = 2.5 \cdot e^{-4}$, $\theta = 1.25 \cdot e^{-3}$	2, 6, 7, 8, 9, 10, 11 ,14*	as above*	as above*	as above
$\rho = 1 \cdot e^{-4}$, $\theta = 5 \cdot e^{-4}$	as above*	2, 6, 7, 8, 9, 11, 14*	as above*	as above
$\rho = 5 \cdot e^{-5}$, $\theta = 2.5 \cdot e^{-4}$	as above*	as above*	as above*	as above
$\rho = 2.5 \cdot e^{-5}$, $\theta = 1.25 \cdot e^{-4}$	as above*	ND	ND	ND
$\rho = 0$, $\theta = 0$	ND	ND	as above*	as above
ND- not designed, *compensator unstable † refer to Table 2.1				

Table 6.1: Modes within the uncertainty set for each design technique and level of control authority in the SISO experiment.

for the MM techniques, two sets of compensators were designed. One set was constrained to be stable, and the other was left unconstrained. For ME and SWLQG, stable compensators were designed by including modes located near the unstable poles in the LQG compensators in the uncertainty set. Note that for designs at $\rho = 2.5 \cdot e^{-3}$, the SWLQG and ME compensators included the eighth mode (13.74 Hz) and fourteenth mode (54.2 Hz) in the uncertainty set for this purpose. At higher levels of

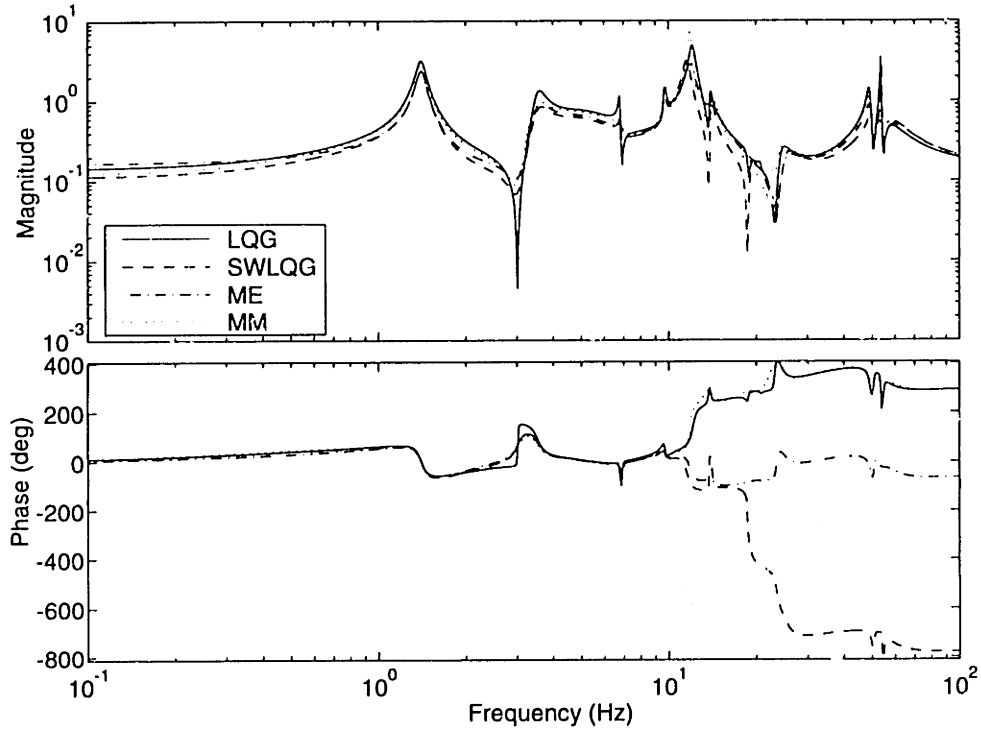

Figure 6.3: LQG, MM, ME and SWLQG compensators with $\rho = 2.5 \cdot e^{-3}$ and $\theta = 1.25 \cdot e^{-2}$.

control authority, however, these same modes were included strictly for robustness reasons. Not all unstable compensator poles could be avoided by including system modes in the uncertainty set. Therefore, not all SWLQG and ME compensators were stable. Table 6.1 indicates which compensators were stable and which were not.

6.1.2 Discussion of Results

The purpose of this section is to present the comparison of the SWLQG, ME and MM techniques based on compensators designed for this SISO loop on the MACE test article. The section begins with a study of the primary and secondary effects of adding robustness using each of the techniques, followed by a comparison based on experimentally measured performance.

To determine the changes in the compensator that result from adding robustness, the robust controllers will be compared to LQG compensators designed with the same values for sensor noise and control weighting. Due to the number of uncertainties, it

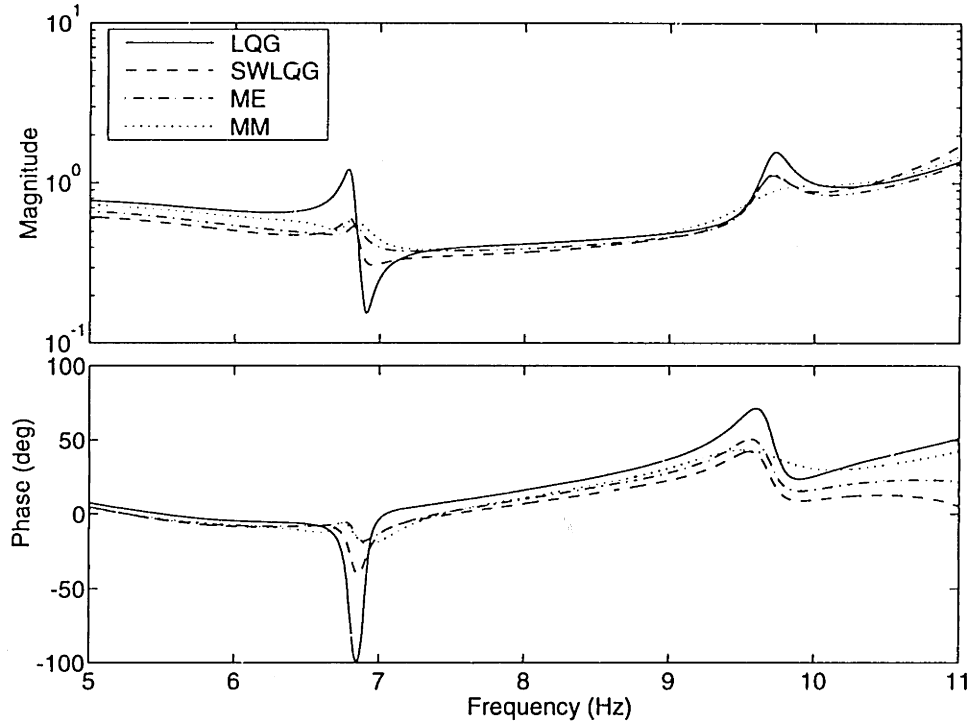

Figure 6.4: LQG, MM, ME and SWLQG compensators with $\rho = 2.5 \cdot e^{-3}$ and $\theta = 1.25 \cdot e^{-2}$ in the 5–11 Hz region.

is quite difficult to correlate the primary effects with the uncertainty that causes the changes in the compensator. However, some primary effects stand out. Figure 6.3 shows the frequency response of the LQG, MM, ME and SWLQG compensators designed with the control weighting $\rho = 2.5 \cdot e^{-3}$ and the sensor noise intensity $\theta = 1.25 \cdot e^{-2}$. Figure 6.4 shows the same transfer functions in the 5–11 Hz region. At this level of control authority, the same six uncertainties were used for the SWLQG and ME designs. The MM design had an additional uncertainty (refer to Table 6.1). Note that the LQG and MM compensators have unstable poles at 12 Hz while the SWLQG and ME compensators are stable. This is evident from the phase of the frequency responses in Figure 6.3.

Primary effects can be distinguished in the vicinity of two of the uncertain modes. Figure 6.4 shows the frequency response of the compensators in the region around the 6.8 Hz and 9.4 Hz plant modes. In the vicinity of the 6.8 Hz mode, it can be seen from both the magnitude and phase plots that the lightly damped pole-zero pair of the

LQG compensator has been damped significantly in the robust compensators. This is very similar to the primary effects encountered in the first sample problem. The primary effects are slightly different Around the 9.4 Hz mode. The LQG compensator does not have a lightly damped pole-zero pair, but rather a lightly damped pole with a more heavily damped zero at the same frequency so that there is an inverted notching effect. Neither the ME nor SWLQG compensators contain the 9.4 Hz mode in its uncertainty set. Therefore there is little change in the inverted notch behavior. The overall gain has been reduced somewhat, but it is more likely that this is due to the weighting of the 6.8 Hz mode and other higher frequency modes. However, the MM compensator did consider the 9.4 Hz mode to be uncertain. From the phase of the frequency response, it can be seen that the MM compensator has a much more heavily damped pole. Thus, there is a nearer cancellation with the heavily damped zero, and the inverted notch is not present. The effects of this change in the compensator should be localized since the gain at frequencies above and below the notch do not change. The effects of the other uncertainties are difficult to isolate.

The most important secondary effect can be seen by comparing the frequency response of each of the compensators (Figure 6.3). Because this problem is output degenerate, the performance can be improved by high gain (provided that sensitivity is low). It is clear from the figure that in the vicinity of the 1.4 and 3.4 Hz modes of the plant, which contribute significantly to the performance (Figure 6.1), the robust compensators have lower gain than the LQG compensator. The LQG compensator, however, has high sensitivity, and in fact drove the system unstable when implemented. None of the robust compensators have sensitivity problems. Therefore high gain at these frequencies implies better performance. It can be seen that, as with the sample problems, the frequency response of the MM compensator is closer in magnitude and phase to that of the LQG compensator outside of the uncertain ranges. This is particularly true in the 1–7 Hz range which is critical for performance. A secondary effect of robustification has been to reduce the gain further in this region for the ME and SWLQG designs.

The same is true at higher levels of authority. Figure 6.5 shows the LQG, MM,

ME and SWLQG compensators designed with the control weighting of $\rho = 5 \cdot e^{-4}$ and the sensor noise intensity of $\theta = 2.5 \cdot e^{-3}$. At this level of authority, it was necessary to consider seven modes uncertain in order to achieve a design for which the open loop data predicted stability. The phase of the compensators is quite different in the 10–25 Hz range. This is due to the presence of unstable compensator poles. The LQG compensator has unstable poles at 9.5 and 12 Hz. The MM compensator has an unstable pole at 12 Hz. The ME compensator has an unstable pole at 23 Hz, while the SWLQG compensator has no unstable poles in the 10–25 Hz range. At frequencies below 10 Hz, the gain in the compensators is quite different. The gain differential is significantly larger than in Figure 6.3. The LQG compensator has the highest gain, but this compensator destabilized the system during the experiment. The Multiple Model compensator has the second highest gain, followed by the Maximum Entropy and SWLQG compensators. Experimentally, all three of the robust compensators were sufficiently robust to improve the performance of the test article. Not surprisingly, with higher gain the MM compensator achieved the best performance improvement followed by the ME and SWLQG compensators.

In the input-output degenerate sample problem, the secondary effects of adding robustness were a lower gain at low frequency and higher gain at high frequency. In the experiment, there is no noticeable increase in gain at high frequency, but there is a large change in the low frequency gain of the robust compensators. Because of the phase lag in the system, the compensators for all of the control techniques use the modally sparse region around 40 Hz for the loop phase to cross $-180°$. For stability, it is required that the loop gain is less than unity at the crossover frequency, which effectively constrains the high frequency gain increase. Thus the the secondary effects are manifested as a drop in gain at low frequency. Figure 6.5 shows that, for a given level of control authority, the Multiple Model compensator has the smallest secondary effects of the robust techniques.

The consequences of the difference in secondary effect can be seen by comparing the performance of the compensators. Figure 6.6 shows the predicted performance of each compensator plotted as a function of control authority. Each 'x' represents

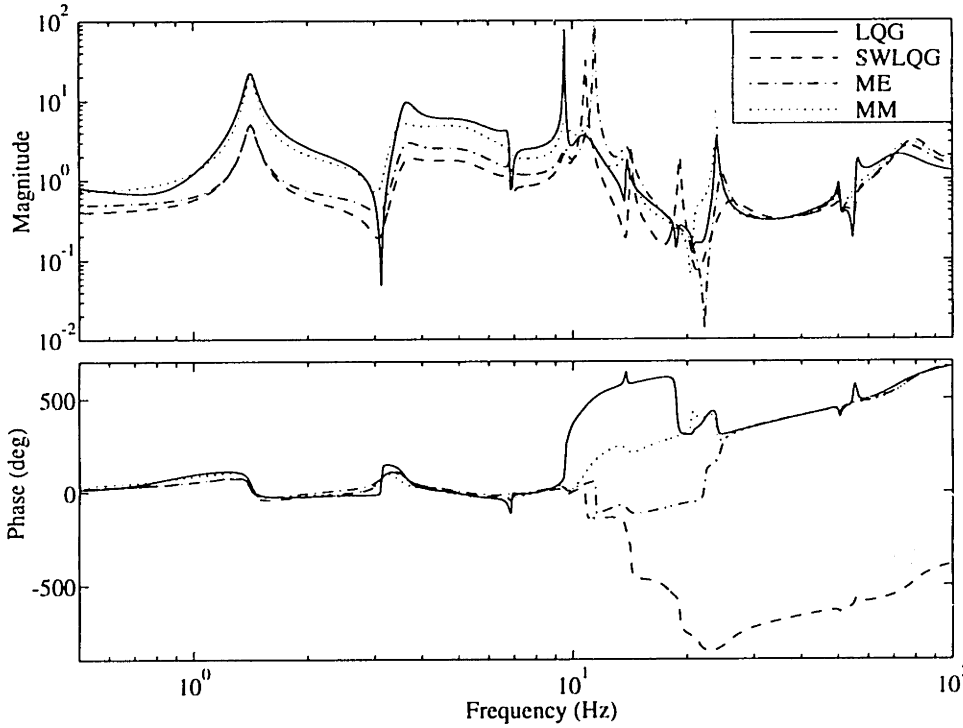

Figure 6.5: LQG, MM, ME and SWLQG compensators with $\rho = 5 \cdot e^{-4}$ and $\theta = 2.5 \cdot e^{-3}$.

the normalized state cost of the closed loop system for a particular value of control weighting (ρ). The normalized performance is the closed-loop state cost, using the design model with no sensor noise, scaled so that the open loop cost is unity. The lines on the plot connect the compensators designed using each technique: LQG, MM, ME, SWLQG, and MM with a stability constraint. For each value of ρ, the figure shows that the state cost is lower for LQG than for any of the robust control techniques. The difference in cost represents the performance that has been sacrificed in order to improve the robustness of the compensator. Note that for MM (both stable and unconstrained) compensators were designed for ρ=0, and thus the locus of points extends beyond the figure. However, the slope of the performance curves for the MM designs shows that the performance asymptotes to a value not much lower than those at $1/rho = 2 \times 10^4$. Finally, the figure shows that the performance sacrificed by the SWLQG and ME techniques is significantly greater than the performance sacrifice of the MM designs. Thus because the secondary effects were smaller in MM, *i.e.* the

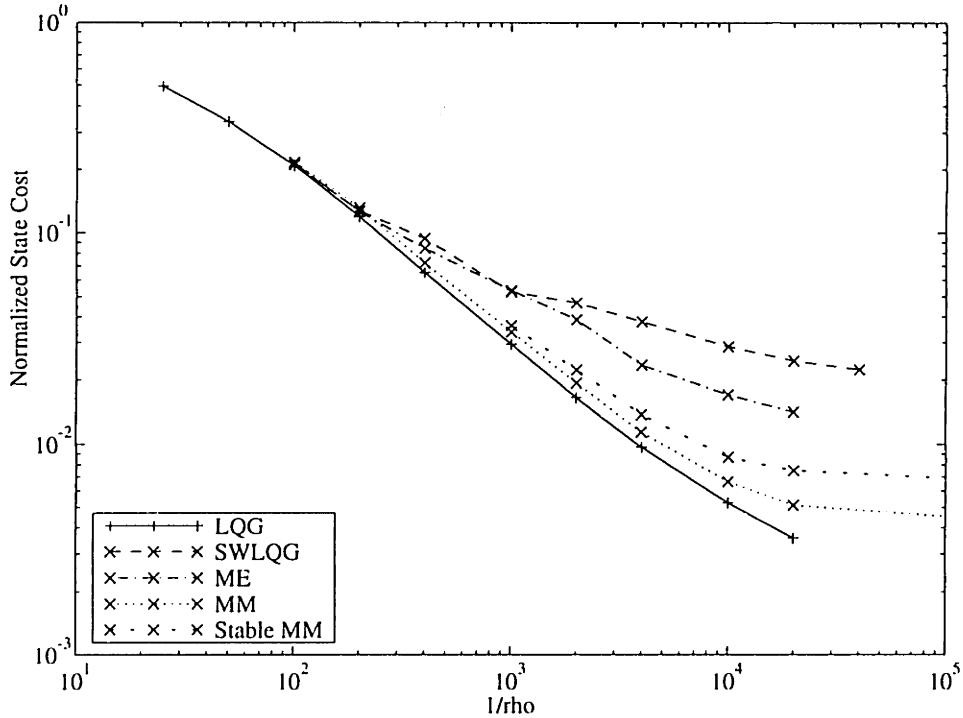

Figure 6.6: Performance on the design model as a function of control authority for LQG and the robust control techniques.

gain was higher, better performance can be achieved with this technique.

So far, only predicted performance has been considered. The experimental results are much more important. More than 40 compensators were designed, and more than 20 of them were implemented. The results are presented in Figure 6.7 and Table 6.2. Figure 6.7 shows the normalized state cost of the closed loop system both for the design model and as determined experimentally. The different line styles distinguish the control techniques. The results based on the model are depicted with an x, and the experimental results are shown by a filled circle.

Two trends can be seen in the figure. First, the performance levels achieved experimentally are lower than those predicted for all compensators. (Note that lower performance corresponds to higher state cost.) This can be attributed to several causes. First, the predictions on the model do not include sensor noise since it was used as a design variable. The experimental results include whatever sensor noise was present when the transfer functions were measured. Therefore, the state cost should

be higher. Also, the open loop cost based on the model and measured experimentally differ by about 5%. In the figure, the state cost for the model predictions is normalized with respect to the open loop model. Experimental results are normalized with respect to the measured open loop.

Second, a trend can be seen in the performance achieved experimentally. It is clear that the LQG compensators were so non-robust that they only improve the performance at the first three levels of authority. This demonstrates the need for robust control and illustrates the importance of this work. Note that several compensators were implemented for each control technique. The maximum performance for each technique was obtained by testing to such a level that instability occurred. The performance of the next lowest authority compensator was then taken as the best performance for the given technique. Hence all of the lines of experimental results in the figure end with a point of infinite cost. It can be seen in the figure that, as predicted by the performance based on the model, the MM compensators achieved better performance improvement than the ME compensators while these achieved better performance than the SWLQG compensators.

Figure 6.7 also shows that not all of the robust techniques destabilized the system at the same level of control authority. To make a fair comparison of the performance which can be achieved with each technique, the maximum performance improvements must be compared. Table 6.2 shows the performance improvement achieved by each compensator that was implemented. From the table, note that the best LQG controller achieved only a 4.5 dB reduction in the RMS X-axis inertial angular displacement of the primary payload. The performance improvement achieved by any of the other techniques clearly shows the benefit of using robust control for this system.

Comparing across the row for which $\rho = 1 \cdot e^{-4}$, it can be seen that at the highest level of authority for which none of the robust techniques destabilizes the system, the MM compensator achieves the best performance. With the constraint that a stable compensator be used, the MM technique sacrifices only 1 dB and achieves 19 dB performance improvement. But, the stable MM compensator maintained system stability at a higher level of control authority. Thus the maximum performance achieved

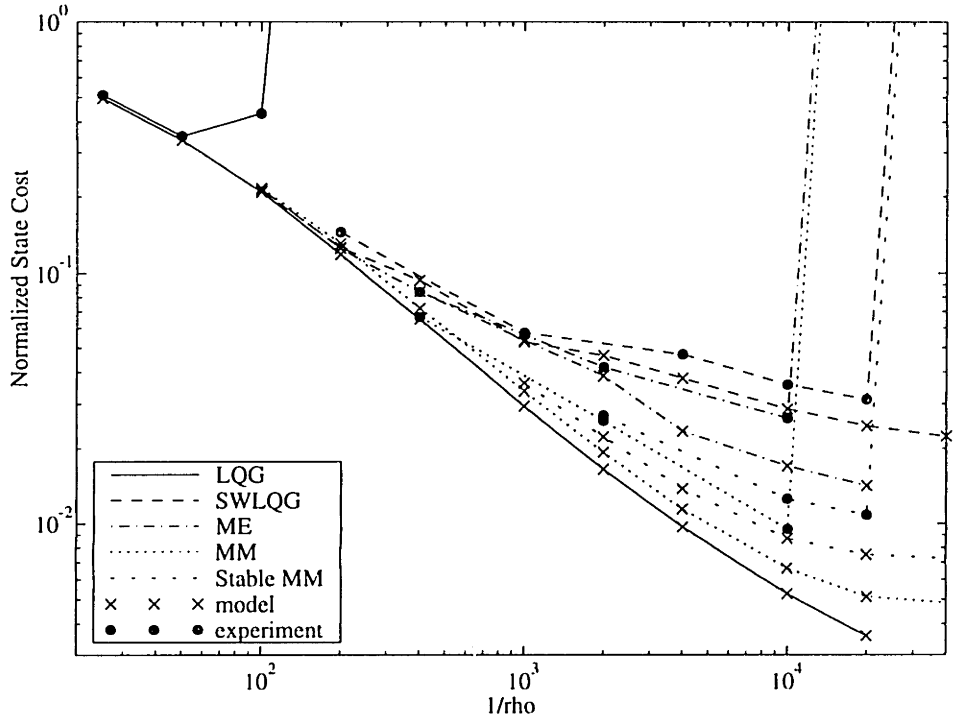

Figure 6.7: Performance as a function of control authority for the control techniques both on the design model and experimentally measured.

by the constrained MM was 19.7 dB; only 0.5 dB less than the best unconstrained MM design.

The Maximum Entropy compensator achieved 15.8 dB improvement while the SWLQG controller achieved 14.5 dB, with $\rho = 1 \cdot e^{-4}$. However, SWLQG remained stable at a higher level of control authority at which it achieved 15.0 dB improvement. Thus the gap between the best performance achievable by these methods was narrowed somewhat.

It is difficult to claim any significance from differences of less than 1 dB. A finer grid of control authority levels would be necessary to get more accurate maximum performance values, but differences on this scale are not significant.

It is useful at this point to show the analysis techniques, described in the preceding chapter, applied to the best compensator. Tthe unconstrained MM compensator that achieved 20.2 dB performance improvement is used for this purpose. For this compensator, Figure 6.8 shows the performance transfer function as predicted by both

Table 6.2: Experimental performance values for each of the control techniques.

Control authority (ρ,θ)		Performance Improvement				
		LQG	SWLQG	ME	MM	stable MM
$\rho = 0.04,$	$\theta = 0.2$	2.9 dB	ND	ND	ND	ND
$\rho = 0.02,$	$\theta = 0.1$	4.5 dB	ND	ND	ND	ND
$\rho = 0.01,$	$\theta = 0.05$	3.6 dB	NI	NI	NI	ND
$\rho = 5 \cdot e^{-3},$	$\theta = 2.5 \cdot e^{-2}$	US	8.4 dB	NI	NI	ND
$\rho = 2.5 \cdot e^{-3},$	$\theta = 1.25 \cdot e^{-2}$	NI	NI	10.8 dB	11.8 dB	ND
$\rho = 1 \cdot e^{-3},$	$\theta = 5 \cdot e^{-3}$	NI	12.4 dB	NI	NI	NI
$\rho = 5 \cdot e^{-4},$	$\theta = 2.5 \cdot e^{-3}$	NI	NI	13.8 dB	15.9 dB	15.7 dB
$\rho = 2.5 \cdot e^{-4},$	$\theta = 1.25 \cdot e^{-3}$	NI	13.3 dB	NI	NI	NI
$\rho = 1 \cdot e^{-4},$	$\theta = 5 \cdot e^{-4}$	NI	14.5 dB	15.8 dB	20.2 dB	19.0 dB
$\rho = 5 \cdot e^{-5},$	$\theta = 2.5 \cdot e^{-4}$	NI	15.0 dB	US	US	19.7 dB
$\rho = 2.5 \cdot e^{-5},$	$\theta = 1.25 \cdot e^{-4}$	NI	US	ND	ND	ND
$\rho = 0,$	$\theta = 0$	ND	ND	ND	NI	US
NI- not implemented, ND- not designed, US- unstable						

the model and the open loop data, and as experimentally measured. Note that both predictions match well with the actual closed loop response. At 20 Hz, the model based prediction deviates from the data prediction and the actual response because of the mismodelling of the modes in this region. Recall that the 18.8 Hz and 22.8 Hz modes have almost 10% errors.

Figures 6.9 and 6.10 show a Nichols plot of the loop transfer function (GK) based on the model and open loop data, respectively. A close inspection will reveal that both plots contain two net left to right passes over the critical point (x). This compensator contained two pairs of unstable complex poles, thus two passes are required for stability. It can also be seen that the gain and phase margins of this

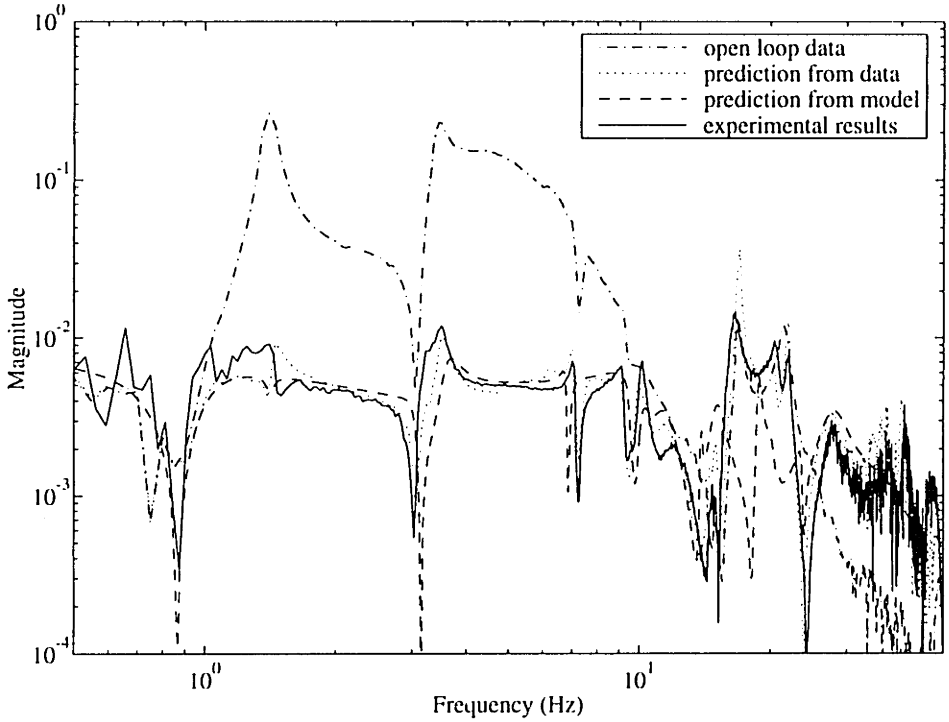

Figure 6.8: Performance transfer function of best SISO compensator experimentally, and as predicted on the data and model.

compensator are very small. These margins were necessary in order to achieve the high level of performance that this compensator achieved.

Finally, Figure 6.11 shows the singular values of $I + GK$ for this compensator. Because this is a SISO compensator, the singular values do not provide any information that can not be inferred from the Nichols plot. However, it is useful to see the relation between proximity to the critical point on the Nichols plot and sensitivity. The singular values of I+GK in the 30–40 Hz range are very small. On the Nichols plot over this frequency range, GK passes just under the critical point. In addition, large singular values of $I + GK$ show that in the 1–10 Hz range the compensator achieves very good disturbance rejection, *i.e.* good performance.

From comparing the compensator transfer functions and the experimental results, it can be observed that Multiple Model compensators had the smallest secondary effects, and achieved better performance as a result. However, the computation required was significantly higher. To this point, only SISO control loops have been

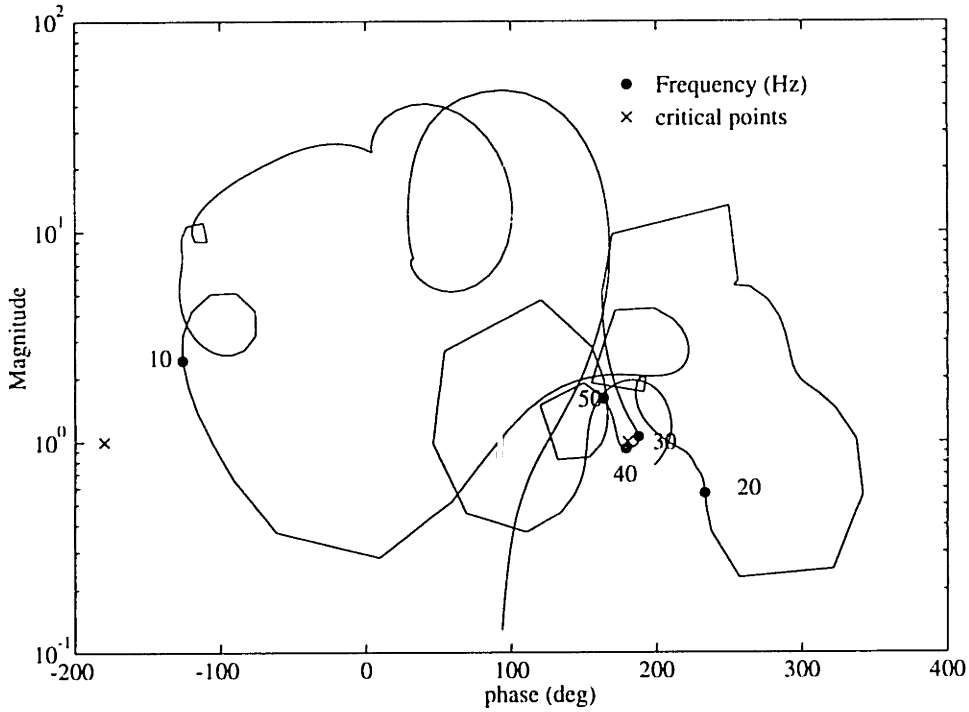

Figure 6.9: Nichols plot of best SISO compensator using the model.

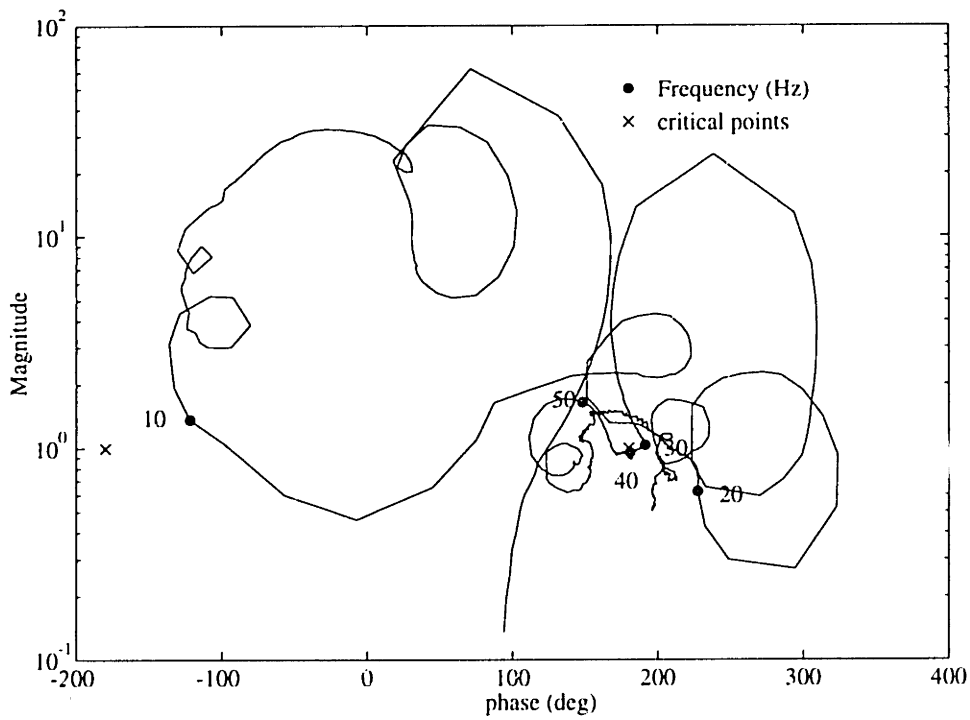

Figure 6.10: Nichols plot of best SISO compensator, using open loop data to predict stability.

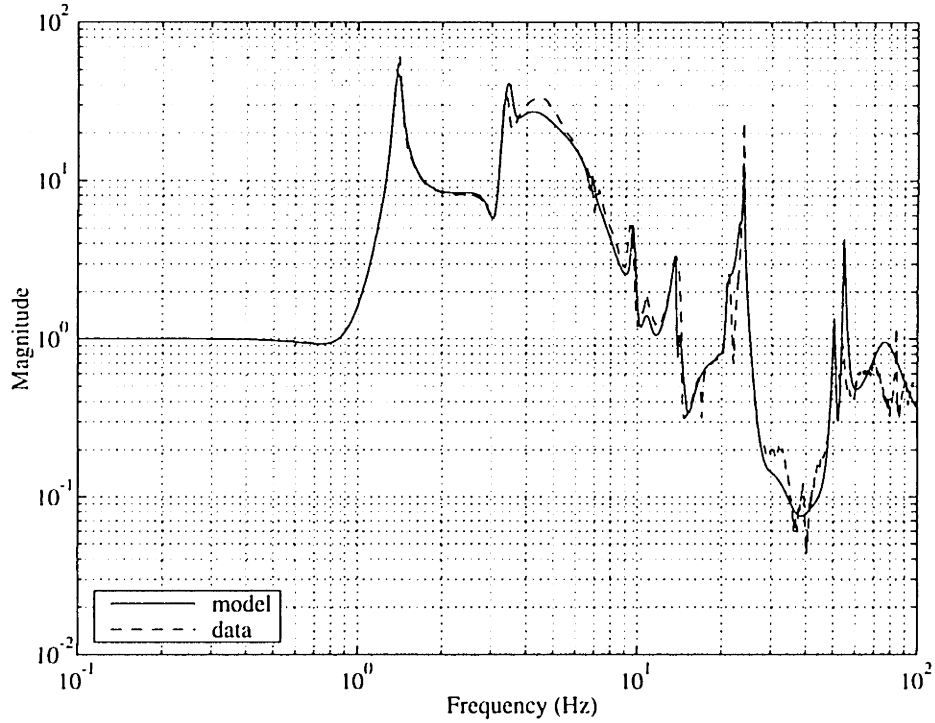

Figure 6.11: Singular values of $I + GK$ as predicted by the model and the open loop data for the best SISO controller.

considered because more decisive analysis is possible for these than for MIMO systems. Before concluding, it is important to investigate a MIMO system so that more general conclusions can be made.

6.2 MIMO Control Designs

To present a thorough comparison of the robust control techniques, it is necessary to consider MIMO systems as well as SISO systems. These systems are much more difficult to analyze, however, so the conclusions drawn from these will be more limited. The most important information that can drawn from these experiments is the maximum performance that can be achieved using each of the control techniques.

The control objective for this problem is to minimize the RMS, inertial angular displacement of the primary payload about the X-axis when disturbed by a white noise relative angle command to the X-axis of the secondary gimbal, just as in the SISO

experiments of the preceding section. For control, three actuators and three sensors are used, providing the multivariable nature of this experiment. The first sensor-actuator pair is the primary gimbal X-axis relative angle command and theprimary gimbal X-axis rate gyro, as in the preceding section. Added on to this are the X and Y-axis reaction wheels as inputs and the X and Y-axis bus rate gyros as sensors (see Figure 2.1). The transfer function for the gimbal loop is shown in Figure 6.2. The transfer function for the X-axis reaction wheels to X-axis bus rate gyro loop is shown in Figure 6.12. The transfer function for the Y-axis reaction wheels to Y-axis bus rate gyro loop is shown in Figure 6.13.

Comparing Figures 6.12 and 6.13 with Figure 6.2, it can be seen that the modelling errors in the two new loops are greater than the errors in the SISO loop used in the preceding section. The X-axis reaction wheel loop has a strong modal contribution from the 1.4 Hz and 3.4 Hz modes which are very important to the performance, which indicates that this loop should be effective at controlling these modes. However, because there are large discrepancies between the measured data and the model at these frequencies, this loop may introduce greater robustness problems. The Y-axis control loop does not indicate a strong influence on the 1.4 Hz or 3.4 Hz modes, but it has a large response to the second and fourth Y-axis bending modes (9.4 Hz and 22.8 Hz), *i.e.* the asymmetric bending modes. These modes had a strong influence on robustness properties in the SISO problem, so better control of these modes may result in better robustness characteristics in this MIMO experiment.

6.2.1 Design Approach

As with the SISO control designs, the methods of Chapter 4 are used to aid in the design of a series of MIMO compensators with different bandwidths for each of the LQG, SWLQG, ME and MM techniques. The same general approach to including uncertainty is used as in Section 6.1.1. A particular modal frequency uncertainty is included in the uncertainty set for each technique only if it is necessary. However, because multiple actuators and sensors are available, the relative weighting of each in control weighting and sensor noise intensity represent additional parameters which

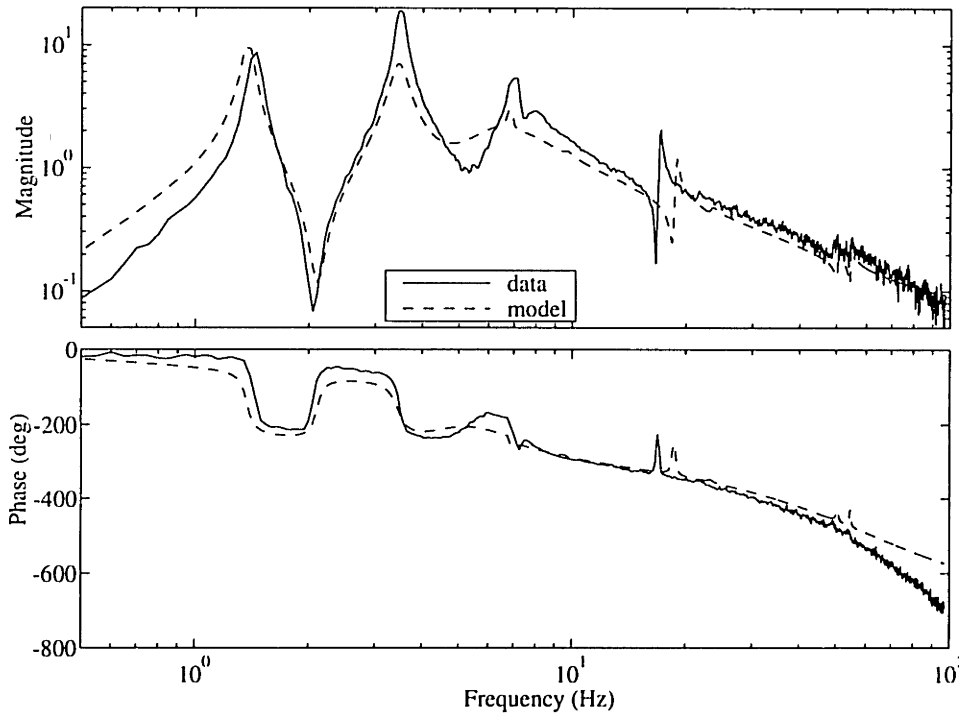

Figure 6.12: Transfer function from X-axis reaction wheels to X-axis bus rate gyro.

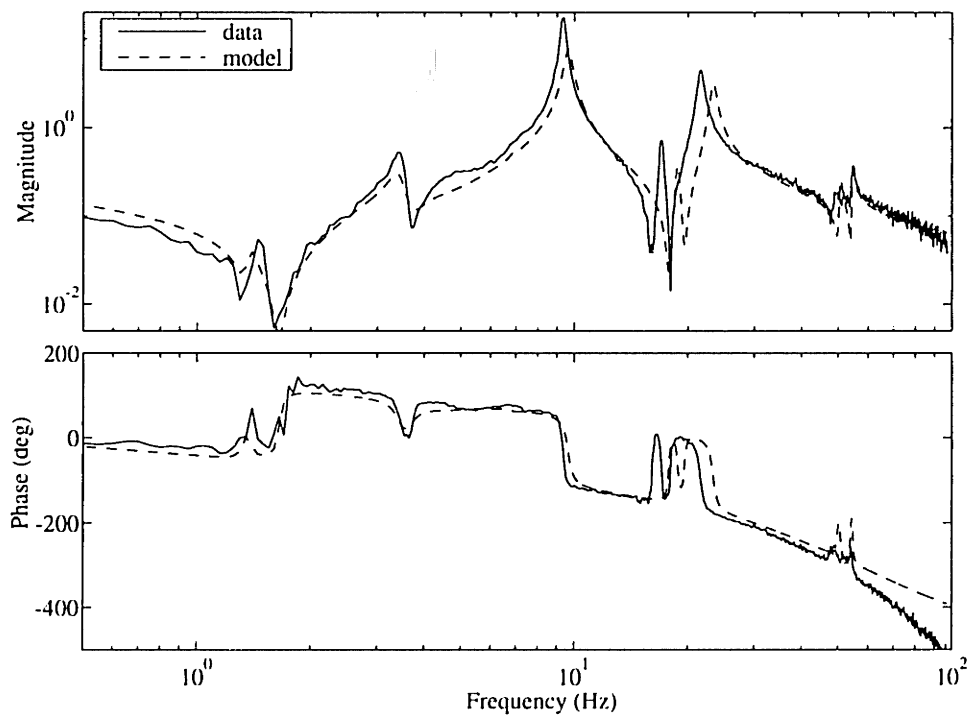

Figure 6.13: Transfer function from Y-axis reaction wheels to Y-axis bus rate gyro.

can be altered to achieve robustness. Before proceeding with MIMO control designs, each of the three collocated actuator sensor loops was investigated to determine a good ratio for sensor noise intensity and control weighting. In all three cases, LQG controllers were designed which achieved equivalent performance, but had different values for ρ and θ. For all three, it was found that a ratio of 1 to 5 (ρ to θ) resulted in good robust designs. Therefore, this ratio was fixed for all subsequent controllers.

Next, it was necessary to investigate the role of the relative weighting of different actuator/sensor pairs. This was done by designing controllers with different values on the diagonal of the control weighting matrix, R_{uu}, and the sensor noise intensity matrix, V_{yy}. Consider the control weighting matrix to have the form $R_{uu} = \rho R'_{uu}$ where ρ is a scalar and R'_{uu} is normalized so that the first element is unity. Similarly, consider the sensor noise matrix to be $V_{yy} = \theta V'_{yy}$ where θ is a scalar and V'_{yy} is normalized so that the first element is unity. Because the ratio of ρ to θ is the same for each of the three sensor/actuator pairs, R'_{uu} and V'_{yy} were set to be equal and θ was set to five times ρ. The relative weighting of the three sensor/actuator loops is then contained in the diagonal elements of the R'_{uu} matrix. Several LQG controllers were designed to determine the best relative weightings. In general, it was found that there was no particular advantage to be gained by weighting one actuator/sensor pair more than another. Therefore, the R'_{uu} matrix was set to the identity matrix.

Having determined the general weightings that were to be used, compensators were designed for 12 levels of control authority. As with the SISO compensator designs, at different levels of authority different modes were considered uncertain. The uncertainty set used in each design is summarized in Table 6.3. Note that except for the third violin mode at 20.68 Hz, all of the modes which were considered uncertain for the SISO designs belong to the uncertainty sets in the MIMO problem. In addition, the X rotation mode at 1.4 Hz is considered uncertain, and a heavily damped servo mode at 4.5 Hz is considered uncertain at high authority in the MM designs.

Note that unlike the SISO compensator designs, no frequencies were considered uncertain so that stable compensators would result. Also, all the MIMO MM com-

pensators were stable. Therefore, there was no need to design MM compensators with a stability constraint.

Finally, while R'_{uu} was in general set to the identity matrix to provide equal control weighting for each actuator, it was often the case that poor performance was predicted in the frequency region around the X rotation mode at 1.4 Hz. It was seen in Figure 6.12 that the X-bus control loop contains significant error. For several controllers, de-emphasizing the use of this actuator was found to improve the predicted performance. Therefore, R'_{uu} was altered to change the relative weighting for the X-bus control loop. Note that the inputs are arranged so that the (1,1) element of R'_{uu} represents the control weighting on the X-axis primary gimbal; the (2,2) element represents the X-axis reaction wheels; and the (3,3) element represents the Y-axis reaction wheels. Similarly, the outputs are arranged so that the (1,1) element in V'_{yy} represents the primary payload X-axis rate gyro; the (2,2) element represents the bus X-axis rate gyro; and the (3,3) element represents the bus Y-axis rate gyro. Table 6.4 shows the values for R'_{uu} that were used in each of the control designs.

6.2.2 Discussion of Results

Much less can be concluded about the MIMO experiments than the SISO experiments. In the SISO experiments it was possible to show the frequency response of the compensators from different techniques and point out primary and secondary effects based on how the loop transfer function was altered. For a MIMO problem, the loop transfer function does not provide stability information. Stability can be determined by the Multivariable Nyquist Criterion. However, very little interpretation of the Nyquist Criterion can be made from plotting the singular values of the frequency response of the MIMO compensator or the frequency response of each individual channel. Therefore it is very difficult to conclusively show primary and secondary effects of robustification. However, it is possible to observe the performance/robustness tradeoff by comparing the performance of different compensators both experimentally, and from predictions based on the model.

Control Authority	Modes in Uncertainty Set†		
	SWLQG	ME	MM
$\rho = 0.05$, $\theta = 0.25$	ND	ND	ND
$\rho = 0.02$, $\theta = 0.1$	ND	ND	ND
$\rho = 0.01$, $\theta = 0.05$	3, 7	3, 7	2, 3, 7, 8, 9, 10, 12, 17
$\rho = 5 \cdot e^{-3}$, $\theta = 2.5 \cdot e^{-2}$	2, 3, 7	2, 3, 7	as above
$\rho = 2 \cdot e^{-3}$, $\theta = 1 \cdot e^{-2}$	2, 7, 8, 10	2, 3, 7, 8, 9	as above
$\rho = 1 \cdot e^{-3}$, $\theta = 5 \cdot e^{-3}$	2, 7, 8, 9, 10, 12	2, 3, 7, 8, 9, 10, 12	as above
$\rho = 5 \cdot e^{-4}$, $\theta = 2.5 \cdot e^{-3}$	2, 7, 8, 9 10, 12, 17	2, 3, 7, 8, 9, 10, 12, 17	as above
$\rho = 2 \cdot e^{-4}$, $\theta = 1 \cdot e^{-3}$	as above	as above	as above
$\rho = 1 \cdot e^{-4}$, $\theta = 5 \cdot e^{-4}$	as above	as above	2, 3, 4, 7, 8, 9, 10, 12, 17
$\rho = 5 \cdot e^{-5}$, $\theta = 2.5 \cdot e^{-4}$	as above	as above	as above
$\rho = 2 \cdot e^{-5}$, $\theta = 1 \cdot e^{-4}$	as above	as above	as above
$\rho = 0$, $\theta = 0$	ND	ND	as above
ND- not designed, † refer to Table 2.1			

Table 6.3: Modes within the uncertainty set for each design technique and level of control authority in the MIMO experiment.

Figure 6.14 shows the normalized closed loop state cost of the model plotted as a function of the control weighting, ρ. Several observations can be made from this figure. First, note that for some values of ρ, the SWLQG and MM control designs result in a lower state cost than LQG. Table 6.4 shows that at these levels of authority, the X and Y axis bus reaction wheels were penalized more heavily in LQG designs than in SWLQG or MM designs. In fact, because the LQG designs use less control in the bus reaction wheel channels, they are actually at lower authority, though due

Table 6.4: Relative weightings on actuators and sensors for each design technique and level of control authority in the MIMO experiment.

Control Authority	R'_{uu}- Relative weighting of actuators and sensors			
	LQG	SWLQG	ME	MM
$\rho = 0.05$, $\theta = 0.25$	I_3	ND	ND	ND
$\rho = 0.02$, $\theta = 0.1$	I_3	ND	ND	ND
$\rho = 0.01$, $\theta = 0.05$	I_3	I_3	I_3	I_3
$\rho = 5 \cdot e^{-3}$, $\theta = 2.5 \cdot e^{-2}$	I_3	I_3	I_3	I_3
$\rho = 2 \cdot e^{-3}$, $\theta = 1 \cdot e^{-2}$	$\begin{bmatrix} 1 & 0 & 0 \\ 0 & 2 & 0 \\ 0 & 0 & 2 \end{bmatrix}$	$\begin{bmatrix} 1 & 0 & 0 \\ 0 & 0.5 & 0 \\ 0 & 0 & 1 \end{bmatrix}$	I_3	I_3
$\rho = 1 \cdot e^{-3}$, $\theta = 5 \cdot e^{-3}$	$\begin{bmatrix} 1 & 0 & 0 \\ 0 & 2 & 0 \\ 0 & 0 & 2 \end{bmatrix}$	$\begin{bmatrix} 1 & 0 & 0 \\ 0 & 0.5 & 0 \\ 0 & 0 & 1 \end{bmatrix}$	I_3	I_3
$\rho = 5 \cdot e^{-4}$, $\theta = 2.5 \cdot e^{-3}$	$\begin{bmatrix} 1 & 0 & 0 \\ 0 & 2 & 0 \\ 0 & 0 & 2 \end{bmatrix}$	I_3	$\begin{bmatrix} 1 & 0 & 0 \\ 0 & 2 & 0 \\ 0 & 0 & 1 \end{bmatrix}$	I_3
$\rho = 2 \cdot e^{-4}$, $\theta = 1 \cdot e^{-3}$	I_3	I_3	$\begin{bmatrix} 1 & 0 & 0 \\ 0 & 2.5 & 0 \\ 0 & 0 & 1 \end{bmatrix}$	I_3
$\rho = 1 \cdot e^{-4}$, $\theta = 5 \cdot e^{-4}$	I_3	I_3	$\begin{bmatrix} 1 & 0 & 0 \\ 0 & 2.5 & 0 \\ 0 & 0 & 1 \end{bmatrix}$	$\begin{bmatrix} 1 & 0 & 0 \\ 0 & 2 & 0 \\ 0 & 0 & 1 \end{bmatrix}$
$\rho = 5 \cdot e^{-5}$, $\theta = 2.5 \cdot e^{-4}$	I_3	I_3	I_3	$\begin{bmatrix} 1 & 0 & 0 \\ 0 & 2 & 0 \\ 0 & 0 & 1 \end{bmatrix}$
$\rho = 2 \cdot e^{-5}$, $\theta = 1 \cdot e^{-4}$	I_3	I_3	I_3	$\begin{bmatrix} 1 & 0 & 0 \\ 0 & 2 & 0 \\ 0 & 0 & 1 \end{bmatrix}$
$\rho = 0$, $\theta = 0$	ND	ND	ND	I_3
ND- not designed, I_3- 3×3 identity matrix				

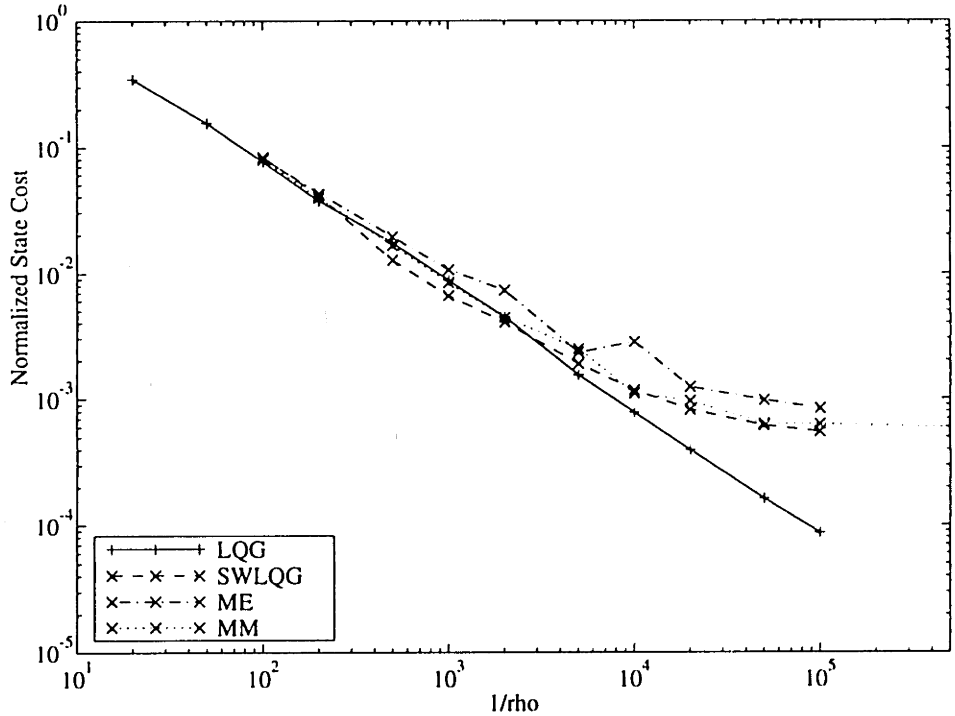

Figure 6.14: Performance on the design model as a function of control authority for LQG and the robust control techniques.

to the normalization, ρ is equal. This illustrates one of the problems in analyzing multivariable controllers.

Note also from Figure 6.14 that for $1/\rho = 10^4$, the ME compensator has a higher state cost than at the previous level of authority. At $1/\rho = 10^4$ it was necessary to increase the weighting on the 1.4 Hz mode by a factor of 10 in order to maintain predicted closed loop stability. This changed the compensator significantly. However, it was still possible at higher levels of authority to further improve the performance which is shown by the closed loop cost for the last three design points for ME in the figure.

Finally, note that for $1/\rho > 10^4$ in Figure 6.14, the performance/robustness trade-off becomes quite evident. All of the robust control techniques tend to level off in the performance that is achievable while the LQG controllers continue to improve. It should be noted that this performance/robustness trade-off occurs at a much lower state cost than in the SISO experiment. However, there appears not to be a signif-

icant difference between the asymptotic performance for each of the techniques. A significant difference between the compensators can be seen by comparing the sensitivities. Figures 6.15, 6.16, and 6.17 show the singular values of $I + GK$ predicted using both the model and the data, for the highest authority SWLQG, ME and MM compensators. All three are very sensitive at 1.4 Hz, the frequency of the X rotation mode, as shown by a very low minimum singular value at this frequency. For each case, closed loop instability was predicted using the data if lower weighting (smaller uncertainty bounds for MM) on the 1.4 Hz mode was applied. Higher weighting resulted in a significant decrease in performance without much change in the sensitivity at this frequency. In the 3–4 Hz range, SWLQG and ME are also very sensitive. Again, little change in the sensitivity resulted from altering the uncertainty weights to the first Y-bending mode, 3.4 Hz. In fact, for SWLQG, any weighting on this mode resulted in increased sensitivity. However, the minimum singular value of $I + GK$ in the 3–4 Hz region for the MM compensator is very close to 1. This indicates that the MM compensator is not very sensitive in this frequency range. Upon implementation, the SWLQG and ME compensators in fact destabilized the system. Thus, while the predicted performance for the three compensators may almost be equal, it is more important to compare the experimental performance.

The final comparison of the compensators is made on the basis of experimentally achieved performance. The performance improvement for each compensator is shown in Table 6.5. In addition, Figure 6.18 shows the normalized state cost of the closed loop system both for the design model and as determined experimentally. The different line styles distinguish the control techniques. The results based on the model are depicted with an x, and the experimental results are shown by a filled circle.

Note that, as with the SISO system, the performance achieved experimentally is less than predicted for all compensators. However, in these experiments, both the predicted and the achieved performance improvement is greater than in the SISO experiments. Because better performance is achieved, sensor noise is a larger portion of the signal that is measured. Since the predictions on the model do not include sensor noise and the experimental results include whatever sensor noise was present

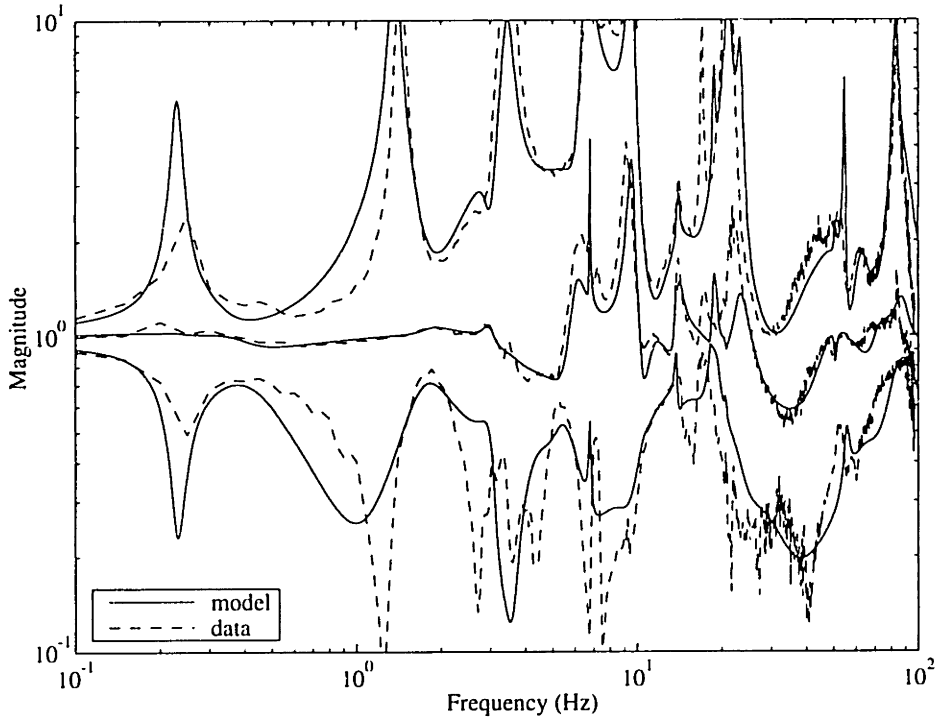

Figure 6.15: Singular values of $I + GK$ as predicted by the model and the open loop data for the highest authority MIMO SWLQG controller.

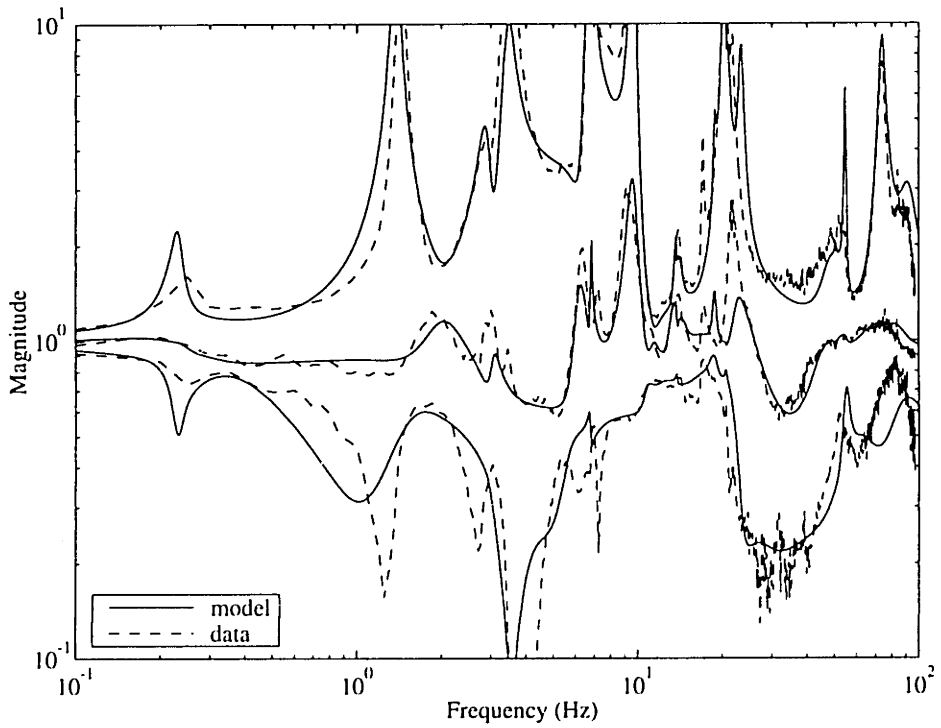

Figure 6.16: Singular values of $I + GK$ as predicted by the model and the open loop data for the highest authority MIMO ME controller.

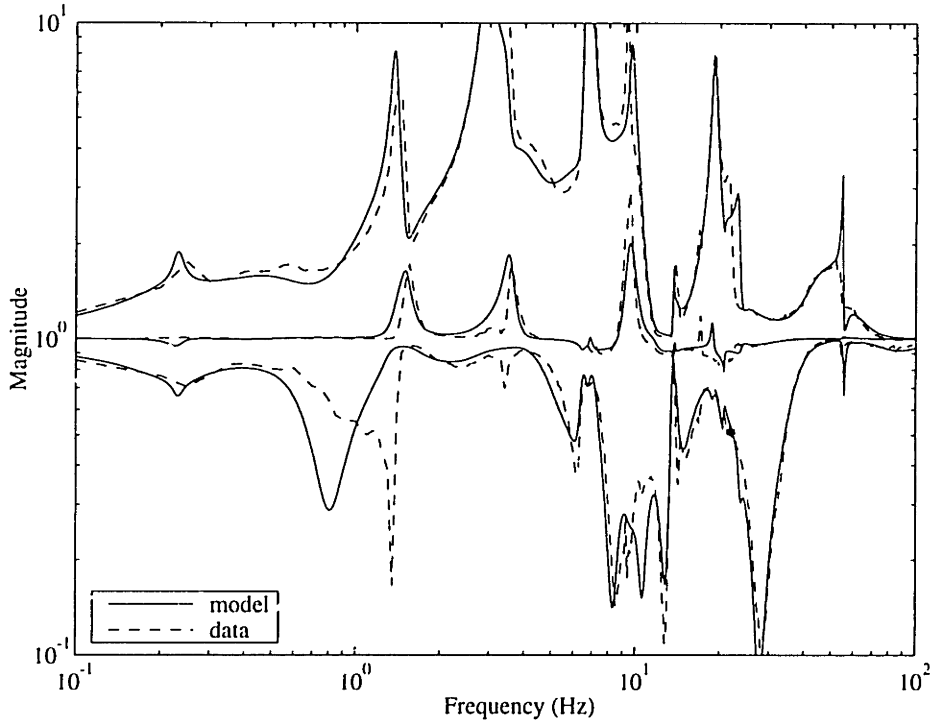

Figure 6.17: Singular values of $I + GK$ as predicted by the model and the open loop data for the highest authority MIMO MM controller.

when the transfer functions were measured, it is not surprising that the response is larger than predicted with the model.

Comparing Figures 6.18 and 6.7, it can be seen that the MIMO LQG controllers have performed much better than the SISO LQG controllers. Table 6.5 shows that the best MIMO LQG controller achieved a 14.9 dB improvement, while Table 6.2 shows only a 4.5 dB improvement using LQG in the SISO loop. It appears that simply adding more actuators and sensors has made this optimal control technique more robust.

Comparing the performance improvement of the robust control techniques, from Figure 6.18 it can be seen the SWLQG compensators have reduced the state cost significantly less than ME and MM compensators. In fact, the performance figures in Table 6.5 show that the best SWLQG control improvement the performance metric by 16.2 dB. This is a better improvement than the SISO SWLQG controllers (15.0 dB), but still much less than the ME and MM performance improvements. The best ME

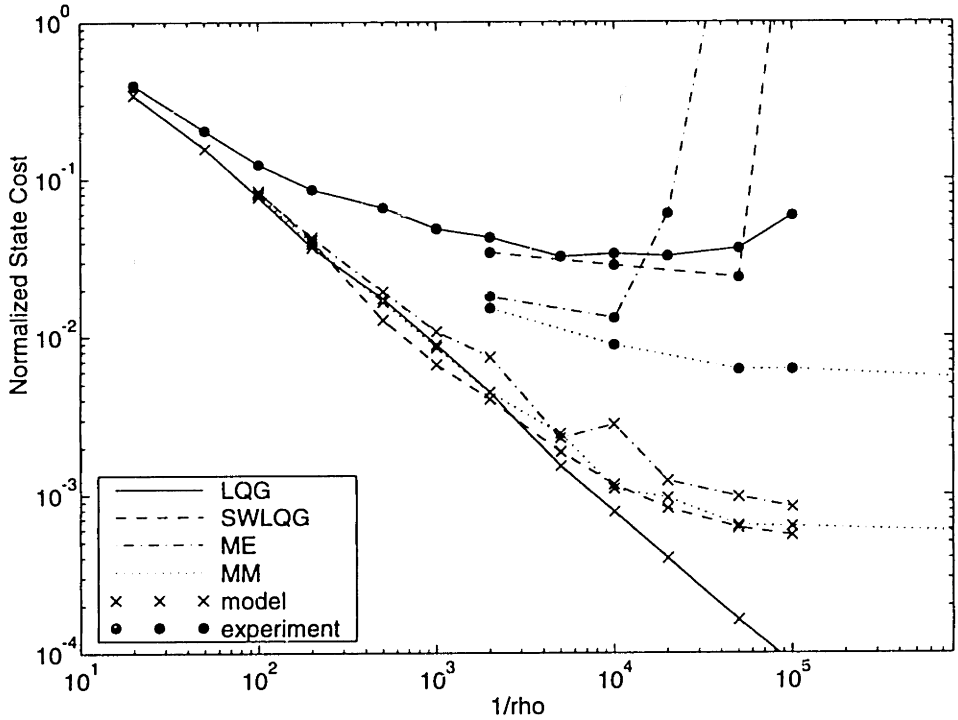

Figure 6.18: Performance as a function of control authority for the control techniques both on the design model and experimentally measured.

compensator achieved an 18.8 dB improvement, while the best MM compensators achieved a 22.6 dB improvement.

Figure 6.18 and Table 6.5 also indicate that compensators from both the SWLQG and ME control techniques destabilized the system at some level of control authority. In both instances, the first Y-axis bending mode (3.4 Hz) was destabilized. Predictions based on the Multivariable Nyquist Criteria indicated that the closed loop system would be stable for these controllers. However, Figures 6.15 and 6.16, which show the sensitivities of the SWLQG and ME compensators for the highest level of control authority, indicate significant differences between the data and model predictions in the frequency range around the 3.4 Hz mode. Both also indicate significant differences near the 1.4 Hz mode of the system. Experimentally, however, no problems were encountered with this mode. Figure 6.17 shows a very large difference in the sensitivity predictions near 1.4 Hz for the MM compensator as well. Again, experimentally, no stability or performance problems were encountered in this region.

The prediction difference near the 1.4 Hz mode is partially explained by the nonlinear nature of the MACE test article. Due to nonlinearity, possibly friction effects in the suspension system, the frequency of the X rotation mode (nominally 1.4 Hz) is shifted when the system is excited by the reaction wheels. Thus the frequency response measured with reaction wheel inputs shows the X rotation mode about 5% lower in frequency than frequency response data with primary gimbal input. Because predictions were made based on these frequency responses, errors occurred.

Note that for all three robust techniques, large weighting (uncertainty bounds for MM) was required on the 1.4 Hz mode to obtain a prediction of closed loop stability. For the SWLQG and ME techniques, these weightings caused increased sensitivity in the 3-4 Hz range. This indicates that for these techniques, the effects of robustifying to the 1.4 Hz mode have caused greater problems to the 3.4 Hz mode. The Multiple Model technique did not encounter this problem, which indicates that the robustifying effects may be more localized.

It is useful at this point to show the analysis techniques described in the preceding chapter applied to the best MIMO compensator, *i.e.* the MM compensator that achieved 22.6 dB performance improvement. For this compensator, Figure 6.19 shows the performance transfer function as predicted by both the model and the open loop data, and as experimentally measured. Note that the predictions are not as good as those in the SISO case (Figure 6.8). For frequencies above 8 Hz, the prediction using open loop data is good. However, below this there are significant deviations. In particular, the data prediction indicates that over the 1–8 Hz range, the response should be much lower than the response that was achieved. The model based prediction shows a much lower response over all frequencies than was achieved. A strong contributor to this could be the absence of sensor noise in the model and the nonlinearity.

Figures 6.20 and 6.21 show a Nichols plot of the multivariable Nyquist Function, Equation 4.1, based on the model and open loop data, respectively. The MM compensator contained only stable poles and therefore no net passes over the critical points should occur. In the two figures, it can be seen that the locus of the Nyquist function

Control authority (ρ,θ)		Performance Improvement			
		LQG	SWLQG	ME	MM
$\rho = 0.05,$	$\theta = 0.25$	4.0 dB	ND	ND	ND
$\rho = 0.02,$	$\theta = 0.1$	6.9 dB	ND	ND	ND
$\rho = 0.01,$	$\theta = 0.05$	9.1 dB	NI	NI	NI
$\rho = 5 \cdot e^{-3},$	$\theta = 2.5 \cdot e^{-2}$	10.7 dB	NI	NI	NI
$\rho = 2 \cdot e^{-3},$	$\theta = 1 \cdot e^{-2}$	11.8 dB	NI	NI	NI
$\rho = 1 \cdot e^{-3},$	$\theta = 5 \cdot e^{-3}$	13.2 dB	NI	NI	NI
$\rho = 5 \cdot e^{-4},$	$\theta = 2.5 \cdot e^{-3}$	13.7 dB	14.6 dB	17.4 dB	18.2 dB
$\rho = 2 \cdot e^{-4},$	$\theta = 1 \cdot e^{-3}$	14.9 dB	NI	NI	NI
$\rho = 1 \cdot e^{-4},$	$\theta = 5 \cdot e^{-4}$	14.7 dB	15.4 dB	18.8 dB	20.5 dB
$\rho = 5 \cdot e^{-5},$	$\theta = 2.5 \cdot e^{-4}$	14.9 dB	NI	12.2 dB	NI
$\rho = 2 \cdot e^{-5},$	$\theta = 1 \cdot e^{-4}$	14.4 dB	16.2 dB	US	22.1 dB
$\rho = 1 \cdot e^{-5},$	$\theta = 5 \cdot e^{-4}$	12.3 dB	US	NI	22.1 dB
$\rho = 0,$	$\theta = 0$	ND	ND	ND	22.6 dB
NI- not implemented, ND- not designed, US- unstable					

Table 6.5: Experimental performance values for the MIMO topology for each of the control techniques.

passes underneath all of the critical points, and therefore stability is predicted on the basis of both the frequency response of the model and the measured open loop frequency response data.

Finally, Figure 6.17 shows the singular values of $I + GK$ for this compensator. Note that at the frequencies at which the locus of the Nyquist function passes near a critical point, the singular values are very low. However, since the determinant does not contain information about the singularity of $I + GK$ (Section 4.3), the singular values can be low without the locus of the Nichols plot passing near the critical point. Hence the need for the test. Finally, note that large singular values

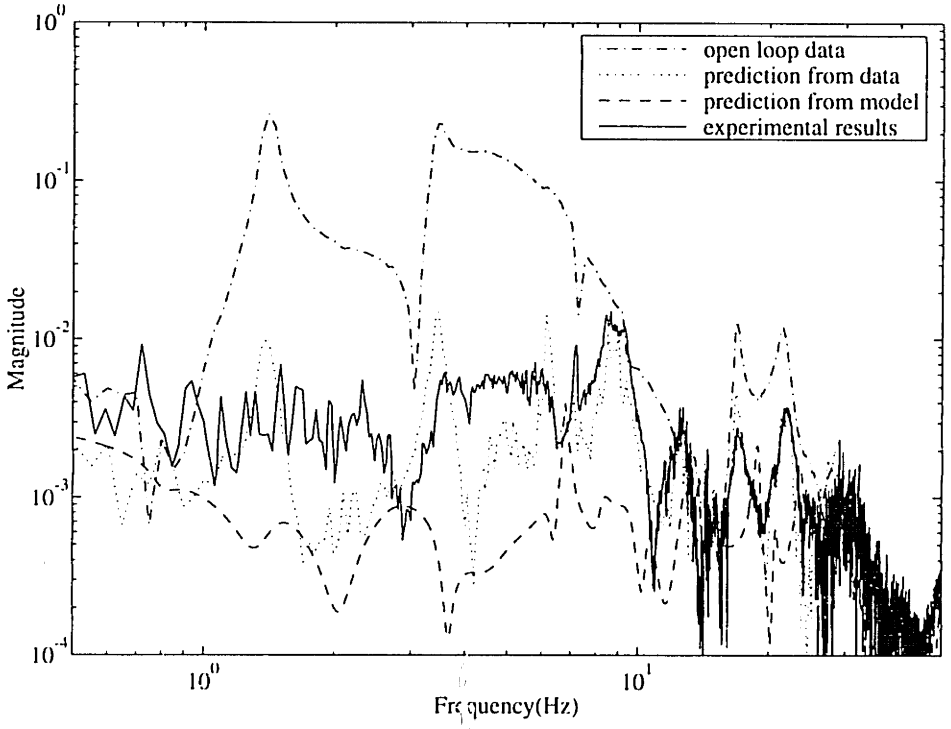

Figure 6.19: Performance transfer function of best MIMO compensator experimentally, and as predicted on the data and model.

indicate that in some "directions" the disturbance rejection is good. The fact that the closed loop performance is better than open loop performance indicates that these directions correspond to those in which the modelled disturbance enters the system. Note, however, that disturbance rejection cannot be guaranteed for all disturbances because the minimum singular value is less than unity.

The conclusions that can be drawn from the MIMO experiments are not as decisive as those from the SISO experiments. Once again, compensators designed by Multiple Model achieved the best performance. This indicates that the Multiple Model technique sacrifices less performance to achieve robust stability than the other techniques. However, the effects of robustification on the compensator have been seen only indirectly. Large weighting on the 1.4 Hz mode was necessary in all three techniques to obtain a stable prediction using the open loop data. For the SWLQG and ME techniques, this weighting caused an increase in the sensitivity to the 3.4 Hz mode. Weighting the 3.4 Hz mode in these techniques reduced this sensitivity somewhat, but

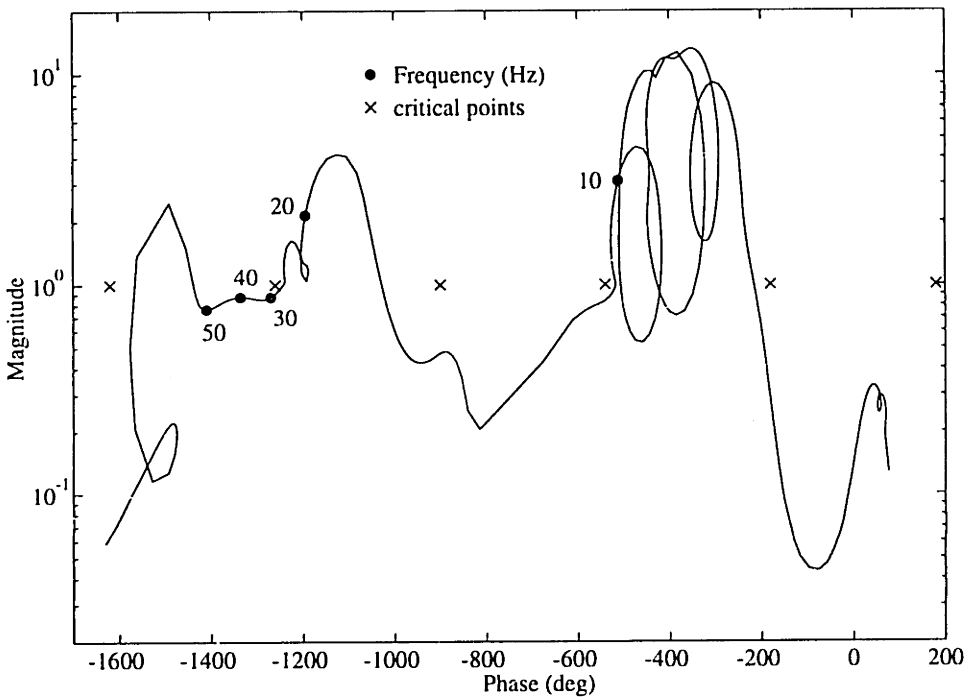

Figure 6.20: Nichols plot of best MIMO compensator using model.

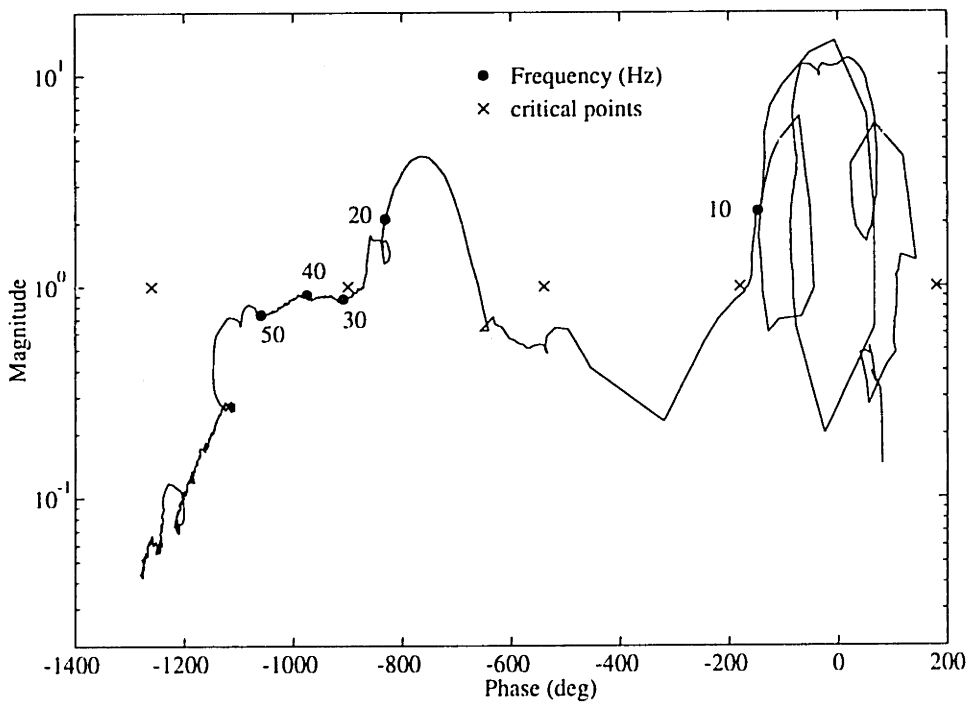

Figure 6.21: Nichols plot of best MIMO compensator, using open loop data to predict stability..

experimentally both destabilized this mode. For the multiple model compensators, it appears that the effects of robustifying to the 1.4 Hz mode were more localized. The sensitivity near the 3.4 Hz mode was not increased, and none of the MM compensators destabilized the system.

In the following chapter, results from both the SISO and MIMO experiments, the sample problem, and computational considerations will be discussed to draw final conclusions.

Chapter 7

Summary of Findings

The comparison of synthesis methods for robust control began with nine robust control design techniques divided into two categories. TSO, SWLQG, PRLQG, and Maximum Entropy are control techniques which achieve robustness by desensitizing the compensator to the uncertain parameters. Multiple Model, the Bourret approximation to the average cost, $\mathcal{H}_\infty$-synthesis, μ-synthesis, and Popov Control Synthesis are control techniques which provide some robustness guarantees.

A high degree of similarity exists between SWLQG and PRLQG. For frequency uncertainty, it is shown in Section 3.2.3 that the two techniques can be made to be identical. Therefore, PRLQG was not considered further.

Similarly, the derivation of SWLQG and TSO is very similar. Some simplifying assumptions are made in the SWLQG derivation which make it less rigorous. However, a substantial gain is made in computational savings. For TSO, $(2n_\alpha^2 + 5n_\alpha + 3)n^{\text{th}}$ order Lyapunov equations, must be solved at each step in an iterative solution process. For SWLQG, the solution of only two n^{th} order Riccati equations is required, and no iteration is necessary. Because of the degree of similarity between these techniques, and the computational simplicity of SWLQG, TSO was not considered further.

The Bourret approximation technique was discarded on the basis of high computational burden and similarity to the Multiple Model technique. The solution procedure for these two methods is similar. Both use a Quasi-Newton optimization process. However, for each Quasi-Newton iteration, the Multiple Model technique must solve

two $(2n)^{\text{th}}$ order Lyapunov equations for each model. The Bourret approximation method requires the solution of a coupled set of n_α $(2n)^{\text{th}}$ order Lyapunov equations. To solve the coupled equations itself requires iteration. In addition, it was shown in Section 3.3.2 that for a single uncertainty, these two techniques have the same solution. Because only a single uncertainty was considered in the sample problems, and the computation is prohibitively expensive for a problem on the order of the MACE examples, the Bourret technique was not considered further.

The Popov Controller Synthesis technique was not pursued in this thesis. Up until very recently, a good solution procedure was not available for the solution of the optimal Popov compensator. The original synthesis procedure used a zeroth order homotopy on the uncertainty bounds to introduce uncertainty to an initial guess provided from another control design technique. In Ref. [49], How illustrates a new algorithm which makes the use of a zeroth order homotopy no longer necessary, and significantly reduces the convergence time. However, the algorithm was not available for this thesis, and therefore for computational reasons, this method was not studied further.

The remaining techniques; SWLQG, ME, MM, $\mathcal{H}_\infty$, and μ-synthesis were used to design compensators for an eighth order sample problem. It was shown in Chapter 5 that all of the techniques are effective at providing robustness to parametric uncertainty. Compensators designed using each technique achieved robustness bounds of greater than $\pm 15\%$ to the frequency of the uncertain third mode of the system. However, the distinction between the methods arises when the cost, in terms of performance decrease, bandwidth increase, computation required, and, for methods which provide guarantees, conservatism is considered.

The $\mathcal{H}_\infty$ technique was found to be very conservative. Despite achieving robustness to greater than 50% uncertainty in the sample problem, $\mathcal{H}_\infty$ designs could guarantee stability for only 2% uncertainty. This is not entirely surprising since it was noted in Chapter 3 that $\mathcal{H}_\infty$ is necessarily conservative for real parameter uncertainty because it considers complex valued uncertainties. Thus the guarantees provided by the $\mathcal{H}_\infty$ controllers for the sample problem were almost negligible. Conservatism

aside, it is still possible to compare $\mathcal{H}_\infty$ compensators with the other techniques on the basis of performance decrease and bandwidth increase for equivalent robustness. Here also, $\mathcal{H}_\infty$ compensators were comparatively poor. Figure 5.28 showed the nominal state cost as a function of achieved uncertainty bounds for $\mathcal{H}_\infty$, SWLQG, ME and MM compensators. For equivalent uncertainty bounds, the $\mathcal{H}_\infty$ compensators sacrificed much more performance than any of the other methods. As well, the bandwidth increase was significantly greater than any of the other methods. Based on these results, it was determined that using $\mathcal{H}_\infty$ synthesis for real parameter uncertainty such as frequency errors on structural systems was unsuitable. Thus, the $\mathcal{H}_\infty$ technique was pursued no further.

The μ-synthesis technique was found to be unsuitable as well, but for substantially different reasons. The closed loop performance of the μ compensators designed for the first sample problem was very good. No significant decrease in performance was observed. However, this was partly due to stringent performance requirements and weak constraints on the high frequency response,which resulted in large bandwidth increases. However, while the bandwidth increase was significantly larger than for the $\mathcal{H}_2$ designs, it was less than the bandwidth increases that resulted in the $\mathcal{H}_\infty$ compensators.

The reduction in conservatism over $\mathcal{H}_\infty$ was significant as well. Compensators were designed which guaranteed robust performance for up to 6% uncertainty in the frequency of the third mode of the system, compared with 2% for $\mathcal{H}_\infty$. However, because μ considers the uncertainty to be complex, conservatism was still present. The compensator which guaranteed robust performance for 6% uncertainty achieved robust stability for up to 18% uncertainty. Even by weakening performance and bandwidth constraints, it was still not possible to design a compensator which would guarantee stability for 8% uncertainty.

The major drawback of μ-synthesis, however, is computation. The D-K iteration solution procedure of μ-synthesis was outlined in Section 3.3.4. The procedure contains alternating analysis (D) and synthesis (K) steps. For each synthesis step, an $\mathcal{H}_\infty$ compensator is designed for the system DGD^{-1} where D is a state space fit of the D-

scales obtained from the analysis step. Thus the order of the system for which an $\mathcal{H}_\infty$ compensator is designed is increased by twice the order of D. For the sample problem, the D scales were fit with a system roughly three times larger than the original system dynamics. The resulting $\mathcal{H}_\infty$ compensator was over 70 states for this 8 state system. It is true that the order of the compensator could be reduced significantly *a posteriori*. However, it is necessary to first solve for the full order compensator. In a system with multiple uncertainties, each additional uncertainty adds another set of D-scales which further increases the order of the system. The state inflation caused by the D-scales makes μ-synthesis impractical for designing compensators for large order systems with multiple uncertainties such as MACE. Therefore, the μ-synthesis technique was not investigated further.

The remaining three robust control techniques; SWLQG, ME, and MM were further investigated on a second sample problem, and both SISO and MIMO control experiments on the MACE test article. All three techniques were found to be effective, and each was found to have its own advantages.

SWLQG has a clear computational advantage over either ME or MM. The SWLQG compensator is derived from the solution of two n^{th} order Riccati equations, just as LQG. However, there are no robustness guarantees, and an iteration is required to find sensitivity weights that yield the desired robustness. The major disadvantage of SWLQG is that, of the $\mathcal{H}_2$ techniques, it sacrifices the most performance and results in the largest bandwidth increase. Experimentally, the SWLQG compensators consistently provide good performance (15 dB in Table 6.2 compared to 4.5 dB for LQG). This shows SWLQG to be a useful and effective technique. However, ME and MM compensators could achieve better performance (15.8 dB and 20.2 dB, respectively). In the MIMO experiment, SWLQG achieve 16.2 dB performance improvement compared with 18.8 dB for ME and 22.6 dB for MM.

Computationally, the Maximum Entropy technique is significantly more complex than SWLQG. For frequency uncertainty, a new homotopy algorithm has been developed [28] which provides an efficient solution to the coupled set of two n^{th} order Lyapunov and two n^{th} order Riccati equations. Table 3.1 shows that the computa-

tion required for an ME compensator is significantly more than for SWLQG, but also significantly less than for MM. For the 8^{th} order sample problem, the computation for ME compensators took 6.4 Mflops, compared with 1.0 Mflops for SWLQG and 98.2 Mflops for MM. Unfortunately, like SWLQG, ME provides no robustness guarantees. Therefore it requires an iterative process to determine the uncertainty weightings that achieve the desired robustness.

In all respects, the Maximum Entropy technique appears to lie between SWLQG and MM. In the first sample problem, there were no significant differences in the performance of the three $\mathcal{H}_2$ techniques. In terms of bandwidth, SWLQG resulted in higher bandwidth compensators than ME which had higher bandwidth than the MM compensators. In the second sample problem, the ME compensators were between the MM and SWLQG compensators in terms of both bandwidth and performance. In both the SISO and MIMO experiments, as well, the ME compensators performed better than SWLQG compensators, but not as well as MM compensators. Therefore, its advantage is being computationally easier to calculate than MM compensators while generally achieving better performance than SWLQG compensators.

The MM technique is the most computationally intensive of the three $\mathcal{H}_2$ techniques, requiring the solution of two $(2n)^{th}$ order Lyapunov equations for each model at each iteration in a Quasi-Newton optimization. Also, the number of models can increase combinatorially with the number of uncertainties. Throughout this thesis, however, a smaller set of models has been used for MM design. Rather than including a model for each combination of upper and lower estimates of the uncertain parameters, only three separate models were used in each design. These three models consist of the nominal, one with all the uncertain parameters perturbed to their respective upper estimates, and one with all uncertain parameters at their respective lower estimates. Although this introduces correlation between the uncertainties, this set of models has been found to be very effective.

It has already been reiterated that the Multiple Model compensators consistently achieved the best performance and sustained the least increase in bandwidth in each of the sample problems and the MACE experiments. The remaining issue to discuss

is conservatism. The multiple model technique provides some robustness guarantees. Namely, it guarantees stability on every model in the design set. In the first sample problem, with one uncertainty, it was shown that MM is much less conservative than either $\mathcal{H}_\infty$ or μ-synthesis. In both sample problems, it was shown that the achieved robustness bounds were very close to the design points for which MM is guaranteed to be stable. One implication of showing little conservatism is that if uncertainty bounds are known, excessive performance will not be sacrificed by designing a compensator to guarantee robustness to those uncertainty bounds.

Another drawback of the computational procedure for the Multiple Model technique is the requirement for an initial guess which stabilizes all of the models in the design set. Because optimal LQG controllers are often not sufficiently robust they cannot be used, except in a homotopy procedure from low authority. Instead, a procedure that worked extremely well in this thesis is to use an SWLQG (or ME) compensator as an initial guess.

This procedure has been refined into a design methodology that combines the techniques in three different stages. The first stage in the process is the recognition of the parameters in the system which *must* be considered part of the uncertainty set for robust control. Because there is a performance/robustness trade off for every uncertainty, inclusion of a parameter in the uncertainty set results in some degradation in performance. By reducing the uncertainty set to only those parameters that are important to the control, higher performance is possible. In this first stage, a sequence of controllers is designed at different levels of control authority. In order to determine which uncertainties actually cause robustness problems, controllers at different levels of authority are evaluated using the prediction methods in Chapter 4 until a robustness problem arises. The critical parameters can then be included in the uncertainty set and controllers robust to these uncertainties can be designed for subsequently higher levels of authority until all the critical uncertainties are identified. It is best to use a fast robust control technique (SWLQG or ME) for this stage.

The second stage is the optimization of sensitivity weights on the uncertainties that have been identified so the best SWLQG controller results. The final stage is to

use this SWLQG as an initial guess for a Multiple Model controller which includes the parameters identified through the design of the SWLQG controller in the uncertainty set.

This design process has the advantage of using a design technique which requires very little computation (SWLQG), in an iterative scheme to identify the critical uncertain parameters in a system. This is followed by the design of a compensator using a computationally intensive routine which results in very good performance. This process has distinct advantages over using either of the techniques individually. First, because it uses iterative SWLQG designs to determine the critical uncertainties, it is faster than if the same iterative process were used with Multiple Model alone. Second, because it uses SWLQG as an initial guess, it avoids the need for a homotopic approach for an initial guess using Multiple Model. Thus, it again saves time and computation. Finally, because a Multiple Model controller is designed with only the critical uncertain parameters included in the uncertainty set, it avoids sacrificing performance on parameters which do not need to be in the uncertain set, and thus is capable of greater performance.

Chapter 8

Conclusions

The purpose of this thesis has been to compare robust control techniques applied to uncertain structural systems. Compensators were designed for two systems: the first, an analytical, low order sample problem; the second, an experimental system, the Middeck Active Control Experiment (MACE) test article. The use of these two systems has permitted two different and complementary approaches to comparison.

The first approach is essential in comparing the performance that robust controllers sacrifice, when compared to optimal control techniques, in order to achieve robustness. On a sample problem, it is possible to manipulate the uncertainty in the parameters. Then, the achieved robustness bounds can easily be quantified, and compensators can be compared on the basis of the performance that is sacrificed in order to achieve certain bounds.

The second approach is essential for comparing the performance gain that these controllers achieve *because* they are robust. As shown in Chapter 6, for real systems, compensators designed for optimal performance are often not sufficiently robust to maintain stability. These techniques are then limited to low authority. However, it is possible to implement higher authority robust compensators and thus achieve better performance on the test article than lower authority optimal compensators.

The sample problems and experimental results in Chapters 5 and 6 demonstrate these robustness/performance trades. However, to achieve good experimental performance it is important that one determines the parameters that are uncertain, and of

these, the ones that are most critical for stability. A number of analysis tools have been used both to aid in the identification of uncertainties and to aid in the design and comparison of different compensators. These tools are discussed in Chapter 4. The Multivariable Nyquist Criteria and singular values of $I + GK$ based on open loop data and the frequency response of the model were found to be particularly useful for predicting stability and sensitivity problems. These tools form an essential part in the synthesis methodology for robust control design.

In terms of performance achieved, Multiple Model was the best of the robust control techniques. However, difficulty with the computation of these controllers has led to the development of the design methodology discussed in the preceding chapter. This methodology combines the use of the predictive analysis tools and computational advantages of Sensitivity Weighted LQG (SWLQG) with the performance and robustness advantages of the Multiple Model technique. The results in this thesis have demonstrated this to be a powerful robust control synthesis technique for uncertain structural systems.

8.1 Future Work

A logical extension of the comparison of robust control techniques contained in this thesis is to compare new robust control techniques as they are developed. Since the start of work on this thesis, at least two significant developments have been made in robust control. The first, Popov Control Synthesis [13], is touched on in Section 3.3.5. This is a promising technique which incorporates the Popov stability criteria from absolute stability theory into an $\mathcal{H}_2$ controller synthesis technique. The resulting compensator provides guarantees of stability and performance. This technique was not pursued because software was still in an early stage of development. Recently [49] a homotopy approach for solving for the optimal Popov multiplier has been introduced which advances the synthesis significantly. Comparing controllers designed using Popov Control Synthesis would complement the work contained in this thesis.

The second major development in robust control theory during the preparation of

this thesis is the extension of μ-synthesis to include real parameter uncertainty [50]. An upper bound to μ for the case of real parameter uncertainty and mixed real and complex uncertainties has been developed. The calculation of the upper bound involves a minimization over two sets of scaling functions (D and N). The D-scales in mixed-μ are identical to the D-scales in complex μ. The N-scales are included to introduce phase information to the uncertainty. Both are frequency dependent functions. Real μ analysis has very close connections with the Popov stability criteria [35]. In fact, the Popov analysis test is equivalent to real μ analysis with constant D and N-scales. A synthesis technique has been developed which combines the mixed-μ analysis with an $\mathcal{H}_\infty$ synthesis. This is similar to the D-K iteration, and is known as the D-N-K iteration. The K step for mixed-μ synthesis is considerably more complex than for complex-μ. An $\mathcal{H}_\infty$ compensator is designed for a system which includes the state space representation of D and D^{-1}, as well as powers of N. As a result, the number of states in the system is considerably more than would be included for the complex-μ synthesis alone. Thus, this technique likely suffers from the same problems of computational burden as μ synthesis. However, comparing compensators developed using mixed-μ synthesis for the sample problem, would complement the work contained in this thesis.

References

[1] Tahk, M. and J. L. Speyer, "Parameter Robust Linear-Quadratic-Gaussian Design Synthesis with Flexible Structure Control Applications," *AIAA Journal of Guidance, Control, and Dynamics*, Vol. 12, No. 4, Aug. 1989, pp. 460–468.

[2] Doyle, J. C. and G. Stein, "Multivariable System Design: Concepts for a Classical/Modern Synthesis," *IEEE Trans. on Automatic Control*, Vol. AC–26, No. 1, Feb. 1981, pp. 4–16.

[3] Tahk, M. and J. L. Speyer, "Modeling of Parameter Variations and Asymptotic LQG Synthesis," *IEEE Trans. on Automatic Control*, Vol. AC–32, No. 9, Sept. 1987, pp. 793–801.

[4] Cheung, M.-F. and S. Yurkovich, "On the Robustness of MEOP Design Versus Asymptotic LQG Synthesis," *IEEE Trans. on Automatic Control*, Vol. AC–33, No. 11, Nov. 1988.

[5] Hyland, D. C., "Maximum Entropy Stochastic Approach to Controller Design for Uncertain Structural Systems," *Proceedings, American Control Conference*, Arlington, VA, June 1982, pp. 680–688.

[6] Okada, K. and R. E. Skelton, "Sensitivity Controller for Uncertain Systems," *AIAA Journal of Guidance, Control, and Dynamics*, Vol. 13, No. 2, 1990, pp. 321–329.

[7] Sesak, J. R., *Sensitivity Constrained Linear Optimal Control Analysis and Synthesis*, Ph.D. thesis, University of Wisconsin, 1974.

[8] Ashkenazi, A. and A. E. Bryson Jr., "Control Logic for Parameter Insensitivity and Disturbance Attenuation," *AIAA Journal of Guidance, Control, and Dynamics*, Vol. 5, No. 4, July 1982, pp. 383–388.

[9] MacMartin, D. G., S. R. Hall, and D. S. Bernstein, "Fixed Order Multi-Model Estimation and Control," *Proceedings, American Control Conference*, Boston, MA, June 1991, pp. 2113–2118.

[10] Hagood, N. W., *Cost Averaging Techniques for Robust Control of Parametrically Uncertain Systems*, Ph.D. thesis, Department of Aeronautics and Astronautics, M.I.T., Cambridge, MA, June 1991.

[11] Doyle, J. C., K. Glover, P. P. Khargonekar, and B. A. Francis, "State-Space Solutions to Standard $\mathcal{H}_2$ and $\mathcal{H}_\infty$ Control Problems," *IEEE Trans. on Automatic Control*, Vol. AC–34, No. 8, Aug. 1989, pp. 831–847.

[12] MuSyn Inc., *μ-Analysis and Synthesis Toolbox: User's Guide*, The Math Works, Inc., 1991.

[13] How, J. P., *Robust Control Design with Real Parameter Uncertainty using Absolute Stability Theory*, Ph.D. thesis, Department of Aeronautics and Astronautics, M.I.T., Cambridge, MA, Jan. 1993.

[14] Glaese, R. M., *Development of Zero-Gravity Structural Control Models from Ground Analysis and Experimentation*, Master's thesis, Massachusetts Institute of Technology, 1994.

[15] McLaren, M. D. and P. Y. Chu, "Slew Disturbance Compensation for Multiple Payloads of a Flexible Spacecraft," *Proceedings, AIAA Guidance, Navigation, and Control Conference*, Hilton Head, SC, Aug. 1992.

[16] Crawley, E. F., J. de Luis, and D. W. Miller, "Middeck Active Control Experiment (MACE) Phase A Final Report," Tech. Rep. SERC #16-90-R, Space Engineering Research Center, Massachusetts Institute of Technology, June 1989.

[17] Kienholz, D. A., "A Pneumatic/Electric Suspension System for Simulating On-Orbit Conditions," *Proceedings, Winter Annual Meeting of the American Society of Mechanical Engineers*, Dallas, TX, Nov. 1990.

[18] Kwakernaak, H. and R. Sivan, *Linear Optimal Control Systems*, Wiley-Interscience, 1972.

[19] Safonov, M. G. and M. Athans, "Gain and Phase Margin for Multiloop LQG Regulators," *IEEE Trans. on Automatic Control*, Vol. AC–22, No. 2, Apr. 1977, pp. 173–179.

[20] Doyle, J. C., "Guaranteed margins for LQG regulators," *IEEE Trans. on Automatic Control*, Vol. AC–23, 1978, pp. 756–757.

[21] Bernstein, D. S. and D. C. Hyland, "Optimal Projection Equations for Reduced-Order Modelling, Estimation, and Control of Linear Systems with Multiplicative White Noise," *Journal of Optimization Theory and Applications*, Vol. 58, No. 3, Sept. 1988, pp. 387–409.

[22] Weinmann, A., *Uncertain Models and Robust Control*, Springer-Verlag, 1991.

[23] Yedevalli, R. K. and R. E. Skelton, "Controller Design for Parameter Sensitivity Reduction in Linear Regulators," *Optimal Control Applications and Methods*, Vol. 3, 1982, pp. 221–240.

[24] Wagie, D. A. and R. E. Skelton, "Model Reduction and Controller Synthesis in the Presence of Parameter Uncertainty," *Automatica*, Vol. 22, No. 3, 1986, pp. 295–308.

[25] Blelloch, P. A. and D. L. Mingori, "Robust Linear Quadratic Gaussian Control for Flexible Structures," *AIAA Journal of Guidance, Control, and Dynamics*, Vol. 13, No. 1, Jan. 1990, pp. 66–72.

[26] Bernstein, D. S. and D. C. Hyland, "The Optimal Projection/Maximum Entropy Approach to Designing Low-Order, Robust Controllers For Flexible Structures,"

Proceedings, IEEE Conference on Decision and Control, Ft. Lauderdale, FL, Dec. 1985, pp. 745–751.

[27] MacMartin, D. G., *A Stochastic Approach to Broadband Control of Parametrically Uncertain Structures*, Ph.D. thesis, Department of Aeronautics and Astronautics, M.I.T., Cambridge, MA, June 1992.

[28] Collins Jr., E. G., L. D. Davis, and S. Richter, "A Homotopy Algorithm for Maximum Entropy Design," preprint, submitted to 1993 American Control Conference.

[29] Bernstein, D. S. and D. C. Hyland, "The Optimal Projection Approach to Robust, Fixed-Structure Control Design," in *Mechanics and Control of Space Structures* (Junkins, J. L., ed.), pp. 237–293, AIAA, Washington, D. C., 1990.

[30] Scales, L. E., *Introduction to Non-Linear Optimization*, Springer-Verlag, New York, 1985.

[31] Mustafa, D., *Minimum Entropy $\mathcal{H}_\infty$ Control*, Springer-Verlag, 1990.

[32] Maciejowski, J. M., *Multivariable Feedback Design*, Addison-Wesley, Wokingham, England, 1989.

[33] Doyle, J. C., "Analysis of Feedback Systems with Structured Uncertainties," *IEE Proceedings*, Vol. 129, Part D, No. 6, Nov. 1982, pp. 242–250.

[34] Young, P. M. and J. C. Doyle, "Properties of the Mixed-μ Problem and its Bounds," Preprint, submitted to *IEEE Transactions on Automatic Control*, Oct. 1992.

[35] How, J. P. and S. R. Hall, "Connections between the Popov Stability Criterion and Bounds for Real Parameter Uncertainty," *Proceedings, American Control Conference*, San Francisco, Inst. of Electrical and Electronics Engineers, Piscataway, NJ, June 1993, pp. 1084–1089. Submitted to *IEEE Trans. on Auto. Control.*

[36] Willems, J. C., "Dissipative Dynamical Systems, Parts I and II," *Archive Rational Mechanics Analysis*, Vol. 45, 1972, pp. 321–351,352–393.

[37] Ogata, K., *Modern Control Engineering*, Prentice-Hall, Inc., Englewood Cliffs, NJ, 1970.

[38] Lehtomaki, N., *Practical Robustness Measures in Multivariable Control System Analysis*, Ph.D. thesis, Massachusetts Institute of Technology, May 1981.

[39] Lublin, L., *Multivariable Stability Robustness for Control of Flexible Beams and Trusses*, Master's thesis, Massachusetts Institute of Technology, 1992. MIT SERC report # 6-92.

[40] Grocott, S. C. O., J. P. How, D. W. Miller, D. G. MacMartin, and K. Liu, "Robust Control Implementation on the Middeck Active Control Experiment (MACE)," Dec. 1993. Submitted to the *AIAA Journal of Guidance, Control, and Dynamics.*

[41] Blevins, R. D., *Formulas for Natural Frequency and Mode Shape*, Robert E. Krieger Publishing Company, Malabar, Florida, 1979.

[42] Campbell, M. E., *Neo-Classical Control of Structures*, Master's thesis, Department of Aeronautics and Astronautics, M.I.T., Cambridge, MA, Feb. 1993.

[43] MacMartin, D. G. and J. P. How, "Implementation and Prevention of Optimal Unstable Compensators," Sept 1993. Submitted to the *1994 American Control Conference.*

[44] Karlov, V. I., R. M. Glaese, D. W. Miller, and E. F. Crawley, "Physical Model-Set Identification for Robust Control of Flexible Structures," Presented at *AIAA Guidance, Navigation and Control Conference*, Aug. 1993.

[45] Karlov, V. I., D. W. Miller, W. E. Vander Velde, and E. F. Crawley, "Identification of Model Parameters and Associated Uncertainties as a Basis for Robust Control," Submitted to *AIAA Journal of Guidance, Control, and Dynamics.*

[46] Petersen, I. R. and C. V. Hollot, "A Riccati Equation Approach to the Stabilization of Uncertain Linear Systems," *Automatica*, 1986, pp. 397–412.

[47] Grocott, S. C. O., D. G. MacMartin, and D. W. Miller, "Experimental Implementation of a Multi-Model Design Technique for Robust Control of the MACE Test Article," *Proceedings, Third Internation Conference on Adaptive Structures*, San Diego, CA, Nov. 1992, pp. 375–387.

[48] Francis, B. A., *A Course in $\mathcal{H}_\infty$ Control Theory*, Springer-Verlag, 1987.

[49] How, J. P., E. G. Collins, Jr., and W. M. Haddad, "Optimal Popov Analysis and Synthesis for Systems with Real Parameter Uncertainties," Sept 1993. Submitted to the *1994 American Control Conference* and the *IEEE Transactions on Control Systems Technology.*

[50] Young, P. M., M. P. Newlin, and J. C. Doyle, "μ Analysis with Real Parametric Uncertainty," *Proceedings, IEEE Conference on Decision and Control*, Brighton, England, Dec. 1992, pp. 1251–1256.